Steady state experimental evaluation of a novel Raney-Ni/PTFE gas diffusion electrode in an alkaline fuel cell

Khan, Khan Abbas A., M.S.
King Fahd University of Petroleum and Minerals (Saudi Arabia), 1993

Order Number 1354019

Steady state experimental evaluation of a novel Raney-Ni/PTFE gas diffusion electrode in an alkaline fuel cell

Khan, Khan Abbas A., M.S.

King Fahd University of Petroleum and Minerals (Saudi Arabia), 1993

U·M·I
300 N. Zeeb Rd.
Ann Arbor, MI 48106

Steady State Experimental Evaluation of a Novel Raney-Ni/PTFE Gas Difffusion Electrode in an Alkaline Fuel Cell

BY

Khan Abbas A. Khan

A Thesis Presented to the

FACULTY OF THE COLLEGE OF GRADUATE STUDIES

KING FAHD UNIVERSITY OF PETROLEUM & MINERALS

DHAHRAN, SAUDI ARABIA

In Partial Fulfillment of the
Requirements for the Degree of

MASTER OF SCIENCE

In

CHEMICAL ENGINEERING

June, 1993

KING FAHD UNIVERSITY OF PETROLEUM AND MINERALS
DHAHRAN 31261, SAUDI ARABIA

COLLEGE OF GRADUATE STUDIES

This thesis, written by *ABBAS ALI A. KHAN* under the direction of his thesis advisor and approved by his thesis committee, has been presented to and accepted by the Dean of the College of Graduate Studies, in partial fulfillment of the requirements for the degree of *MASTER OF SCIENCE IN CHEMICAL ENGINEERING*

Thesis Committee

Chairman (Dr. Selahattin Gultekin)

Co-Chairman (Dr. Muhammad A. Al-Saleh)

Member (Dr. Abdullah S. Al-Zakri)

Dr. Dulaihan K. Al-Harbi
Department Chairman

Dr. Ala H. Al-Rabeh
Dean, College of Graduate Studies

Date: 10-7-93

THIS IS DEDICATED TO MY

BROTHERS

ACKNOWLEDGMENT

I would like to sincerely thank my thesis advisor, Dr. Selahattin Gultekin for his invaluable guidance and co-operation during the course of my studies. I am grateful to my co-advisor, Dr. Muhammad Al-Saleh for his excellent guidance and constant encouragement throughout this thesis. I am also indebted to Dr. Abdullah Al-Zakri for his critical comments, fruitful suggestions and generous assistance in this project. I would like to thank Dr. Dulaihan Al-Harbi, Chemical Engineering Department Chairman for his marvelous assistance during my research work. Special thanks are also due to my friends Aleem Paracha and Saleem ur-Rahman for their help in the project. I am grateful to all the faculty members and graduate students of Chemical Engineering Department who made my stay in the university pleasant and memorable one.

ABBAS ALI A. KHAN

Dhahran/Saudi Arabia

June 1993

TABLE OF CONTENTS

Chapter 7-EXPERIMENTAL RESULTS AND ANALYSIS

LIST OF FIGURES

LIST OF TABLES

Nomenclature

A = External surface area of electrode,cm^2

ä = Electrode activity

C_o = Solubility of hydrogen in KOH ,mol/cm^3

D_L = Effective diffusion coefficient of H2 in electrolyt flooded pores

E_a = Apparent activation energy for H2 oxidation reaction

F = Faraday constant

f° = Active surface area of electrode per unit volume,cm-1

I = Total current, Ampere

i = Current density,mA/cm2

i_o = Exchange current density ,mA/cm^2

K_d = Deactivation rate constant

L = Electrode thickness,cm

n = Number of electrons transferred

R = Average radius of catalyst grain, cm

t = Time on stream, hr

T = Absolute temperature

z = Stoichiometric number

Greek Letters

α = Charge transfer coefficient

ε_{mac} = Macroporosity of the electrode

ε_{mic} = Microporosity of the electrode

η = Measureable overpotential on the electrolyte side, mV

θ = Contact angle

κ_e = Effective ionic conductivity, $\Omega^{-1}cm^{-1}$

ξ = Dimensionless electrode thickness

ϕ = Dimensionless overvoltage

ملخص الأطروحة

الأسم : عباس علي خان

عنواو الاطروحة : تقييم تجربي لاقطاب نيكل اسفنجي غازية جديدة عند حالة الاستقرار في خلايا الوقود القلوية.

التخصص : هندسة كيميائة
التاريخ : يونيو ١٩٩٣

أجريت قياسات استقطابية عند حالة الاستقرار لقطب نيكل اسفنجي غازي جديد، ومطلي بأول أكسيد النحاس، و قدتم رصد أداء القطب على المدى الطويل في نصيف خلية تحتوي ٤٥٪ من محلول هيدروكيد البوتاسيوم . ضخ غاز هيدروجين نقي لنصف الخلية تحت ضغط ١ . ٤ بار، وغيرة الحرارة من ٢٥° م إلى ٧٥°م، يعزى الأداء الأفضل (الاستتقطاب أقل) عند كثافات تيار كهربائي عالية لاضافة النحاص للقطب.

تم تطبيق نموزج داني الكروي لامتزار وذلك لتقرير:
الوسائط الكايناتيكية، كثافات التيار المتبادلة، و معامل انتقال الشحنة للقطب. ووجد أن قيم كثافات التيار المتبادلة تحت درجات حرارة مختلفة تتراوح ما بين ٢ . ٦ x ١٠إلى ١ . ٣x١-٤ أمبير/سم وه علامة أسّية مع درجة الحرارة. وجد أيضاً أن طاقة التنشيط الظاهرية للقطب تساوي ٢٨ كيلوجول/مول، وهي أقل من القيم المنشورة. أما طاقةالتنشيط الأقل لتفاعل أكسدة الهيدروجين فإهنا تعني نشاطاً أعلى لمثل هذا النوع من الاقطاب.

على المدى الطويل بينت الاختبارات أنّ جهداً قطبياً أعلى من ٥٠ ملي فثولت يُسبب تقليلاً سريعاً لنشاط القطب حُسبت ثوابت التقليل الظاهري للنشاط فكانت تتغير ما بين ٠.٠٤، إلى ٠.٣٦، لكل ساعة، وكان معدل تقليل النشاط أكثر عند درجات حرارة أعلى .

درجة الماجستير في العلوم

جامعة الملك فهد للبترول والمعادل

الظهران ، المملكة العربيةالسعودية

ABSTRACT

Steady state polarization measurements on specially prepared Raney-Ni/PTFE gas diffusion electrode impregnated with copper oxide were carried out. The long term performance of the electrode was also investigated in a half cell setup with 25% KOH solution. Pure hydrogen gas was fed to the half cell at a pressure of 1.4 bar. The electrolyte temperature was varied from 25°C to 75°C. The better performance (less polarization) at higher current densities is attributed to the addition of copper to the electrode.

Spherical Raney-catalyst grain model was applied to determine the kinetic parameters, exchange current density(i_o) and charge transfer coefficient(α) for the electrode. The values found for the exchange current densities at various temperatures were 6.6×10^{-6} to 3.1×10^{-4} Acm^{-2}. Exchange current density followed an exponential relation with temperature. Apparent activation energy for the electrode was found to be 28 kJ/mol lower than that reported in the literature. The lower activation energy for hydrogen oxidation reaction implied higher electroactivity of the electrodes of this type.

Long term performance tests showed that electrode overpotential greater than 50 mV cause rapid deactivation of the electrode. The apparent deactivation constants estimated for the electrode varied from 0.004 hr^{-1} to 0.032 hr^{-1}. The rate of deactivation is more at higher temperatures.

Chapter 1

INTRODUCTION

1.1 Basic Concept of a Fuel Cell

Fuel cell is an electrochemical device which converts the energy of chemical bonding to electrical energy. Unlike conventional batteries, fuel cells are fed continuously with their appropriate reactants a fuel and an oxidant. The reactants are stored outside the cell. Fuel cell comprises of two electrodes which are immersed in an electrolyte. The fuel which is a reducing agent such as hydrogen is fed to the anode. The oxidizing agent(air or oxygen) is fed to the cathode.(see fig. 1.1)

The oxidation of fuel at the anode and simultaneous reduction of oxidant at the cathode causes a potential difference. This potential difference promotes electron flow in an external circuit, where a load is connected. Thus useful work is obtained from a cell by physical separation of the electrode processes. To keep the electrode electrolyte invariant the reaction products are discarded.(1)

Theoretically any spontaneous chemical reaction could be used in a fuel cell. Because of unlimited supply of oxygen in the air combustion reactions are usually preferred for fuel cells. Most systems under development rely on hydrogen as the fuel.(1)

In practice, voltages of 0.7-0.8 V can be obtained in fuel cells with current densities of 100-300 $mAcm^{-2}$ of electrode surface(2). Fuel cells are

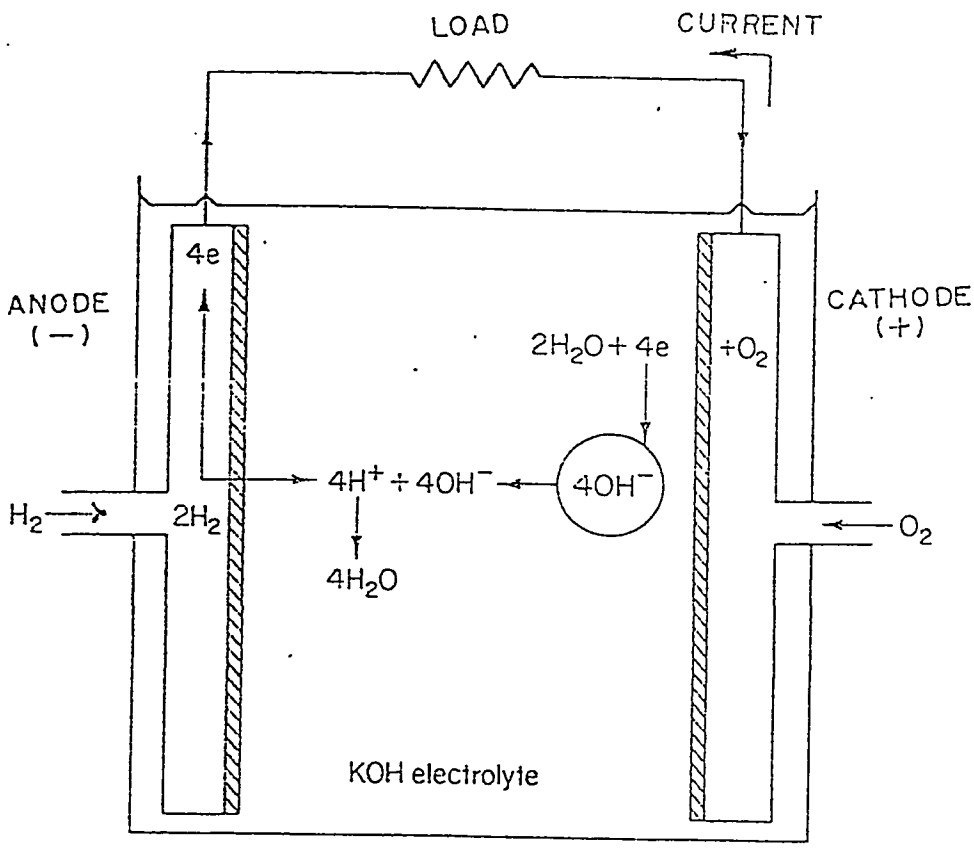

Fig. 1.1 Schematic Representation of a Fuel Cell

usually connected in series or in parallel to obtain higher voltages or currents. Such an arrangement is called a fuel cell stack.

1.2 Advantages and Disadvantages of fuel cells

Fuel cell operation is not dependent on flow of heat between sources and sinks hence it is not subject to Carnot limitations. In fuel cells 100% efficiency can be approached through appropriate design. Because of high thermodynamic effeciency, energy produced per unit weight is relatively high.(3)

Besides high energy production of electrical energy, the fuel cell has several other advantages. There are no moving parts involved so no friction losses. Atmospheric pollutants produced are minimal(4). The operation of a fuel cell is quite simple and reliable.

Within broad limits, effeciency of a fuel cell is independent of size. Therefore smaller modular units could be installed in areas of high electrical demand. This results in decreased in power line investment and transmission losses. Waste heat from fuel cell can be used for space heating ,raising steam . The combined efficiency for electricity and heat production can be as high as 98%.(5)

The disadvantages of fuel cell include actual efficiency, reliability and overall cost. Sources of irreversible behavior such as ohmic losses and sluggish kinetics limit fuel cell efficiency below 50% . The specific power obtained from a fuel cell is very low. Other disadvantages of fuel cell include larger weight and volume of gas fuel storage system, liquification expenses for the fuel, cleaning requirements for the reactants ,deactivation of electrode catalyst etc.(6)

1.3 Applications of Fuel Cells

The major applications of fuel cells can be divided into Remote power, Portable power and Electric utility applications(7). Table 1.1 gives potential fuel cell applications. Remote power applications include space missions, submarine applications, navigational aids, automated weather stations remote beacons, pipeline cathodic protection systems and communication system. Portable power applications are mostly for military purposes. Electric utility applications could further be classified as (a)on-site power plants (40-400kW) close to the point of energy demands,(b)electric utility power plants (5-50MW) located at utility substations with the option of the waste thermal energy being used for commercial heating,(c)electric utility power plants (100-500 MW)located at large central stations. Other possible applications of fuel cells could be to power electric vehicles and emergency power supply.(7,8)

At present very few of this applications are commercialised. With the advancement of technology in future these applications will become economically viable.(9)

1.4 Classification of Fuel Cells

Fuel cells can be configured in many ways with a variety of electrolytes,electrodes, fuels, operating temperatures and catalyst involved. Fuel cells are generally classified according to electrolyte type, since the electrolyte limits the operating temperature range and together these tend to define the fuel option. Table 1.2 gives classification of fuel cells based on electrolyte (10).

Table 1.2 Fuel Cell Classification Based On Electrolyte

Electrolyte	Operating temperature (°C)	Fuel	Oxidant
Aqueous acid		Hydrogen	Air, O_2 (pure)
Phosphoric acid	150–220	Indirect methanol, hydrocarbon, coal	Indirect H_2O_2
Solid polymer	<100		
Aqueous alkaline	<260[a]	Hydrogen, hydrazine	O_2 (pure)
		Indirect ammonia	Indirect H_2O_2
Molten carbonate salt	600–700	Direct methane or methanol	Air[b]
		Indirect methanol, hydrocarbon, coal	
Solid oxide	1000–1100	Hydrogen	Air
		Direct methane or methanol	
		Indirect methanol, hydrocarbon, coal	

[a] For long life with inexpensive materials, temperatures are limited to less than 100°C.
[b] Also requires CO_2 to complete cathode reaction.

Table 1.1 Possible Applications of Fuel Cells

Application	Efficiency		Emissions/noise		Cost
	Weight/volume	Fuel cost	Environmental	Detectability	
Remote					
Space	2	3	3	3	3
Submarine	1–2	2	3	2	2–3
Portable					
Military	1–2	3	3	2	2–3
Recreational	3	2	3	3	1
Utility					
Small (<1 MW)	3	2	2	3	1–2
Large	3	2	2	3	2
Other					
Emergency	3	3	2	3	1
Transportation	1	2	2	3	1

[a] 1, Very important, difficult to achieve targets.
2, Very important, targets achievable.
3, Relatively unimportant (compared with other requirements).

1.5 H_2 /O_2 Alkaline Electrolyte Fuel Cell(AFC)

Alkaline electrolyte fuel cells can be operated at much lower temperatures(<120^0 C) using less concentrated alkali (usually 25-30 % KOH). The lower temperature helps in retaining the electrolyte on matrices and also increases the life of other components.(11)

The advantages of AFC are higher performance and reduced cost. The major disadvantage is the degradation of electrolyte caused by CO_2,CO present in air or in fuel gas. The removal of CO_2,CO gas results in decrease in efficiency of an alkaline fuel cell.(12)

In this thesis work the electrolyte used is KOH in the temperature range 25^{0}C to 75^0 C. In a H_2/O_2 alkaline fuel cell the reactions taking place on the anode and cathode are as follows (9),

$$H_2(g)+2OH^-(aq) = 2H_2O(l)+2e^- \quad \text{Anodic reaction}$$

$$0.5\ O_2(g)+H_2O(l)+2e^- = 2OH^-(aq) \quad \text{Cathodic reaction}$$

$$H_2(g)+0.5\ O_2(g) = H_2O(l) \quad \text{Overall reaction}$$

1.6 Fuel Cell Electrodes

A good electrode structure must be able to bring gas and electrolyte together so that the reaction can be easy and fast and must be able to keep them apart to prevent undesirable mass transfer e.g. bubbling, floating, weeping. Bringing gas and electrolyte with maximum effectiveness requires an enlarged surface and a porous structure(13). Typical gas diffusion electrodes involve 3 phases namely gas, electrolyte and catalyst. A gas diffusion electrode for a liquid electrolyte contains several layers frequently a backing layer or gas diffusion layer, an electrocatalyst layer and a conducting grid or perforated metal foil for support and current conduction. The gas diffusion layer serves as a barrier between the electrolyte and the gas phase. In the gas-diffusion electrode, reactant gas is supplied to the active sites of the electrode by a diffusion process thereby producing higher current densities(14).

Platinum group metals(usually Pt, Ag, Ni) are important electrocatalysts used for alkaline fuel cell electrodes. In alkaline fuel cells Raney-Ni is commonly used as the catalyst in the anode section while Raney-Ag is used in the cathode section(9).

1.7 Over Potential Concept

The flow of electric current through a fuel cell changes the potential of the electrode from its equilibrium value. This is called polarization. The difference between polarization potential E_p,and equilibrium potential E_r both with respect to the same reference electrode is known as the overvoltage of the electrode. The overvoltage is represented by the symbol η at a given current density.

Thus

$$\eta = E_p - E_r \tag{1.1}$$

If the cathode is polarized then it is called cathodic polarization and it is given a negative sign. In the opposite case of anodic polarization ,anodic overvoltage is positive.

The overvoltage represents efficiency loss in an electrochemical device. The polarization losses(fig. 1.2) include the following(11),

1. Activation Polarization This represents energy losses associated with the electrode reactions. For electrochemical reactions the activation energy lost in overcoming the energy barrier takes the form

$$\eta_{act} = a + b\ln i \tag{1.2}$$

Where η_{act} is the activation polarization, a, b are constants and i is the current density.

2. Ohmic polarization It represents the summation of all the ohmic losses within the cell ,including electronic impedances through electrodes ,contacts, and current collectors and ionic impedances through the electrolyte. These losses follow ohms law (V = IR).

3. Concentration polarization It represents the energy losses associated with mass transfer effects. For example the performance of an electrode reaction may

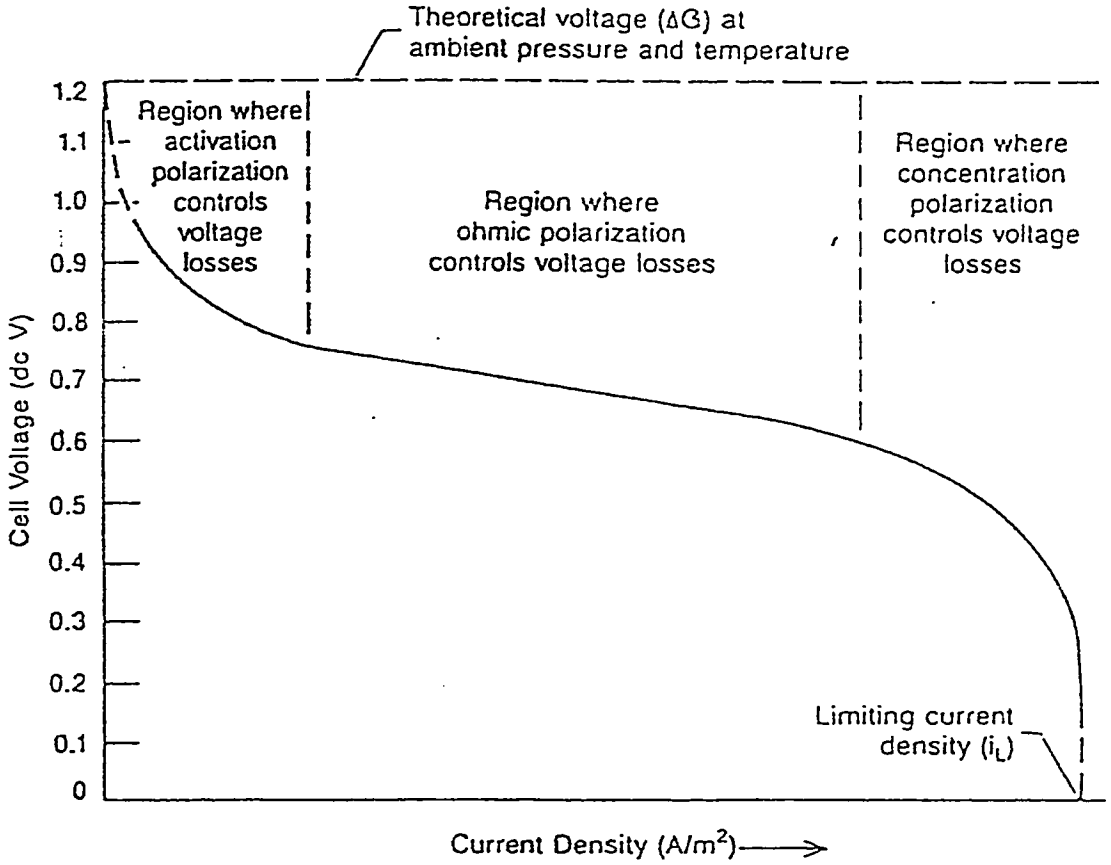

Fig. 1.1 Typical Plot of Cell Potential and Current

be inhibited by the inability of the reactants to diffuse toward, or of products to diffuse away from, the reaction site. In fact at some current, the limiting current density i_L where the current is completely limited by the diffusion process(see fig 1.2).

The performance of a fuel cell is given by the following equation

$$E=E_r-\eta_{c,act}-\eta_{a,act}-\eta_{c,con}-\eta_{a,con}-IR_i \qquad (1.4)$$

Where Er is the reversible potential ,$\eta_{act}$and η_{conc} terms represent the activation and concentration overpotential at the corresponding electrodes and IR is the ohmic overpotential.

At temperatures below 200^{0}C activation overpotential is the main cause of efficiency losses in fuel cells. The hydrogen overpotential is low compared to oxygen overpotential in acid as well as in alkaline electrolyte fuel cells. Therefore oxygen overpotential is responsible for the departure of the cell potential from the reversible value at desired current densities.

1.8 Objectives

The research objectives of this dissertation are as follows

1) Testing the operability of the equipment and electronic instruments involved.
2) Reproducing the steady state polarization behavior of Ni/PTFE gas diffusion electrode used by Celikar(15) at 35^{0}C and 55^{0}C.

3) Investigating the steady state polarization behavior of a new Ni/PTFE gas diffusion electrode in the temperature range of 25^{0}C -75^{0}C with pure hydrogen gas in a half cell setup.

4) Investigating the long term performance of this new Raney Ni/PTFE electrode.

5) Characterization of the fresh and used electrodes by SEM, ICP-AES, BET surface area measurement.

6) Determination of exchange current density, charge transfer coefficient by the application of mathematical model developed earlier by Celikar et al.(15).

7) Determination of the apparent activation energies for the electrochemical reaction taking place on the electrode.

8) Determination of the apparent and intrinsic deactivation constants at various temperatures.

Chapter 2

LITERATURE REVIEW ON H_2 ELECTRODE

The maximum power density obtained from alkaline fuel cells has undergone many advances in recent years due to improved catalyst and electrode materials, and also due to operating conditions and fuel cell design. Theoretical understanding of the electrochemical reactions taking place at the catalyst surface and the influence of electrode structure has improved in recent years(16). Despite all these advances the production of fuel cell electrode is more of an art than a scientifically well founded process.

Kordesh(17) has given a comprehensive review of fuel cell developments during the period 1951-1976. Bacon(18) first produced a biporous electrode with a stable meniscus to be used as an anode in a H_2/O_2 fuel cell. In Bacon`s biporous electrode the coarse pore layer is for the gas side and the fine pore layer is for the electrolyte side.

Double skeleton(DSK) electrodes are developed by pressing and sintering carbonyl nickel powder with Raney nickel powder. DSK electrodes were first produced in former West Germany. DSK electrodes have high catalytic activity of Raney powder and the mechanical rigidity and electrical conductivity of bulk metals. DSK Bacon electrodes were made entirely of the electrocatalyst.

Most of the porous electrodes employed in fuel cell research are produced by deposition of the catalyst on a substrate. A typical porous fuel cell

electrode consists of a metal screen, elecrtocatalyst, catalyst support and the binder(19). In alkaline fuel cells for anode mostly Ni, Cu screens are used while PTFE is used as a binder.

In H_2/O_2 alkaline fuel cell Raney-Ni alloy is used for hydrogen electrode and Raney-Ag alloy for oxygen electrode. Aluminum present in the alloy is leached out by using caustic solutions. So far in the open literature only one paper describes the method of fuel cell electrode preparation.(20).

Mund et all.(21) used 5 % titanium containing Raney-nickel catalyst which showed superior performance from Electrocatalytic activity and stability point of view. The catalyst layer in the electrode was supported by asbestos covering layer on the electrolyte side and by a metal screen on the gas side. They have measured the polarization resistance as a function of catalyst loading and studied the influence of electrolyte temperature on polarization behavior. Impedance measurements have also been used to characterize the electrodes.

Ewe et. all(22) studied the preservation of Raney-nickel and of various blended Raney-nickel catalyst by slow oxidation of samples in atmospheric oxygen followed by controlled heat treatment and reduction. They have found that undoped 1% Ti alloyed Raney nickel gave the best current voltage performance. Catalyst doped with Fe or Mo have been observed to deteriorate under preservation. The method of preservation is useful when it causes a strong increase of exchange current density with insignificant decrease of surface diffusion.

Tomido and Nakabayash(23) .prepared hydrogen electrodes of fuel cell by an innovative method. They sprayed molten aluminum by an acetylene-oxygen

flame gun on both sides of a spongy plate of nickel as substrate. The spongy nickel electrodes were activated by alloying at 50°C to 75° C and leaching the aluminum from the alloy in alkaline solution. With the experimental results they concluded that spongy Raney nickel electrode have very low polarization resistance.

The influence of contact pressure on the performance of supported gas diffusion electrodes in alkaline H_2/O_2 fuel cells has been studied by Ewe et.all(24). A half cell assembly with variable contact pressure facility is constructed and used to measure the polarization of Raney-Ni and Raney-Ag electrodes as a function of contact pressure in KOH electrolyte. They have found that the current densities at constant polarization are increased significantly by the optimization of the contact pressure.

Ewe et. all (25) found that the catalytic properties of Ti doped by Raney Ni (for hydrogen anodes of alkaline fuel cells)could be improved by $Ni(OH)_2$ surface coating which is obtained by carefully optimized oxidation. It is observed that $Ni(OH)_2$ content of 5-6 % increased the attainable current density by a factor of 3 to 4. Also it is observed that the exchange current densities increased significantly up to a $Ni(OH)_2$ content of 5 % but remained constant with further increasing the $Ni(OH)_2$ percentage. As a continuation of this study it has also been shown that oxide surface coating may be stabilized by an annealing of the slowly air oxidized and $Ni(OH)_2$ coated catalyst in hydrogen at 35°C, followed by an air oxidation again(26). It is observed that the formed mixture of NiO and $Ni(OH)_2$ coated improved the catalytic properties and structure. The optimum annealing parameters were determined. The experiments were carried out using a Ti-containing Raney-Ni as catalyst with 6M KOH electrolyte operating at 80°C.

In a following study ,Ewe et.all(27)studied the aging rate of annealed catalyst which was found to be very small at polarization below a critical value of 50mV. Aging rates increased exponentially when polarization was above 50mV. The best catalyst with the lowest aging rate under μV/hr was prepared by using a Raney-Ni(containing 2 % Ti)catalyst with 4-6% initial $Ni(OH)_2$ content, which was heat treated in hydrogen atmosphere at 35^{0}C for 5 minutes. Brennecke et.all (28) studied the kinetics of the electrodes used by Ewe (24,25)by means of impedance measurements. A sine wave generator and a potentiometer regulator was used in the measurements.

Kenjo(29)used a PTFE bonded Raney Ni hydrogen electrode prepared by milling a PTFE dispersion with caustic -leached Raney metal with subsequent calendar rolling of the electrode paste into sheets. The electrode polarization were measured in 6M KOH electrolyte at 62^0 C. The influence of the pressure of the press machine and of the PTFE content on the polarization have been investigated. The polarization resistance as a function of catalyst loading is also determined. It was observed that the polarization resistance decreases with the catalyst loading in the manner to be expected from the reaction mechanism of the gas diffusion through electrolyte film.

Kenjo and Nakajima(30)measured the polarization characteristics of PTFE bonded Raney-Ni hydrogen electrode as a function of the catalyst layer. The polarization curve of the electrode was analyzed based on the electrolyte film. With the thickening of the catalyst layer the performance of the electrodes approached asymptotically to an upper limit. The catalytic activities of Raney-Ni catalysts are enhanced with progression of the polarization while the resistivity of

the electrolyte film remains essentially constant. A slight surface oxidation for the Raney-Ni is understood to be responsible for the enhanced catalytic activities.

Canday and Foilloux (31) used a passivated Raney powder which is mixed with a slurry of PTFE(85.5 % and 12.5% respectively)and sprayed into nickel-grid support. The wafer obtained is heated to sinter the fluorinated plastic which acts as a binder. They also prepared another electrode where the water repelling effect was obtained by charcoal particles with fluorinated oil. The binding material in this case was polyvinylidine fluoride. The electrode was characterized in 5M KOH by using an impedance technique.

Markina et. all (32) prepared a $NiCO_2O_4$ electrode(nickel -cobalt spinels) by thermal decomposition of a mixture of nickel hydroxide and cobalt hydroxide. Moren (33) developed a cell for determining structure parameters such as interstice tortuosity, film tortuosity, effective specific film resistance, effective pore length ,mean film thickness, and film area on operating porous gas diffusion electrodes. Ni electrodes and 5M KOH solution were used in the experiments.

Padyukova(34) studied the state of hydrogen in a Raney-Ni catalyst prepared from Ni-Al alloys(40 -60 mass % Ni) having different degrees of dispersion by using thermal desorption and potentiodynamic measurements. It was found that the composition of the Ni-Al alloys and their particle size have important influence on the adsorption behavior of the Raney-Ni.

Kenjo(35) found that the tenth percent of chromium markedly enhances and stabilizes the activity of Raney-Ni. Hydrogen electrodes catalyzed with chromium dope are prepared and their polarization characteristics are measured. It

was found that the chromium doped Raney Ni was more active than the Titanium-doped catalyst and it provided a high activity over a wide range of the dopant content.

Mund et. all(36)prepared Raney-Ni electrodes which contained 2% Ti. The Raney catalyst powder obtained from Raney alloy had a BET area of 80 m^2/g . A mean pore radius of 2×10^{-7} cm is found in the catalyst particles. They have found that the steady state current voltage characteristics of supported Raney-Ni hydrogen anodes are linear up to a polarization of 0.1V in 6M KOH as electrolyte. The influence of the electrolyte temperature on the current -voltage relation is also studied with a catalyst loading of 0.1 g/cm^2.The influence of the electrolyte concentration on polarization is drastic and observed to lead in diluted alkali to limiting current behaviour. Impedance characteristics were also studied.

Pattabiraman et.all(37)studied the preparation and polarization characteristics of hydrogen and oxygen gas diffusion electrodes for use in low temperature alkaline fuel cells. The electrodes they fabricated had a geometric surface area of 30 cm^2 and employed skeletal Ni obtained from Ni-Al alloy containing Ti promoter as electrocatalyst for hydrogen electrode. The hydrogen electrode was found to show a high polarization beyond 30 mA/cm^2.

Grune(38)studied the dynamic behavior of porous gas diffusion electrodes in fuel cells. In this study all measurements were carried out in a half cell with electrodes having 1cm^2 external surface area ,using 6M KOH as electrolyte at 80^0C.

Abramazon et. all(39)developed a technique to determine the specific activity of disperse Ni catalysts. The specific activity of the type of Nickel catalyst examined is practically independent of the way of preparation.

Jenset et. all(20) have given the production steps of Raney-Ni based PTFE bonded hydrogen anodes for lightweight alkaline fuel cells. The Raney-Ni catalyst has been made by leaching the Ni-Al alloy and additional stabilisation. The electrode is fabricated by mixing the catalyst with copper oxide for enhancing the electronic conductivity and aqueous PTFE emulsion as hydrophobic binder. Based on the experimental findings they concluded that a load of approximately 8-9% PTFE and 15 weight % copper gives optimal performance. They showed that at an overpotential of 100mV the optimized hydrogen anode exhibits at negligible excess hydrogen pressure(1.02 bar)a current density of nearly 400 mA/cm^2 at 80^0C in 30 weight % KOH. They also showed the long term performance of the electrode.

Chapter 3

ELECTRODE KINETICS AND ELECTROCATALYSIS

3.1 Introduction

The real efficiency of an electrochemical energy producing device such as an AFC depends upon the power per unit weight. The power per unit weight also depends on the rate of electrochemical reaction taking place at the elecrode. Thus electrode kinetics determines the real efficiency of an AFC.

Electrocatalysis is the enhancement of a particular electrode reaction by the appropriate choice of electrode material. The Electrocatalytic reaction depends upon the nature of the electrode, presence of an electric field across the electrode-electrolyte interface and nature of the electrolyte. Electrocatalyst is a material which makes electrode reaction cost effective.

3.2 Current-Potential relation at a single Electrode

The reaction rate in electrode kinetics is measured by the current density at the electrode. Thus the current across 1 cm^2 of electrode surface gives the reaction rate. By Faraday's law the reaction rate is(40)

$$r = \text{reaction rate in mole sec}^{-1} = -\frac{dz}{dt} = \frac{I}{nF}$$

and per 1 cm^2 of the electrode of area A, the reaction rate is

$$r = \frac{I}{AnF} = \frac{i}{nF} \tag{3.1}$$

Thus the current density is a direct measure of the reaction rate.

Consider the following electrochemical reaction

$R^+ + e^- \rightarrow$ Rads$\rightarrow\rightarrow\rightarrow$----------pP

Let the first reaction which is charge transfer step be rate determining. In this case the relation of the electrode potential to the current is given by(41)

$$i = i_o[\exp\{\frac{\alpha F\eta}{RT}\} - \exp\{-\frac{(1-\alpha)F\eta}{RT}\}] \tag{3.2}$$

Equation 3.2 is called the Butler-Volmer relation. It is a standard model that describes the current - overpotential relationship for an electrode at a given temperature, pressure and concentration of reacting species.

If the overpotential is large and positive, then the first exponential term in equation 3.2 is much larger than the second term. In this case of large anodic polarization the equation 3.2 simplifies to

$$i = i_o \exp(\frac{\alpha\eta}{RT}) \tag{3.3}$$

where i_o is the exchange current density ,α is transfer coefficient and η is overpotential.

It is remarkable to note that for a change in overpotential by 0.5 V ,the reaction rate changes by 4 to 8 orders of magnitude. Elecrocatalysis is the science of minimizing the overpotential terms given by equation 3.3.

Equation 3.3 can also be written as

$$\eta = a + b\ln i \qquad (3.4)$$

expression 3.4 is called the Tafel equation. The Tafel parameters are characteristics of the electrode and are obtained experimentally from a plot of η Vs logi.

In the case of small overpotential($|\eta| < RT/F$) the Butler-Volmer equation can be linearised as

$$i = \frac{2i_o \alpha F \eta}{RT} \qquad (3.5)$$

3.3 Electrocatalysts

Electrocatalysts are selected or designed for each electrode reaction from a knowledge of the chemical and structural properties of potential catalyst materials. If the mechanism of the same overall reaction is different on various substrates. Then depending on the value of overpotential ,one or other is a better substrate from the practical point of view. Owing to a different mechanism of the reaction resulting in transfer coefficient α being different.(42)

Factors which determine Electrocatalytic activity are as follows(43)

1) Chemical composition of the Catalyst

Electrocatalysts are always based on transition metal atoms or ions. Therefore the design of an electrocatalyst requires the placing of the transition metal in a matrix which optimizes unpaired electron density and the spacing of transition metal centers. For transition metal species unpaired d-electrons and unfilled d-orbitals are available for forming bonds with adsorbates. The catalyst is most effective when the bond is of intermediate strength. Geometric arrangement of the catalyst centers is also important. The geometric and electronic factors are dependent on each other. Together they decide the relationship between the catalytic activity and chemical composition.

2) Real surface area

The current density for an electrode can be increased by deliberately creating a rough surface. By making electrode surface rough the area available for electrochemical reaction is greatly increased as compared to planar surface.

3) The catalyst support

Commonly electrocatalysts are expensive and are therefore prepared either in the form of small particles dispersed on a cheaper substrate or as a thin layer.

4)Catalyst structure on an atomic scale

Size and shape of small centers the presence of grain boundaries ,lattice defects and special sites e.g. kinks, edges or screw dislocation also determine Electrocatalytic activity.

A good electrocatalyst should have

a) High exchange current density and /or

b) A low Tafel slope.

c) A tendency to inhibit side reactions.

d)Stability

3.4 Design of Electrodes

Any practical electrode should have high activity for the desired reaction which is stable over a long period of time. This generally means the ability to deliver a current-density of 0.1-1 A cm^2 at an acceptable overpotential of less than 100mV and this performance must be maintained for the service interval of the cell. The requirements for light weight AFC are as follows,

1. Operating Temperature should be less than 100°C
2. Operating pressure should be less than 4 atm.
3. Insensitivity to impurities in feed gas.
4. O.C.V. should be at least 90 % of reversible E.M.F.
5. High Exchange current density, limiting current density
6. Low overvoltage
7. High gas consumption efficiency i.e. maximum conversion of feed gas
8. High performance at operating load
9. Inexpensive
10. Sufficient life time

Factors which lead to the loss of electrode activity are

1)Mechanical erosion or damage during servicing or handling.

2)Corrosion in the electrolysis medium either when the cell is on load or standing on open circuit.

3)Poisoning by side reactions or adsorption of an impurity from the electrolyte medium.

4)Re crystallization leads to loss in surface area.

The electrode material must show the desired selectivity. In practice the selectivity is based on kinetics rather than thermodynamics.

The electrodes used in AFC are porous in structure. The porous electrode is made by compressing onto a conducting grid a mixture of the catalyst, a conducting powder and a hydrophobic material e.g. PTFE. The gas is then passed over the back of the electrode so that a three phase interface between gas ,electrolyte and catalyst is formed within the pores.

Gas consuming porous AFC electrodes have a triple layered structure. The active electrode surface constitutes the primary(chemical) structure of the active electrode surface. The secondary structure consisting of the inner surface of the catalyst or its support is determined by the fine porosity(dp = 1-10 nm).The third structure is the intermeshed dual system of coarser pores (dp >5μm) between the catalyst particles one part of which is hydrophobic and conducts the gases into fuel cell electrode supplying the electrode wetted catalyst -particles with gas, whereas the second ,hydrophilic pore system containing the electrolyte enables the passage of ionic currents towards the counter electrode.(16)

3.5 Electrode study Techniques

Steady state and unsteady state techniques are used for the study of fuel cell electrodes(44). Table 3.1 gives the various techniques that are commonly employed in fuel cell electrode research. Any change in one of the variables e.g. pressure, temperature, concentration etc. in an electrochemical reaction will cause a time dependent change on other variable. All these variables reach a steady state after a certain period of time. Steady state electrochemical techniques are used to

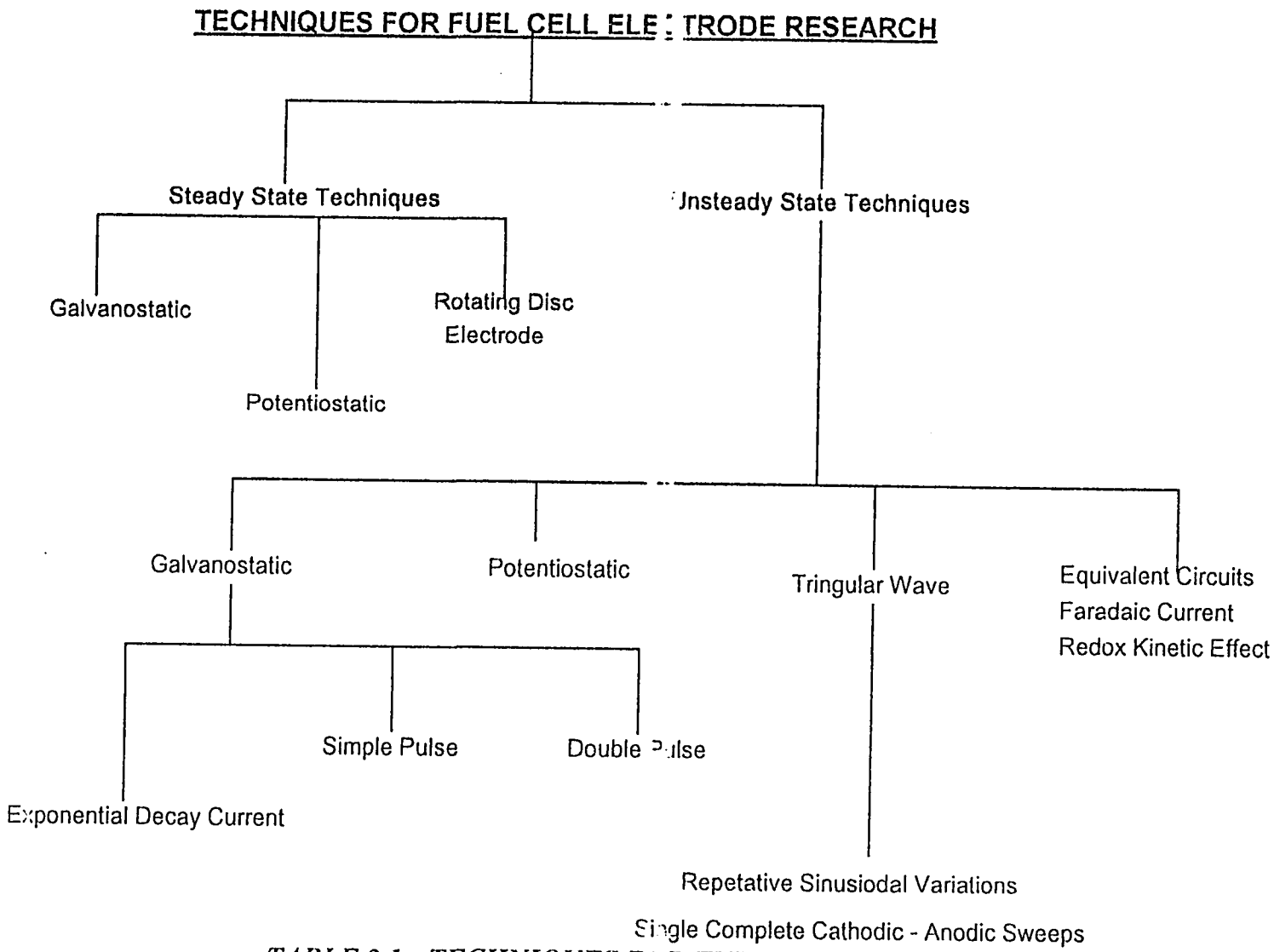

TABLE 3.1 : TECHNIQUES FOR FUEL CELL ELECTRODE RESEARCH

study the functional relationship between variables. Polarization curves(current density Vs potential curves)provide useful information on suitable working potentials, possible current densities and current efficiencies. Steady state polarization curves are utilized to get kinetic information on the overall reaction, reaction orders and to determine charge transfer coefficents, exchange current densities and limiting current densities.

In steady state technique there are again two methods namely galvanostatic and potentiostatic. In galvanostatic method the electrochemical reaction is forced to proceed at a chosen rate by keeping the current flow constant. In this method the current required is changed in steps through a galvanostat and the corresponding potential at the working electrode is measured against a reference electrode under steady state conditions.

In potentiostatic method a potentiostat is used to keep the potential between the working and reference electrode constant at a chosen value by allowing a passage of current through the working and counter electrode. The required voltage values are then changed in steps and each time corresponding current is allowed to come to steady state.

In a non deactivating system ,under steady state conditions the galvanostatic and potentiostatic polarization techniques gives same results. In this work galvanostatic method is used to investigate the performance of specially prepared Raney-Ni hydrogen electrode for AFC.

Unsteady state techniques are used to get double layer capacity, adsorption coverage ,diffusion coefficients etc.

3.6 Importance of Half Cell Studies

Half cell measurements give information about the magnitude of activation, concentration and ohmic polarization occurring in each electrode. The ohmic polarization is measured separately by IR drop measurement techniques. The activation and ohmic polarization are isolated by analyzing the polarization curves. Using a half cell, the reaction at each electrode is studied separately. In this case current is supplied from an external source to the working electrode. The overall reaction taking place in a half cell is different from that occurring in complete cell. A schematic diagram of the half cell used in this study is given in Fig. 3.1.

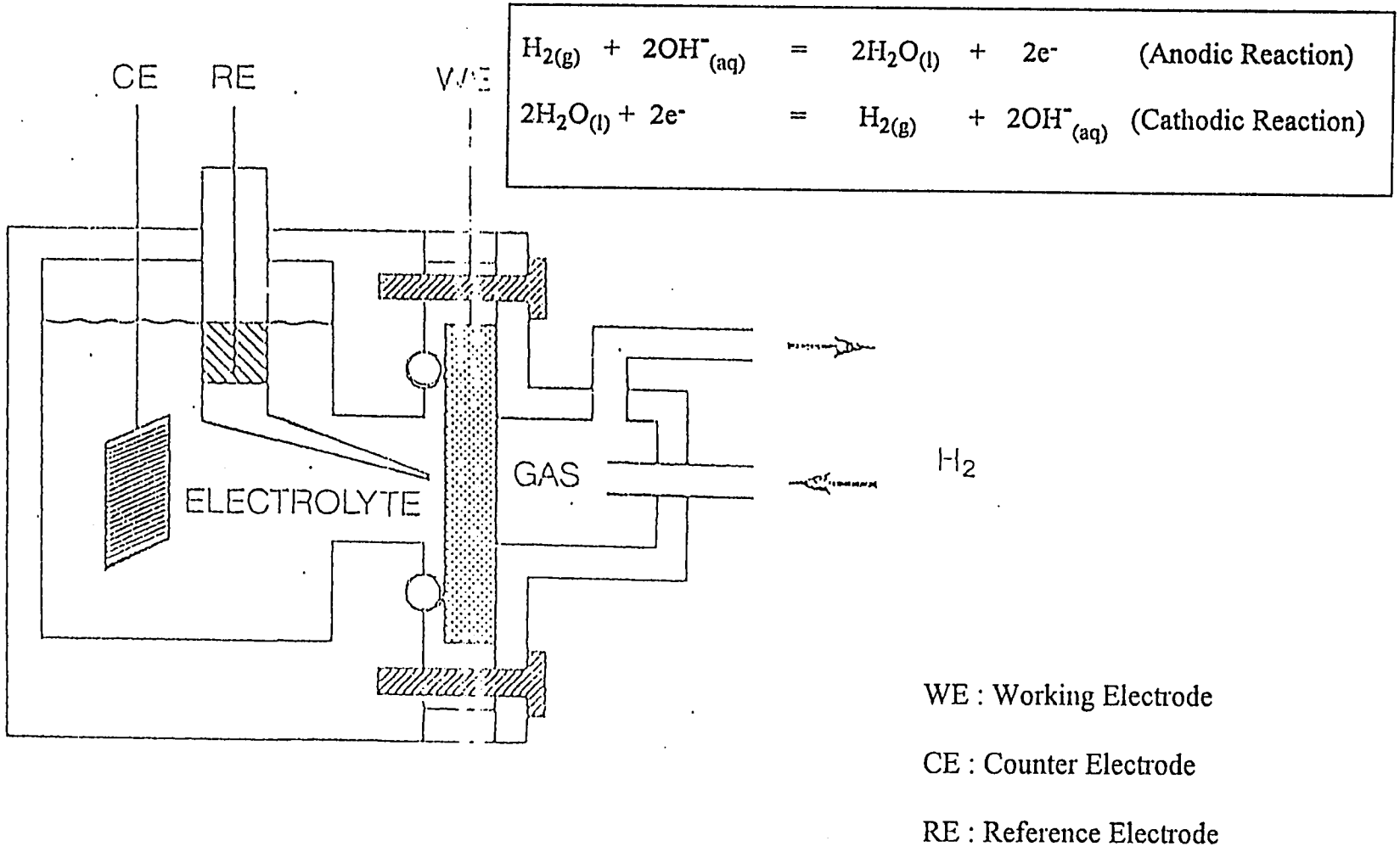

Fig. 3.1 Schematic Representation of a Hydrogen Half Cell

Chapter 4

REVIEW OF MATHEMATICAL MODELS FOR POROUS FUEL CELL ELECTRODES

In order to increase the power density in alkaline fuel cell the activation, concentration and ohmic polarization should be made as small as possible. In order to determine the polarization behavior of electrodes numerous and expensive tests need to be performed. Moreover, the interaction among the three types of polarization causes difficulties in isolating the characteristics of a particular type of polarization. Mathematical models of AFC electrodes can help in determining how changes in parameters and operating conditions affect the various types of polarization , which subsequently influence the performance of a fuel cell.

The AFC electrode models can help in identifying the parameters and concepts that limit the performance of the fuel cell based on today's state -of-the art technology. The mathematical model can also be used to investigate the effect of hypothetical advances in technology on the predicted performance.

The exact theoretical analysis of porous electrode is difficult to carry out because of the following reasons ,

(1) Precise knowledge of the structural details of electrode is unavailable.

(2) Non-linear multidimensional and coupled equations describing the mass transport and partial distributions.

(3) Difficulties encountered in defining the three phase boundaries.

Because of these problems idealizations of various types have been used in the modeling. Thus in the literature there are many models due to diversified design of porous gas diffusion electrodes, controlling factors and operating regimes(42). The models which are mostly used for the description of current-potential relation are the following:

1. Simple Pore Model
2. Thin Film and Meniscus Models
3. Hydrophobic Electrode Models
4. Hydrophilic Electrode Models
5. Cylindrical Gas Pore Model
6. Flooded Agglomerate Model

In the simple pore model developed by Austin et.all (45) it is assumed that the reactant gas diffuses into the pores, dissolves in the electrolyte and further diffuses in solution to reach the catalytic sites where the three-phase boundary of solid -liquid-gas comes into contact.

Experiments with partially submerged electrodes show that the electrode reaction occurs mainly in a region where the electrolyte forms a thin meniscus and a film at the electrode-gas interface. This film helps in molecular diffusion of the gaseous reactant through the thin film of the electrolyte. This is the basis of Thin film and Meniscus model.(46)

Hydrophobic electrode models can be classified into three basic types(47). In the first type hydrophobic gas pores are formed by agglomerates of PTFE in a hydrophilic medium consisting of catalyst particles separated by the

electrolyte. In the second type hydrophobic pores are formed by agglomerates of catalyst located in a hydrophobic medium consisting of PTFE particles with the space occupied by the gas. In the third type the contact angle at the boundary of the liquid is determined by PTFE concentration at the surface of gas pores .The activity of hydrophobic electrode is determined not only by the pressure difference but by the hydrophobizer concentration. The polarization distribution in the electrode is determined by solving differential equations which involve a probability factor of the position of PTFE grains in crystal lattices.

Hydrophilic electrode models include dual porosity models and the models of intersecting capillaries. The dual porosity model treats a porous electrode as containing both wide and narrow pores. The wide pores are filled with gas but their walls are covered with a solution film, and the narrow ones are flooded. Models of intersecting capillaries assumes that the current generation is localized in the neighborhood of intersection of pores.(48)

The pressure differential between the gas and electrolyte solution determines the distribution of gas and liquid and the electrochemical activity of hydrophobic electrodes. The performance characteristics of hydrophobized electrodes depend upon the degree of hydrophobization. The Cylindrical gas pore model was proposed to explain the fact that as Teflon concentration is increased the electrochemical activity goes through a maximum.

In the cylindrical gas pore model suggested by Burshtein et.all (49) and Chirkov(50) gas filled pores are assumed to be circular cylinders of constant radius. These cylinders are assumed to be arranged in a regular manner with walls composed of a mixture of PTFE and catalyst moistened with the electrolyte.

Lampinen, M. J. and Viitanen, M. (51) have proposed a mathematical model in which the agglomerates of catalytic particles are described as cylinders whose axes are perpendicular to the surface of the electrode. The model takes into account the diffusion of gas, the electrochemical reaction taking place, ionic ohmic drop in the cylinder and also electronic ohmic drop due to the finite conductivity of solid materials. The structure of fuel cell electrode can be optimized by this model.

In the agglomerate model the catalyst particles and liquid filled pores coexist in a homogeneous continuum surrounded by the gaseous species. Giner's(52) model accounts for the diffusion of a dissolved gaseous species with electrochemical reaction in a cylindrical agglomerate and considers the variation in the solution phase potential. The model doesn't take into consideration the gas phase and solid phase resistances. The Giner`s model predicts the performance of the electrode as a function of agglomerate radius and catalyst utilization for low current density. Cutlip's analytical model (53) considers mass-transport process occurring in gas diffusion electrodes. In this model catalyst effectiveness factors are used to modify the electrocatalyst based on different shape factors. Cutlips model predicts that the coupling of the gas-phase diffusional resistance and electrode thickness strongly influence the limiting current density.

Iczkowski and Cutlip (54) proposed a fairly complete model of a three-phase electrode. This model accounts for the gaseous diffusion resistance ,solution phase diffusional resistances, and solid and liquid potential variations. Based on this model they suggested that the gas diffusion resistance is about 38% and ohmic loss in the electrolyte contributes 48% of the total voltage drop in fuel cell cathode.

Celikar et. all (55) have proposed flooded Raney catalyst grain model to describe the working mechanism of PTFE - bonded Raney catalyst gas diffusion electrodes. In this model Raney metal catalyst grains in the electrode are considered to be spherical in shape and flooded with electrolyte during operation and are surrounded by hydrophobic gas pores. Analytical equations are derived to evaluate the performance of a single catalyst grain in the presence of diffusion limitations. The current generation expression for each grain is then combined with the potential distribution differential equation to predict the complete electrode performance. The radial degree of utilization of the spherical grains for current generation and also the degree of utilization of the whole electrode in the axial direction can be investigated by the model equations. This model predicts the polarization behavior in terms of experimentally measurable properties e.g. porosity's, current density, potential catalyst loading, electrode thickness.

Kimble and White(56) have for the first time proposed a complete mathematical model of an alkaline fuel cell that contains both the electrodes and the separator. This model assumes a macro homogeneous, three phase electrode structure to describe the processes occurring in the solid, liquid, and gaseous phases of the anode, separator and cathode regions. This model accounts for the one-dimensional transport of reactant gases, water vapor, solution phase concentrations, solid and solution potential variations, and the volume - average velocity. Limitations to attain high power densities are given and methods to increase the maximum attainable power density are suggested based on the model.

In a following paper Kimble and White (57) have carried out parameter sensitivity and optimal design analysis for a hydrogen/oxygen alkaline fuel cell. The optimal electrode thicknesses for the anode and cathode reaction layers and

the gas and liquid phase porosity in the cathode reaction layer are determined by maximizing the power density. Based on the model prediction the authors suggest a significant improvement in the fuel cell performance can be achieved by increasing the gas - liquid interfacial area followed by increasing the Electrocatalytic activity and decreasing the separator thickness.

Yang and Bjornbom (58) have developed a mathematical model for alkaline fuel cell cathode by using concentrated solution transport theory. The model assumes an electrode with two layers: gas supply layer and reaction - active catalyst layer. Application of this model is useful in understanding humidity content management during electrode operation.

Chapter 5
ELECTRODE MANUFACTURE AND CHARACTERISTICS

5.1 Manufacture of Hydrogen Anodes

At present production of fuel cell electrode requires experience and a very good knowledge of material properties. As the volume of research in this area is increasing electrode manufacture will become a scientifically well founded process.

For the production of hydrogen anodes from Raney-nickel for lightweight akaline fuel cell pulverized aluminum-nickel alloys are taken. These alloys are then leached with KOH solution to remove aluminum. This leaching process results in a highly porous structure. Large amounts of adsorbed hydrogen is found in freshly leached Raney nickel. This adsorbed hydrogen is then removed by slow and controlled oxidation before further processing the material.

Polytetrafluorethylene(PTFE) in powder or aqueous emulsion form is used as a binder in AFC electrode manufacture. This PTFE binder provides cohesion between the catalyst particles and firm mechanical contact of the catalyst with the supporting metal screen. The hydrophobic material for the gas conducting pore system is also provided by PTFE.

The depyrophorised and thermally stabilized catalyst and PTFE powder is then intensively blade-milled. This through mixing produces a fluffy mass by which the catalyst and PTFE particles become indistinguishable from each other. This mixture of catalyst and PTFE is then mixed with Cu_2O. The fluffy mass is

then cold rolled into a felt. This cold rolling process results in cross linking of the catalyst particles by PTFE-fibers which is brought about by stress and friction from the initially globular PTFE- particles. This cold rolling of the mixture is the most important step in the production of AFC electrodes. This is where the art factor in the manufacture of fuel cell electrode comes into picture. A very good knowledge of material properties and experience is required for cold rolling step.(59)

When PTFE in powder form is used then the process of electrode manufacture is called dry method. While the manufacturing process with PTFE emulsion is called wet method.(9)

High rolling pressure and strain are required for dry method than wet method. High rolling pressures and stress are supposed to induce a layered structure of the electrode and in particular alignment of the PTFE fibers parallel to the electrode surface. The felt is then rolled onto a metallic screen (fig. 5.1). The metallic screen can be of nickel or copper. The metallic screen acts as a support and current collector. Since at the potential of the hydrogen anode Ni or Cu is immune to corrosion. The thickness of the PTFE bonded Raney-nickel felt for the hydrogen anode should not exceed 0.5 mm for optimum performance. The mesh width of the net and diameters of the metallic wire are of the same or comparable size. The freshly prepared electrodes require cathodic conditioning before using them in AFC. The cathodic conditioning reduces the added Cu_2O with the formation of a highly metallic, highly conductive, copper deposits within the fuel cell electrode. In this way a homogeneous deposition of copper in the electrode matrix is achieved. This cathodic treatment also leads additionally to partial reduction of nickel oxide.(60)

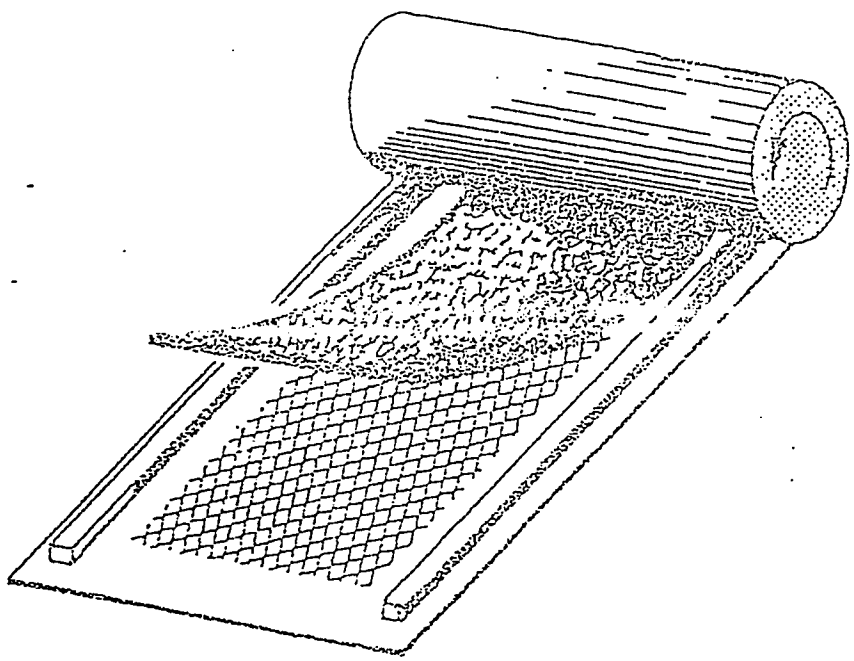

Fig. 5.1 Schematic Representation of Felt Rolling into Metal Net

The novel Raney-Ni/PTFE gas diffusion electrodes used in this study were characterized by a number of techniques which were:

1. BET surface area by nitrogen adsorption
2. Mercury Intrusion Porosimetry
3. Scanning Electron Microscopy
4 Inductively Coupled Plasma(ICP)- Atomic Energy Spectrometry

These characterization results were later used to estimate the physical parameters required for flooded spherical Raney-Ni catalyst grain model developed earlier by Celikar et. all (15). The characterization of the electrode was carried out in the Research Institute of the King Fahd University of Petroleum and Minerals.

5.2 Surface Area

The basic theory behind measuring total surface area of porous structure is by adsorption of a particular molecular species from a gas or liquid onto the surface. If conditions are so adjusted that a complete adsorbed layer, averaging one molecule thick, can be established and the area covered per molecule is known. Then the quantity of adsorbed material gives directly the total surface area of the sample.

In BET surface area by nitrogen adsorption method, the amount of nitrogen adsorbed at equilibrium at the normal boiling point(-195.8°C) is measured over a range of nitrogen pressures below 1atm.

Extension of Langmuir adsorption isotherm to multilayer adsorption gives the following expression for the volume of nitrogen adsorbed at pressure P.

$$\frac{P}{V(P_o - P)} = \frac{1}{V_m C} + \frac{(C-1)P}{V_m C P_o}$$

Here P_o is saturation pressure of adsorbate gas at the experimental temperature and C is a constant which is related exponentially to the heat of adsorption and liquefaction of the gas. More accurate determination of the surface area requires higher C values.

A plot of $P/V(P_o\text{-}P)$ against P/P_o gives a straight line. The reciprocal of the sum of slope S and intercept I of this line gives volume, Vm of gas adsorbed in monolayer. By knowing the average area occupied by an adsorbed molecule the surface area to the catalyst is then calculated. For nitrogen at -195.8°C the surface area per gram is 4.35×10^4 Vm.

The equipment used for the determination of BET surface area of the new electrode was SORPTOMATIC. In this instrument the volume of the gas adsorbed was obtained by measuring the decrease in pressure resulting from the adsorption of a portion of a known gas volume. Predetermined constant volumes of nitrogen were introduced in an evacuated empty burette and kept at liquid nitrogen temperature. After introducing the sample in test chamber a part of nitrogen introduced was adsorbed and the pressure of the gas in equilibrium with the portion adsorbed were recorded. Comparison of the values of pressures with empty

Table 5.1 B.E.T. Surface Area for the Fresh Electrode

SORPTOMATIC B.E.T.

DATE	3/2/93
OPERATOR	
SAMPLE	A-CHE (FRESH)
MONOLAYER THICKN.(A)	4.3
SATUR./LIM. PRESS. (TORR)	760
ADS.MOL.MASS (G/MOL)	28
ADS.LIQ.DENS. (G/CM3)	.808
BUR.TEMPERATURE (C)	-195.82
OPERAT.PRESS. (TORR)	800
TOTAL INTRODUCTION	8
RED. INTRODUCTION	8
REDUCTION FACTOR	.5
BUR.CONST.(CM3/TORR)	.1
SAMPLE MASS (G)	.1041
SAMP.DENS. (G/CM3)	2

CORRECTED BUR. COSTANT (CM3/TORR) = .0993392

ADSORPTION VALUES

P ADS (TORR)	P/PO ADS	VI (CM3)	V ADS (CM3/G)	T (A)	P/(PO-P)
67.5	0.089	7.88	4.130	5.5	.023601
143.4	0.189	15.76	5.329	6.2	.043641
218.2	0.287	23.64	6.912	6.8	.058287
293.6	0.386	31.52	8.285	7.5	.075979
368.4	0.485	39.41	9.862	8.2	
444.9	0.585	47.29	10.858	9.1	
517.3	0.681	55.17	13.278	10.1	
594.2	0.782	63.05	14.128	11.7	
99,0					

VOLUME (MONOLAYER)..... 5.47891 (CM3/G)

SPEC.SURF.AREA..... 23.9409 (M2/G)

BET C VALUE..... 19.9255

TOT. VOL. INTRODUCED.... 63.05 (CM3)

burette gives the gas volume adsorbed at the various equilibrium pressure and hence the isotherm could be calculated.

The results of BET surface area determination of the new electrode by nitrogen adsorption are given in table 5.1.

5.3 Mercury Intrusion Porosimetry

Mercury does not wet most surfaces and therefore doesn't penetrate most pores at atmospheric pressures. Mercury intrusion porosimetry is based on this nonwetting behavior of Hg in capillary. If the contact angle between liquid and solid ,θ is greater than 90°, the interfacial tension opposes the entrance of liquid into pores. This opposition is overcome by external pressure. For a cylindrical pore the force opposing entrance to the pore acts along the circumference and equals $-2\pi r\sigma\cos\theta$, where σ is the surface tension. The external pressure, which opposes this force, acts over the entire pore cross-sectional area and equals $\pi r^2 P$. At equilibrium the two forces are equal and pore radius is given by

$$r = \frac{-2\sigma\cos\theta}{P}$$

Mercury intrusion porosimetry was applied to the new electrode to measure the macroporosity which consisted of pores bigger than 50 A in size. In this method the porous electrode was placed in a cell and evacuated. Hg was then injected into the pores at various pressures and the volume of Hg taken up was obtained as a function of pressure. The results of Hg intrusion porosimetry are given in table 5.2 and 5.3. The total macroporosity for the new hydrogen anode was estimated as $0.0057 cm^3/g$.

Table 5.2 Pore Volume by Hg Intrusion Porosimetry

PORE SIZE, SURFACE, PARTICLE SIZE DISTRIBUTION

DATE	15/2/98
OPERATOR	SAA
SAMPLE	FRESH CHE
CONTACT ANGLE	141.2
SURF.TENS.(DYNES/CM)	480
PRESSURE MAX. (BAR)	2000
DILAT. VOLUME (CM3)	15
CAP.RADIUS (MM)	1.5
COMPRESS. BAR-1.	1.17302-06
MERCURY HEIGHT (MM)	100
SAMPLE MASS (G)	.38
SAMP.DENS. (G/CM3)	2

PORE SIZE (MM2)	PRESSURE (BAR)	SURFACE AREA (A)	DISTRIBUTION (MM3/G)	CUM.VOL. (%)	REL.VOL. (%)	CUM.AREA (CM2/G)	REL. CM
0.71	4.54	15521.3	1.65	3.04	3.0	10	[illegible]
1.41	5.44	14026.6	3.47	6.38	3.3	45	25.9
2.12	6.44	11955.6	5.28	9.72	3.3	76	30.6
2.83	7.24	10545.1	7.11	13.07	3.4	110	34.5
3.53	8.54	8539.2	8.91	16.38	3.3	151	40.5
4.24	9.74	7337.4	10.71	19.70	3.3	197	46.1
4.95	10.63	7174.2	12.53	23.04	3.3	247	50.7
5.65	12.03	6339.8	14.35	26.34	3.3	304	55.7
6.36	12.93	5898.7	16.15	29.68	3.3	366	61.7
7.07	13.93	5475.4	17.96	33.02	3.3	432	66.2
7.78	14.93	5106.9	19.78	36.35	3.3	503	71.0
8.49	16.53	4614.5	21.56	39.64	3.3	580	77.4
9.19	17.53	4351.4	23.38	42.97	3.3	664	83.4
9.90	18.93	4029.7	25.17	46.28	3.3	753	89.1
10.60	19.82	3846.9	26.99	49.62	3.3	847	94.6
11.31	21.92	3479.5	28.75	52.[illegible]	[illegible]	[illegible]	[illegible]
12.02	23.32	3269.9	30.55	56.[illegible]	[illegible]	1056	[illegible]
12.72	25.53	2988.1	32.31	59.40	3.2	1176	117.7
13.43	27.[illegible]	2771.1	34.08	62.65	3.2	1304	127.5
14.14	31.[illegible]	2453.6	35.79	65.77	3.1	1442	136.2
14.84	34.83	2190.4	37.46	68.87	3.1	1596	153.9
15.55	40.53	1882.4	39.06	71.81	2.9	1766	169.9
16.26	45.63	1672.0	40.69	74.80	3.0	1960	194.5
16.96	54.13	1409.5	42.18	77.50	2.7	2169	208.5
17.67	63.43	1202.8	43.59	80.13	2.6	2407	228.2
18.38	74.63	1022.3	44.93	82.61	2.5	2671	253.3
19.08	91.03	838.1	46.04	84.64	2.0	2935	264.1
19.79	108.53	703.0	47.10	86.59	1.9	3235	300.5
20.50	127.13	600.1	48.10	88.43	1.8	3570	335.2
21.21	149.63	509.9	48.93	89.95	1.5	3895	324.2
24.93	252.13	291.3	51.68	94.02	3.4	5493	359.5
25.45	323.13	236.9	52.17	95.91	0.9	5864	407.2
26.15	360.13	211.9	52.58	96.12	0.2	5972	108.3
26.86	394.13	193.6	52.58	96.67	0.5	6280	308.4
27.57	426.13	179.0	52.97	97.38	0.7	6716	436.0
28.27	461.13	165.5	53.22	97.85	0.5	7022	305.3
28.98	496.13	153.8	53.48	98.31	0.5	7350	328.4
29.69	575.13	133.6	53.55	98.32	0.0	7445	395.8
31.10	608.13	125.5	53.91	99.11	0.3	8012	256.1
31.81	645.13	118.3	54.07	99.41	0.3	8284	271.7
32.51	686.13	111.2	54.07	99.41	0.0	8284	0.0
33.22	719.13	106.1	54.39	100.00	0.6	8890	605.8
33.93	760.13	99.6	54.39	100.00	0.0	8890	0.0
34.64	810.13	94.2	54.39	100.00	0.0	8890	0.0
35.34	854.13	89.2	54.39	100.00	0.0	8890	0.0
36.05	902.13	84.0	54.39	100.00	0.0	8890	0.0
36.76	953.13	80.0	54.39	100.00	0.0	8890	0.0
37.46	998.13	76.4	54.39	100.00	0.0	8890	0.0
38.17	1063.13	71.3	54.39	100.00	0.0	8890	0.0
38.88	1114.13	68.5	54.39	100.00	0.0	8890	0.0
39.58	1174.13	65.0	54.39	100.00	0.0	8890	0.0
40.29	1228.13	62.1	54.39	100.00	0.0	8890	0.0
41.00	1282.13	59.5	54.39	100.00	0.0	8890	0.0
41.70	1283.13	55.2	54.39	100.00	0.0	8890	0.0
42.41	1386.13	55.0	54.39	100.00	0.0	8890	0.0
43.12	1438.13	53.1	54.39	100.00	0.0	8890	0.0
43.82	1509.13	50.6	54.39	100.00	0.0	8890	0.0
44.53	1554.13	49.1	54.39	100.00	0.0	8890	0.0
45.24	1615.13	47.2	54.39	100.00	0.0	8890	0.0
45.94	1668.13	45.7	54.39	100.00	0.0	8890	0.0
46.65	1731.13	44.1	54.39	100.00	0.0	8890	0.0
47.36	1773.13	42.9	54.39	100.00	0.0	8890	0.0

SPECIFIC SURFACE AREA (M2/G) = .889 (CYLINDRICAL MODEL)

Table 5.3 Pore Size Distribution for the Fresh Electrode

Pore Size	% Pores
37 - 100 °A	0 %
100 - 1000 °A	17 %
10^3 - 10^4 °A	70 %
> 10^4 °A	13 %

5.4 Scanning Electron Microscopy (SEM)

In SEM an electron spot of about 5 nm minimum is focused on the sample. This spot is then moved over a small area by means of a set of deflecting coils. This area is displayed highly magnified on a cathode ray tube (CRT) screen by causing currents passing through the scanning coils to pass through the corresponding deflecting coils of the CRT while the electrons emitted from the sample are collected, amplified and used to modulate the brightness of the CRT. By verifying the orientation of the specimen with respect to the signal detector, a light/dark effect is produced forming a three-dimensional effect.

The SEM analysis of the electrode was carried out to observe the morphology of the electrode sample and perform EDS analysis for the active layer and metal mesh. The samples were cut and mounted on holders of JSM-840 type SEM, with the help of a double sided adhesive tape. Carbon conducting paint was applied to make the sample conductive. The samples were observed on the CRT screen and energy dispersive spectral (EDS) analysis was performed. After this the samples were coated with a thin layer of gold and micrographs were taken. Two micrographs of the sample were taken to show the cross-sectional area, mesh side or electrolyte facing side. EDS spectra and semiquantitative analysis data was obtained for the mesh and for the electrolyte facing side and back side or gas facing side(figs. 5.2, 5.3, 5.4).

From figs. 5.5 and 5.6 the average grain size and thickness of active χ layer of the electrode sample was estimated to be

Average catalyst grain diameter = 10μm (fig. 5.5)

Average Thickness of Active layer= 380μm (fig. 5.6)

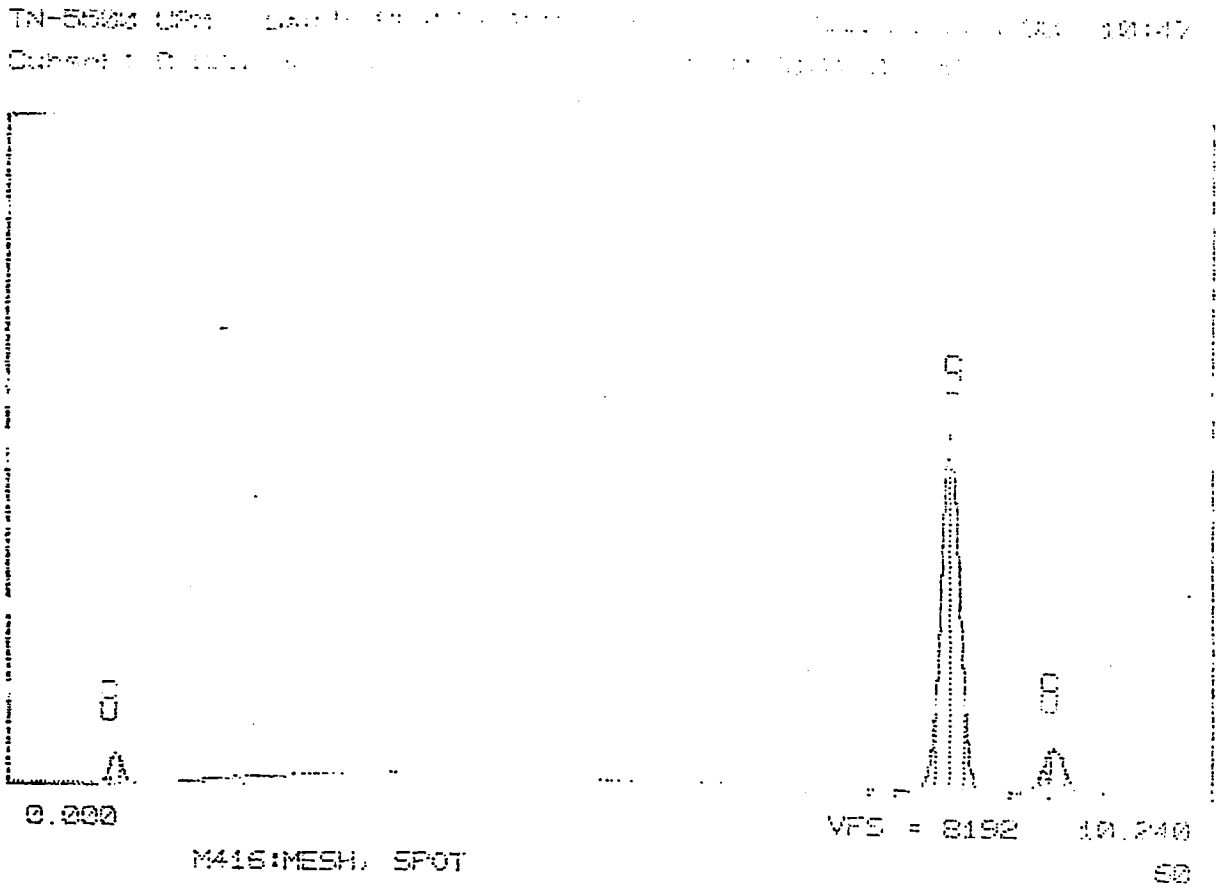

Fig. 5.2 EDS Spectra for the Metal Mesh

SQ0: SSQ

SEMI-QUANTITATIVE ANALYSIS: M416: SQUARE, AREA
EL NORM. K-RATIO

CU-K 0.18185 +- 0.00215
AL-K 0.00962 +- 0.00021
NI-K 0.80251 + 0.00480

ZAF CORRECTION 20.00 KV 40.00 Degs

No. of Iterations 2

	K	[1]	[A]	[F]	[ZAF]	ATOM.%	WT.%	
CU-K	0.181	1.043	0.998	1.000	1.041	16.75	13.52	
AL-K	0.009	0.944	0.281	0.990	0.847	6.15	2.87	*
NI-K	0.803	0.998	1.000	1.00	0.994	77.10	78.61	

* - High Absorbance

SEI.

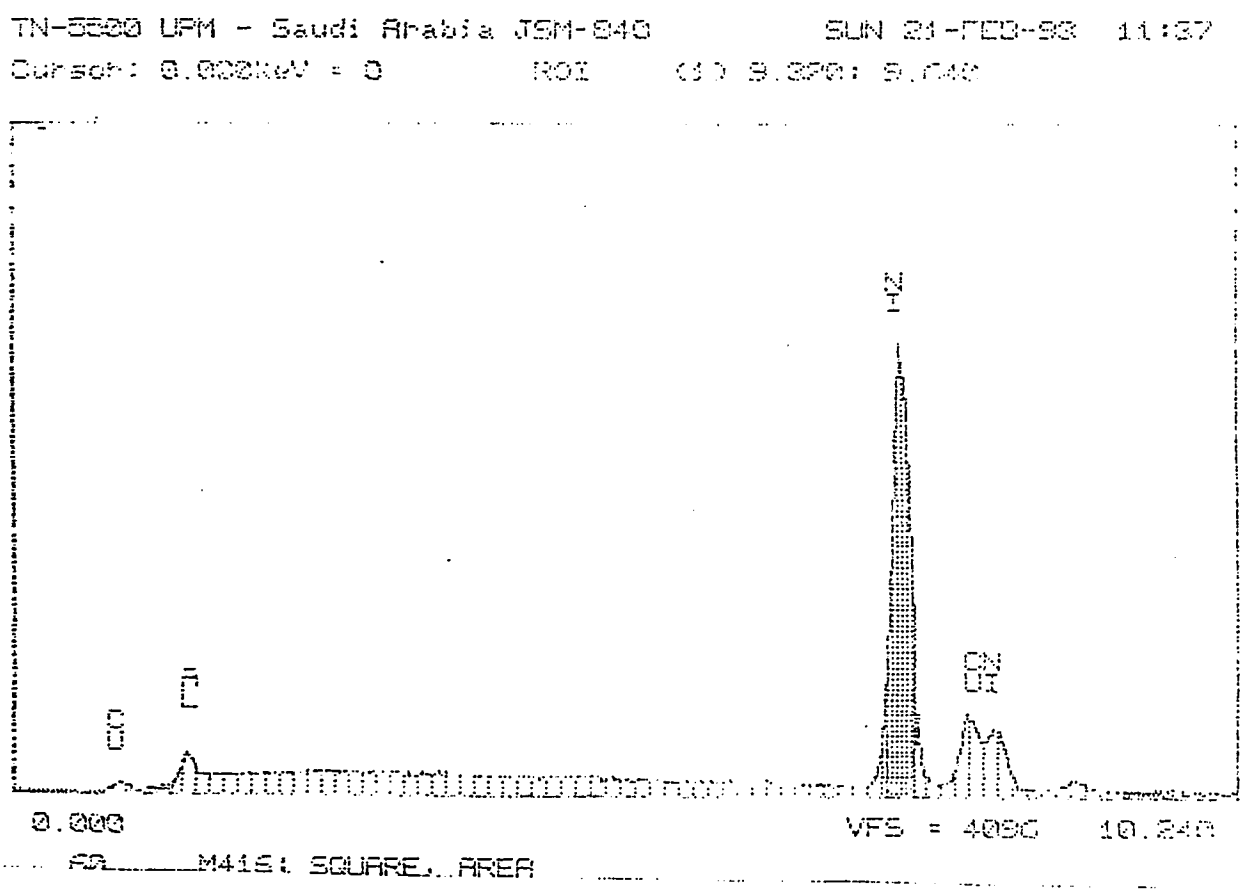

Fig. 5.3 EDS Spectra for the Electrolyte Facing Side of Electrode

SEQ

SEMI-QUANTITATIVE ANALYSIS: M416: BACKSIDE, AREA

EL	NORM. K-RATIO
CU-K	0.23495 +- 0.00243
AL-K	0.00928 +- 0.00021
NI-K	0.75643 + 0.00369

ZAF CORRECTION 20.00 KV 40.00 Degs

No. of Iterations 1

	K	(Z)	(A)	(F)	(ZAF)	ATOM.%	WT.%	
CU-K	0.234	1.040	0.993	1.000	1.039	21.64	23.81	
AL-K	0.009	0.941	3.249	0.999	3.059	5.99	2.78	*
NI-K	0.756	0.991	1.000	1.000	0.991	72.17	73.41	

* - High Absorbance

SEQ:

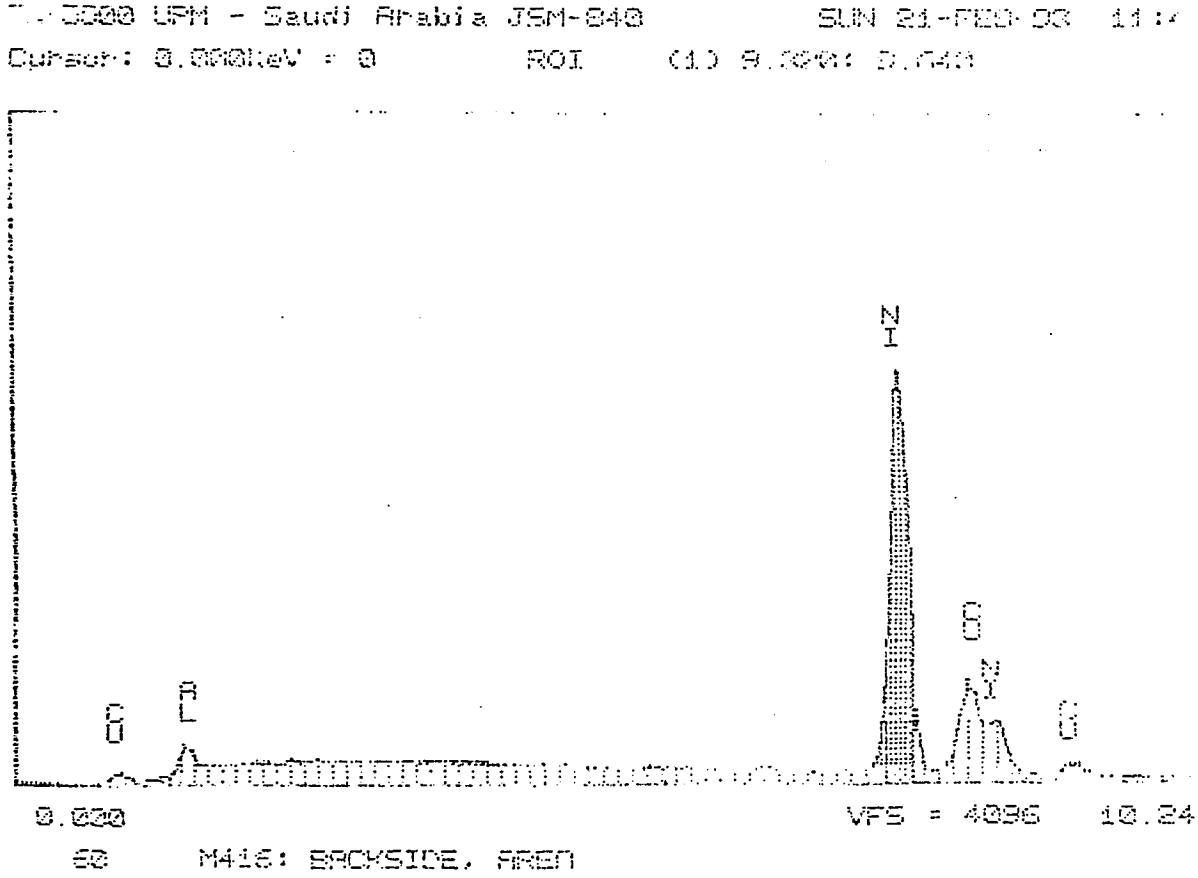

Fig. 5.4 EDS Spectra for the Gas Facing Side of Electrode

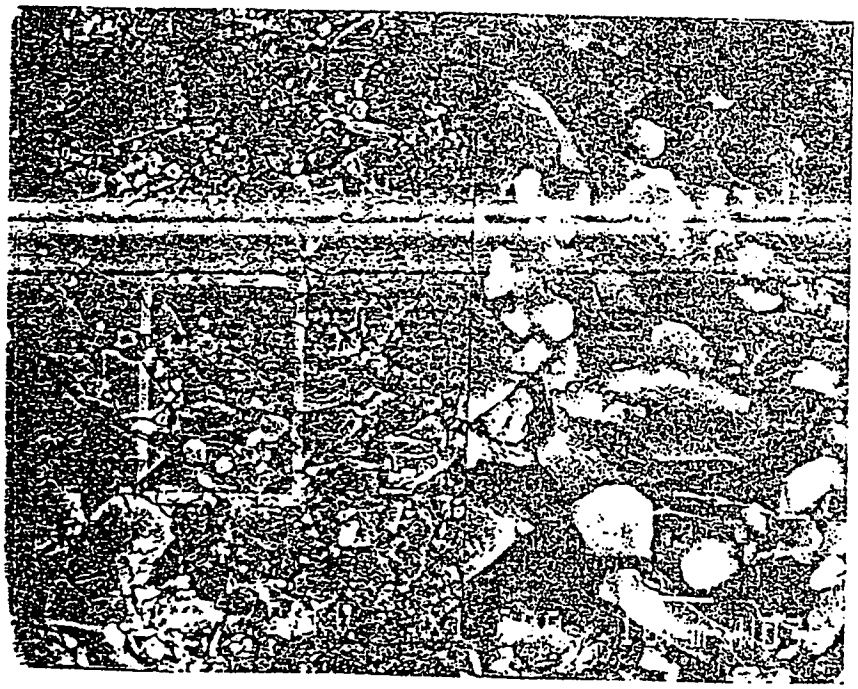

Fig. 5.5 SEM Micrograph of the Active Layer of Electrode

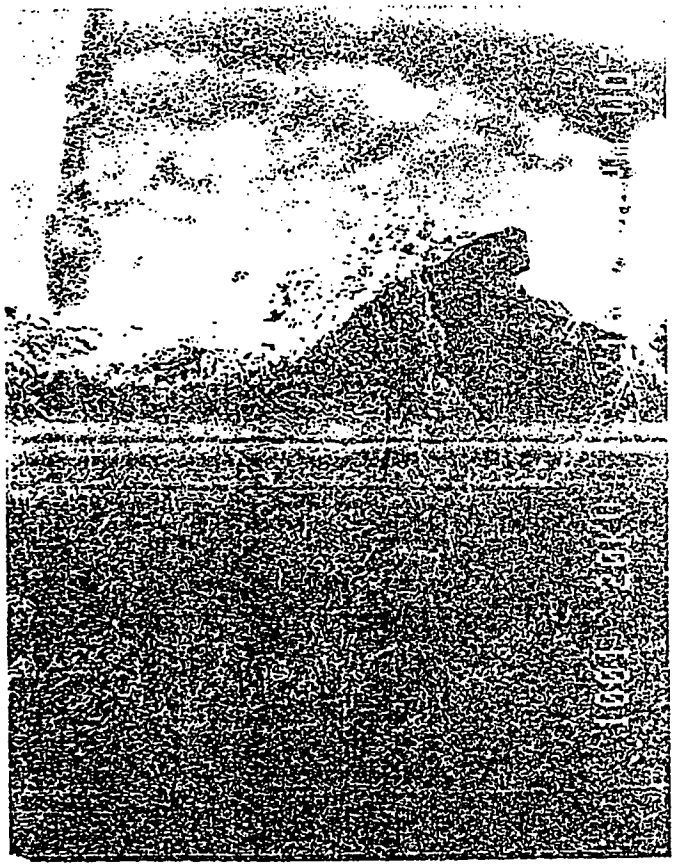

Fig. 5.6 SEM Micrograph of the Cross-section of Electrode

5.5 Inductively Coupled Plasma -AES

ICP-AES analysis gives very accurate determination of the composition of the sample. For this analysis the electrode sample was separated from its metal mesh. The sample was weighed in a digital balance then digested with 25 % HCl under low heat until only white film particles were left. Sample was finally diluted in 5% HCl and screened by ICP to check what elements were there. Final analysis was carried out by ICP which was calibrated with four levels of mixed standards containing the elements that were found from screen test. The results are given in table 5.4.

These results showed that about 27 % PTFE was present in the electrode. This result helped in determining the catalyst loading which was calculated to be 0.08278 g/cm^2 .

5.6 Estimation of Electrochemically Active Surface Area

For estimating electrochemically active surface area a piece of the electrode having external surface area of 4 cm^2 was cut. This piece of electrode was then weighed on a digital balance. After this the copper mesh was separated very carefully from the electrode piece and weighed. From the difference between the total weight and the metal mesh the weight of the active layer in the electrode piece was calculated as follows,

Total weight of 4 cm^2 electrode piece	=	0.6341 g
Weight of copper mesh	=	0.1807 g
∴ weight of active layer in the electrode	=	0.4534 g

Table 5.4 ICP-AES Analysis for the Fresh Electrode

Elements	% By Weight
Al	3.30 %
Cu	7.80 %
Ni	62.0 %
Cr	< 0.05 %
Ti	< 0.01 %
Fe	< 0.05 %
Mn	< 0.05 %

From the BET surface area measurement an area of 24 m^2/g based on total weight was measured. The corrected BET surface area based on the active layer for the electrode was

$$S_{BET}(\text{corrected}) = \frac{24 \quad (0.6341)}{(0.4534)} \quad m^2/g$$

$$= 33.56 \quad m^2/g$$

Surface area based on unit volume of the electrode was calculated as

$$f^o = S_{BET}(\text{corrected})\ \rho\ (1-\theta)$$

$$= 33.56 \times 4.1175 \times (1-0.4)$$

$$= 8.3 \times 105 \quad cm^2/\ cm^3$$

5.7 Estimation of Electrode Macroporosity

For estimation of macroporosity a 4 cm^2 square piece of electrode was carefully cut and weighed on a digital balance. The weight of this sample was found to be 0.6341 g. Hence the area of 1 g of electrode becomes 6.3081cm^2. The product of electrode thickness with the area gave volume of 1 g of electrode to be 0.2429 cm^3/g. Thirty copper wires of 200 μm diameter and 1cm length(L) were counted in 1 cm^2 piece of electrode. From this the volume of wire in 1g of the electrode was calculated as

Volume of wire in 1cm^2 of electrode	$= 30\pi D^2L/4$
1 cm^2 of the electrode	$= 0.009425\ cm^3$
1 g of electrode	$= 0.05945\ cm^3$

Hence corrected volume of active layer $= 0.2429 - 0.05945$

$= 0.1834\ cm^3$

From Hg intrusion porosimetry the total pore volume was found to be 0.0544 cm^3/g . The electrode macroporosity was given by the ratio of void volume which was obtained from Hg intrusion porosimetry divided by the corrected volume. Thus

$$\text{Macroporosity}(\varepsilon_{mac}) = \frac{.00544}{0.1834}$$

$$= 0.2966$$

Table 5.5 gives comparison between the charecteristics of previous elctrode and the new electrode.

Table 5.5 Comparison of Characteristics of the New Electrode with Previous Electrode

Characteristics	Previous Electrode	New Electrode
Avg. Grain Radius(R)	20μm	5μm
Electrode Thickness(L)	320μm	380μm
Macroporosity(ε_{mac})	0.2	0.3
Active Surface Area(f^o)	5.4×10^5 cm^{-1}	8.3×10^5 cm^{-1}
BET Surface Area(S)	30 m^2/g	33.56 m^2/g
Catalyst loading	7 kg/m^2	8 kg/m^2
Cu Content (%)	0 %	7.8 %

Chapter 6

EXPERIMENTAL SETUP AND PROCEDURE

6.1 Experimental Half Cell Setup

A schematic diagram of the half cell assembly used for investigating the performance of the specially prepared Raney-Ni hydrogen electrode is shown in fig.6.1. The half cell is fabricated from plexiglass. It has a gas chamber and an electrode chamber. The gas chamber has an inlet and outlet for the gas while the electrode chamber houses the electrode, a ring shaped PTFE sealing and two nickel wire current collectors. The electrode chamber is screwed to the gas chamber with stainless steel screws. The half cell is mounted into a PTFE container which is filled with 25% KOH solution. A 2.5cm × 2.5cm nickel plate which is welded onto a nickel rod is used as a counter electrode. The counter electrode is fixed onto the plexiglass lid of the PTFE container. As the electrolyte medium is basic therefore a Hg/HgO reference electrode is used. The reference electrode is placed near the electrode in the cell in such a way that shielding effects are minimized. The gas inlet and outlet of the gas chamber are sealed by PTFE tape. The incoming gas is introduced at the side of the chamber while the outgoing gas leaves from the top. The level of water in the back pressure regulator is adjusted to 10 - 15 cm height. A Brooks gas flow controller is used to control the flow rate of hydrogen through the cell. The outlet gas pressure from the hydrogen gas cylinder is kept at 1.4kg/cm^2. The hydrogen gas used in this work has a purity of 99.99%.

The outlet gas stream from the half cell is bubbled through an adjustable height of water column acting as back pressure regulator. The entire half cell

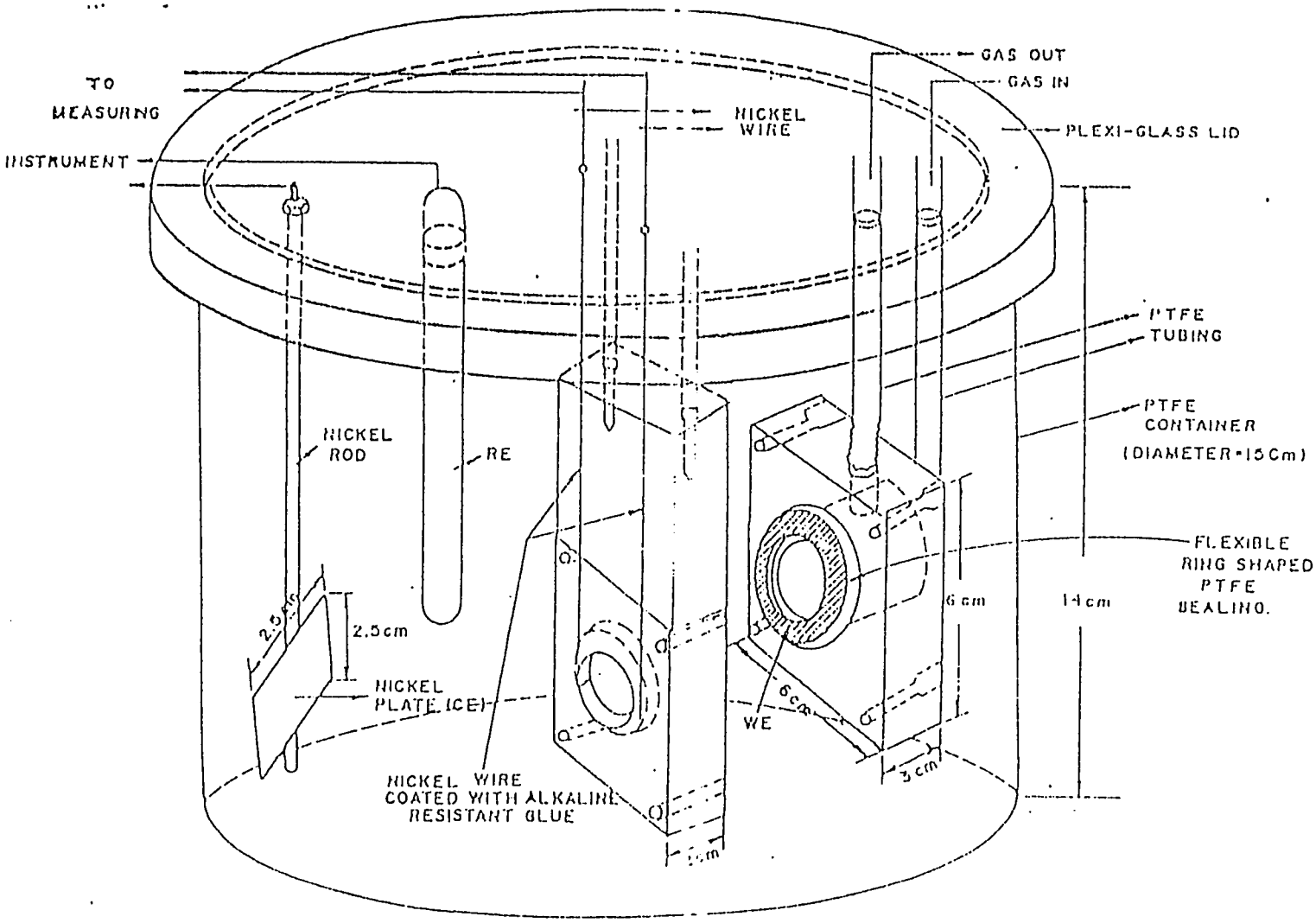

Fig. 6.1 A Schematic diagram o' he Half Cell Assembly

assembly is place in a thermostat water bath for doing experiments at different electrolyte temperatures.

The geometric surface area of the circular shaped electrode used is 6 cm^2 and it is placed in the half cell in such a way that the mesh side faces the electrolyte. Nickel wire current collectors are used to connect the working electrode to external circuit. A Wenking type POS73 potentioscan is used to apply a desire load of current to the working electrode by choosing suitable external resistances. The external resistor is fixed to an interface board. The interface board is also equipped with a solid state relay. Digital multimeter of type METER M-4650 are used as high impedance DC voltmeter and ammeter in the circuit. A dual channel digital storage oscilloscope (Philips ,PM 3302)with a maximum sampling rate of 20 MHz is used for IR drop measurement by current interruption technique using the solid state relay(Teledyne SSP p/N type with 4-10V DC control).

6.2 Activation of the Raney-Ni Electrode

Activation of the Raney-Ni electrode was carried out to precondition the electrode. The activation process results in reduction of the nickel oxide. The activation was done by passing a cathodic current of 25 mA, the electrode being fully immersed in 25% KOH electrolyte.

For the purpose of activation ,a circular shaped electrode of diameter 3.6 cm is cut from the electrode sheet and placed in the electrode chamber in such a way that the metallic mesh touches the current collector wires. A ring shaped PTFE sheet was placed on top of the electrode. The ring acts as a sealing. Then the two pieces of the half cell were brought together and screwed with stainless steel

screws. The gas connections were done and the half cell mounted on the plexiglass lid was slowly lowered into a 25% KOH solution in a PTFE container. The PTFE container was then placed in a thermostat water bath. The level of water in the back pressure regulator was adjusted between 10-15 cm so that neither the gas bubbles in the electrolyte nor the electrolyte leaks into the gas compartment.

The external circuit was connected galvanostatically and a current of 25mA was passed through the cell for 48 hours at 25^{0}C. During activation the electrode potential stayed around -945mV with respect to Hg/HgO reference electrode. Upon stopping the cathodic current the electrode potential falls down to about -922mV.

6.3 Polarization and IR drop Measurements

The working electrode was polarized by changing the settings of the potentiostat and passing anodic current through the cell(fig. 6.2, 6.3). A DC interruption technique which was developed at KFUPM was used to measure the IR drop losses. This IR drop technique utilizes the fact that ohmic overvoltage decays 100 times faster than activation ,concentration overvoltage.

The potentiostat was used as a galvanostat by using an external resistor R_1 whose value determines the current range to be controlled. This resistor was placed between the working electrode and its potentiostatic lead was connected to the point where the external resistor was linked to the working electrode. A solid state relay in series with a milliampmeter was connected to the working electrode of the half cell. Potential difference between the working and reference electrode was measured by a high impedance voltmeter.

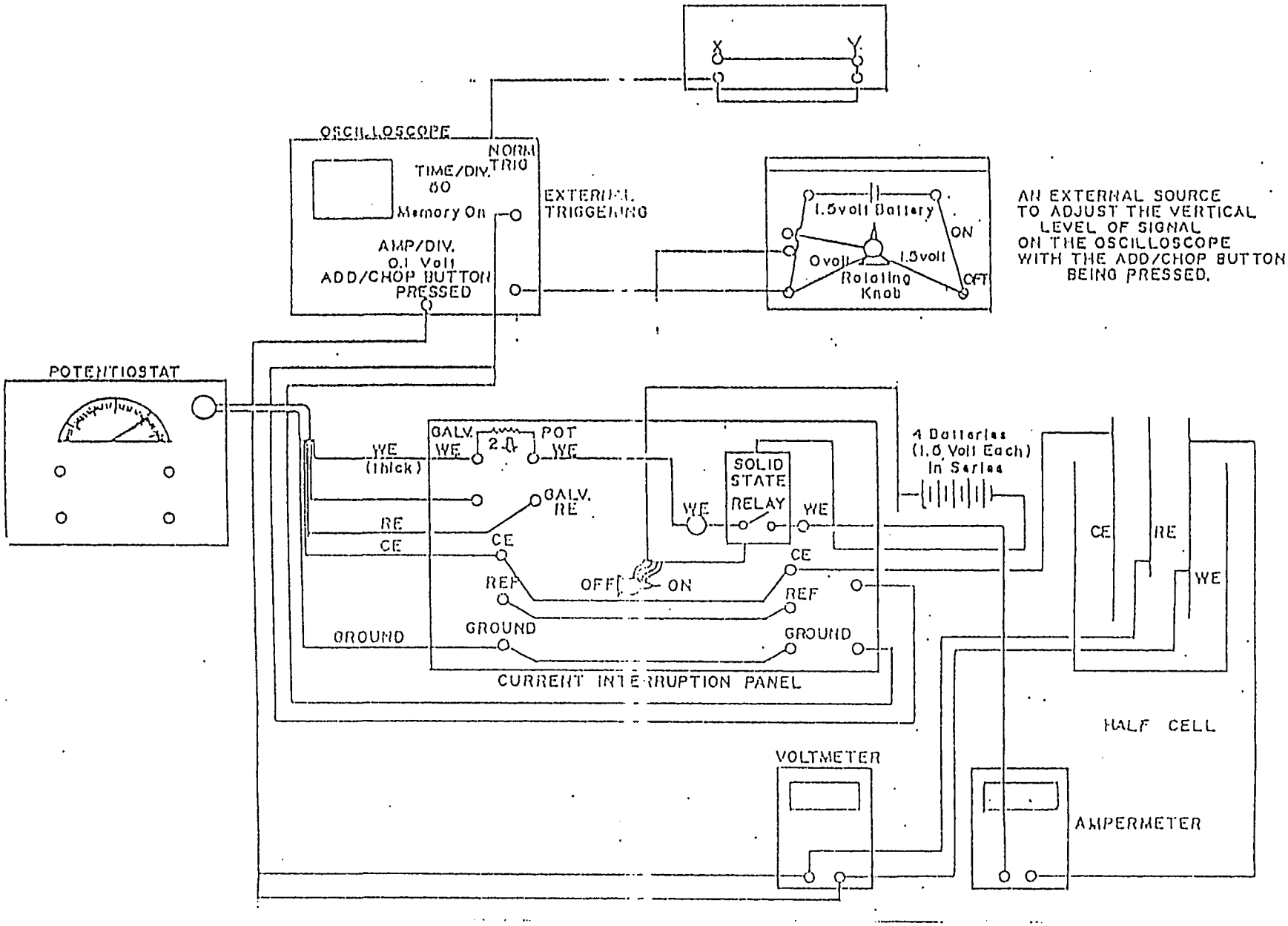

Fig. 6.2 Circuit Diagram for the Galvanostatic Polarization Experiments

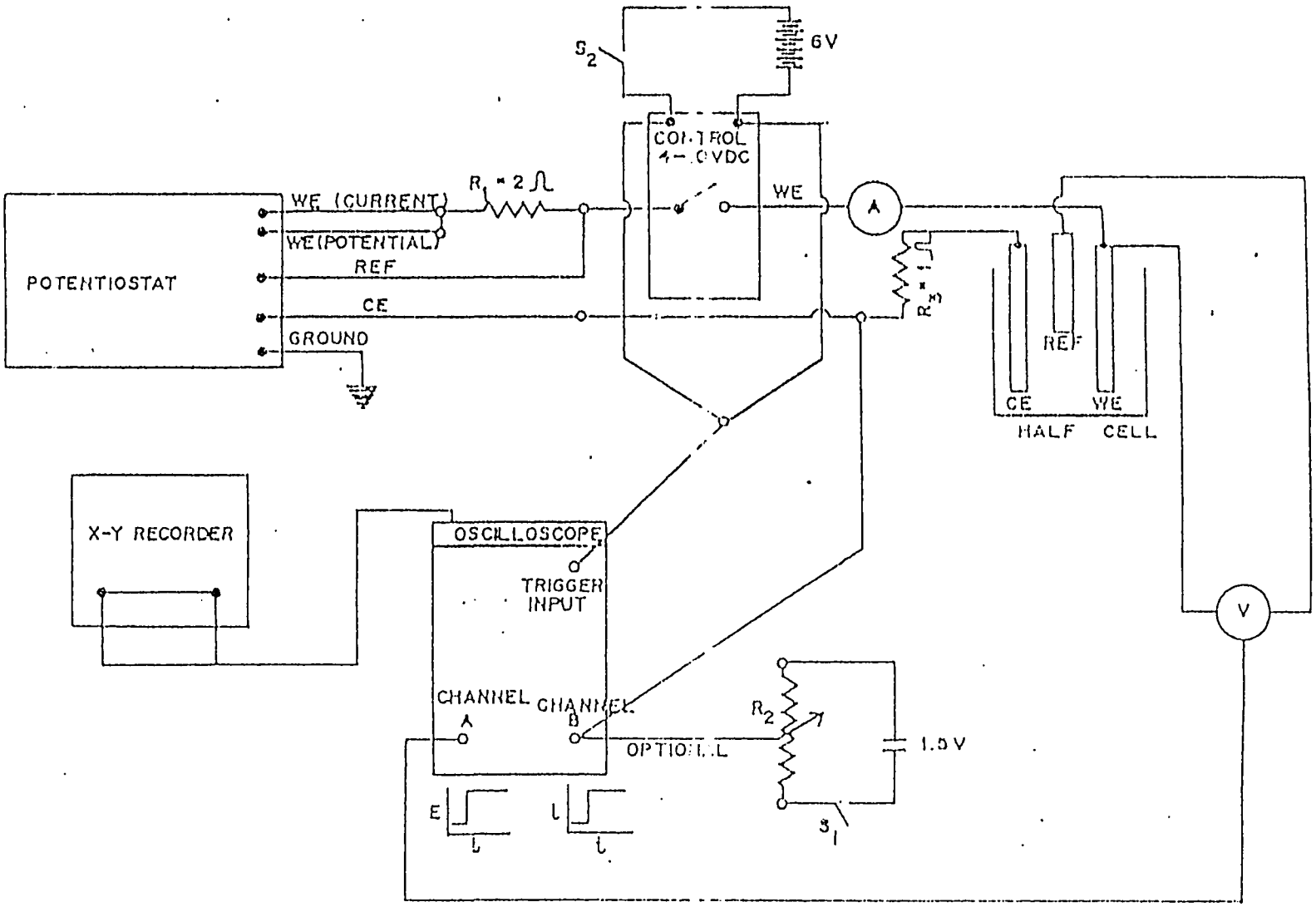

Fig. 6.3 Current Interruption Method for IR Drop Measurement

A dual channel digital storage oscilloscope was used to monitor the working electrode potential and cell current through channels A and B ,respectively. The position of the signal in the Y direction was adjusted by depressing the normal triggering switch and by adjusting the amplifier A and B switches accordingly. The level signal on the oscilloscope was turned slowly till the signal is caught at its present time base values. The cell current transient was recorded as a voltage drop across an accurately known resistor ,R_3.Mechanical switch S_2 when opened ,activates the batteries in series which then deenergizes the relay breaking the circuit current. Without using any pulse generator, switch S_2 was simultaneously used for pre-triggering the oscilloscope with shielded concentric cables. In addition the oscilloscope itself has built in four levels of pre triggering before the event which are namely zero, two, three, four quarter on the screen. Either one quarter or one half pre triggering was used in all the experiments. All the connecting wires to the instruments were kept as short as possible to minimize the pickup of stray capacitances and inductances.

The initial instantaneous jump of the voltage recovery upon going from an operating load to open circuit was recorded as the IR drop in the half cell. At oscilloscope sweep rates of 50ms/div. ,sharp steps corresponding IR drop was easily recorded and measured. It was observed that this event is completed in about 30-35msec. The reproducible delay in the opening of the solid state relay and the adjustment of level of the signal provided a ready synchronization with oscilloscope sweep rate at a present trigger level. The signal was digitally recorded in the memory of the oscilloscope and then plotted on an X-Y plotter. A variable resistor R_2, a mechanical switch S_1,and a 1.5 V battery was connected in series to adjust the vertical level of signal in channel B. This was optional and only

necessary when high sensitivities of deflection per division were required in the vertical direction of the screen.

Thus the experimental procedure involved loading the working electrode with a current density and measuring the resulting potential of the electrode with respect to Hg/HgO reference electrode. The IR drop measured from the oscilloscope and the XY plot of voltage against time. The same process was repeated at different current densities and at different electrolyte temperatures.

For the long term electrode performance test the half cell was connected to the potentiostat in potentiostatic mode. In potentiostatic mode a predetermined overvoltage was applied to the working electrode so as to pass a constant current through the counter and working electrode. Fig. 6.4 gives the circuit diagram for the potentiostatic experimental setup. The decay of this current was then followed as function of time.

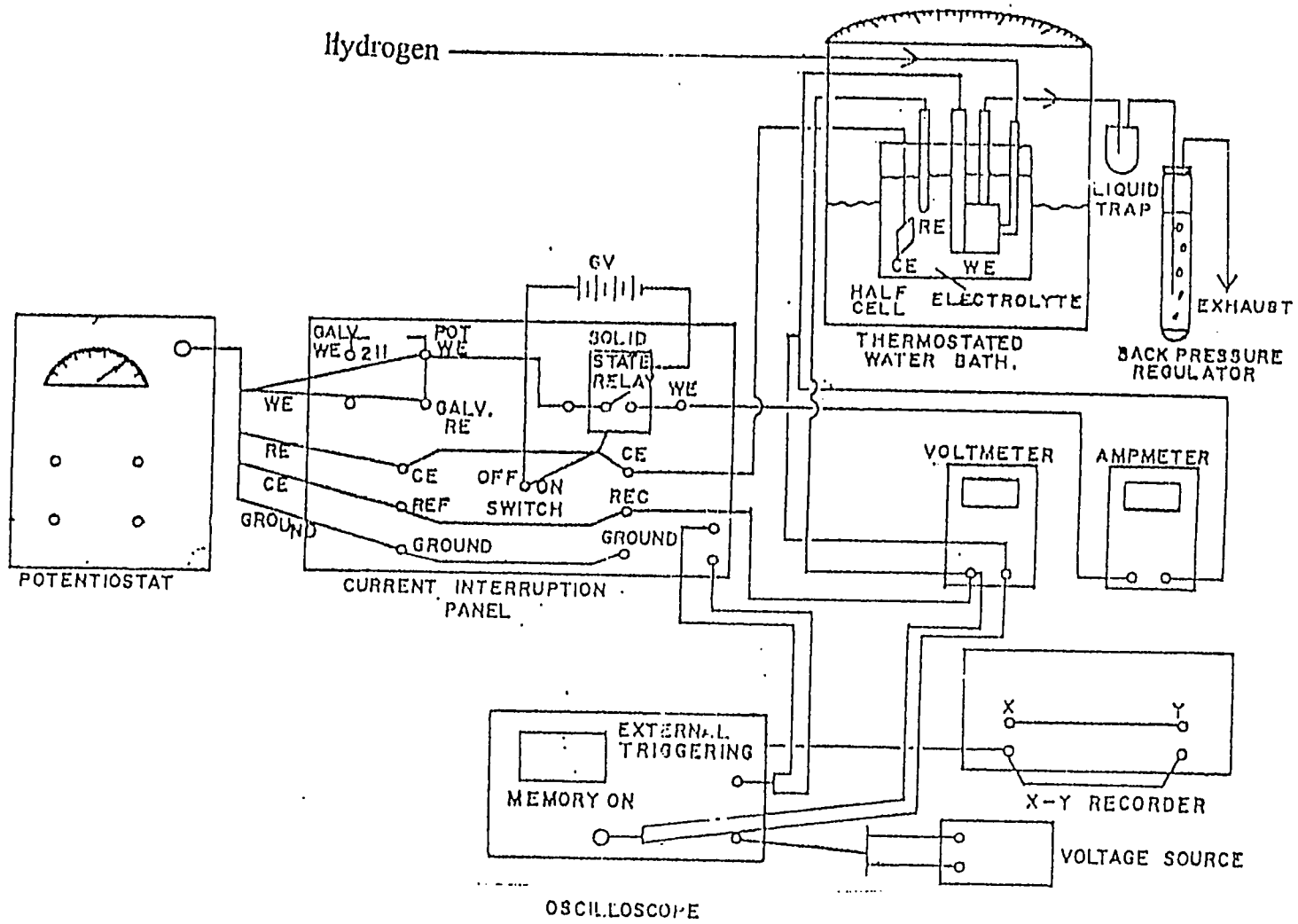

Fig. 6.4 Circuit Diagram for Potentiostatic Experiments

Chapter 7
EXPERIMENTAL RESULTS AND ANALYSIS

7.1 Polarization Measurements Results

In order to ascertain the validity of experimental setup galvanostatic polarization runs were carried out with the old electrode. Fig. 7.1 shows the reproducibility run carried out with the old electrode at 35°C and 65°C as compared to the previous data(15). The measured cell current was divided by the electrode external surface area to get the current densities. Fig. 7.2 shows the reproducibility run carried out with another piece of the new electrode. This run was carried out to ascertain the homogenity of the electrode.

The voltage drop in the electrolyte(IR) was measured by current interruption method. The electrolyte resistance was calculated by dividing IR drop by the measured cell current. Fig. 7.3 shows the electrolyte resistance at various temperatures. Table 7.1 gives the average electrolyte resistance at various temperatures (25°C-75°C). Steady state galvanostatic polarization curves obtained for the new electrode at various temperatures in the half cell setup are shown in figs. 7.4 to 7.9. The open circuit voltage read on the voltmeter and IR drop voltage measured by current interruption method was subtracted from the polarized electrode potential to get IR free overpotential.

$$\text{IR free overpotential} = E_P - \text{O.C.V.} - \text{IR}$$

For the polarization curves this overvoltage versus the current densities at various temperatures were plotted.

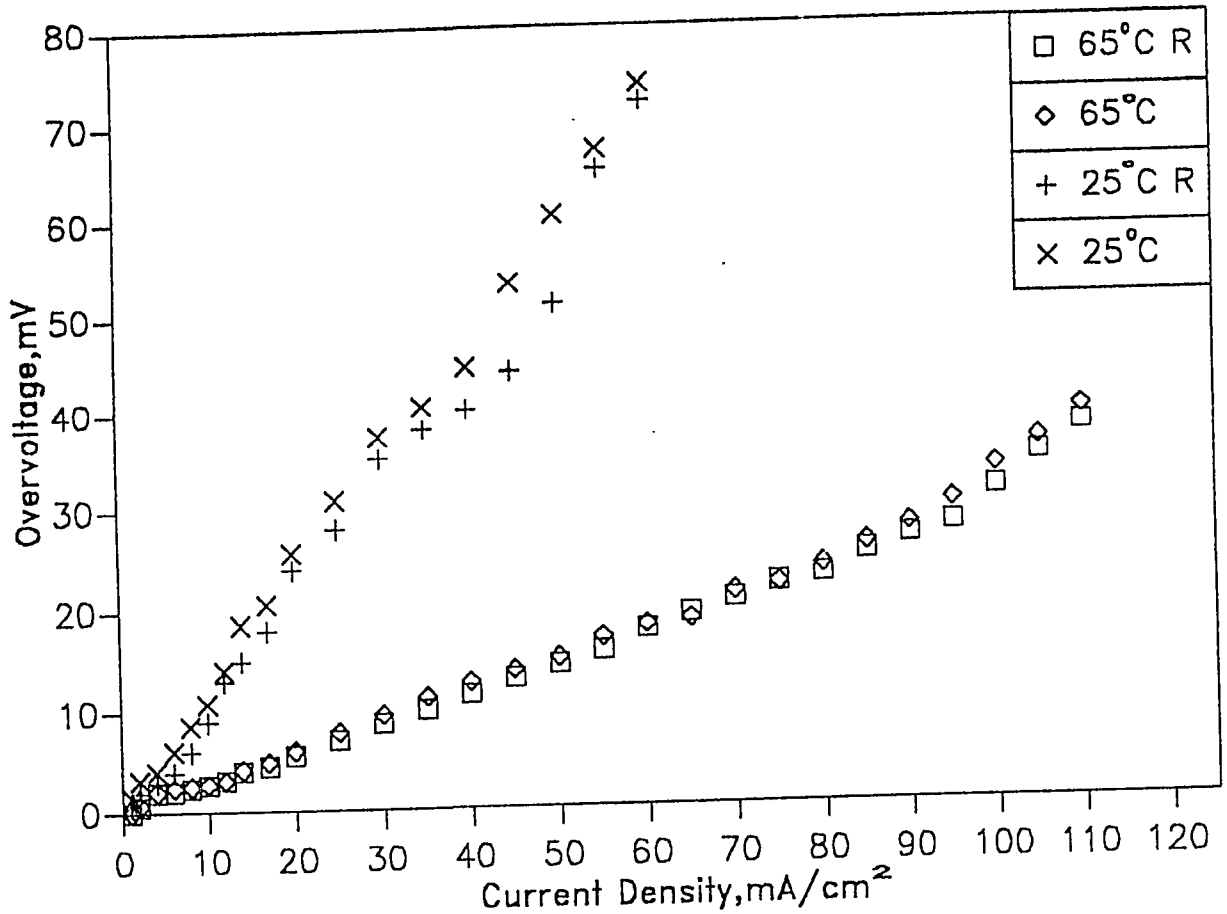

Fig. 7.1 Reproducibility Runs with the Old Electrode at 35°C and 65°C

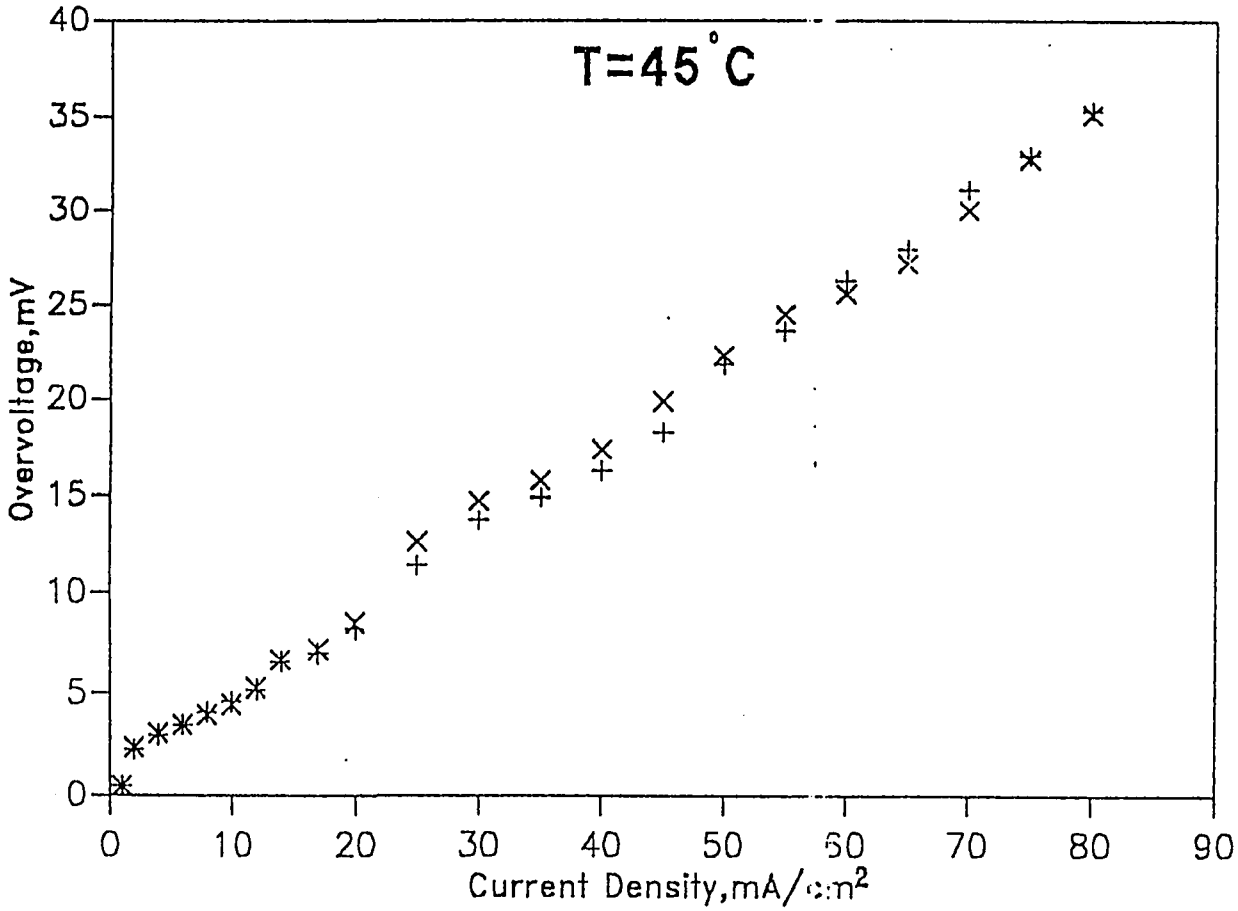

Fig. 7.2 Reproducibility Run with the New Electrode at 45°C.

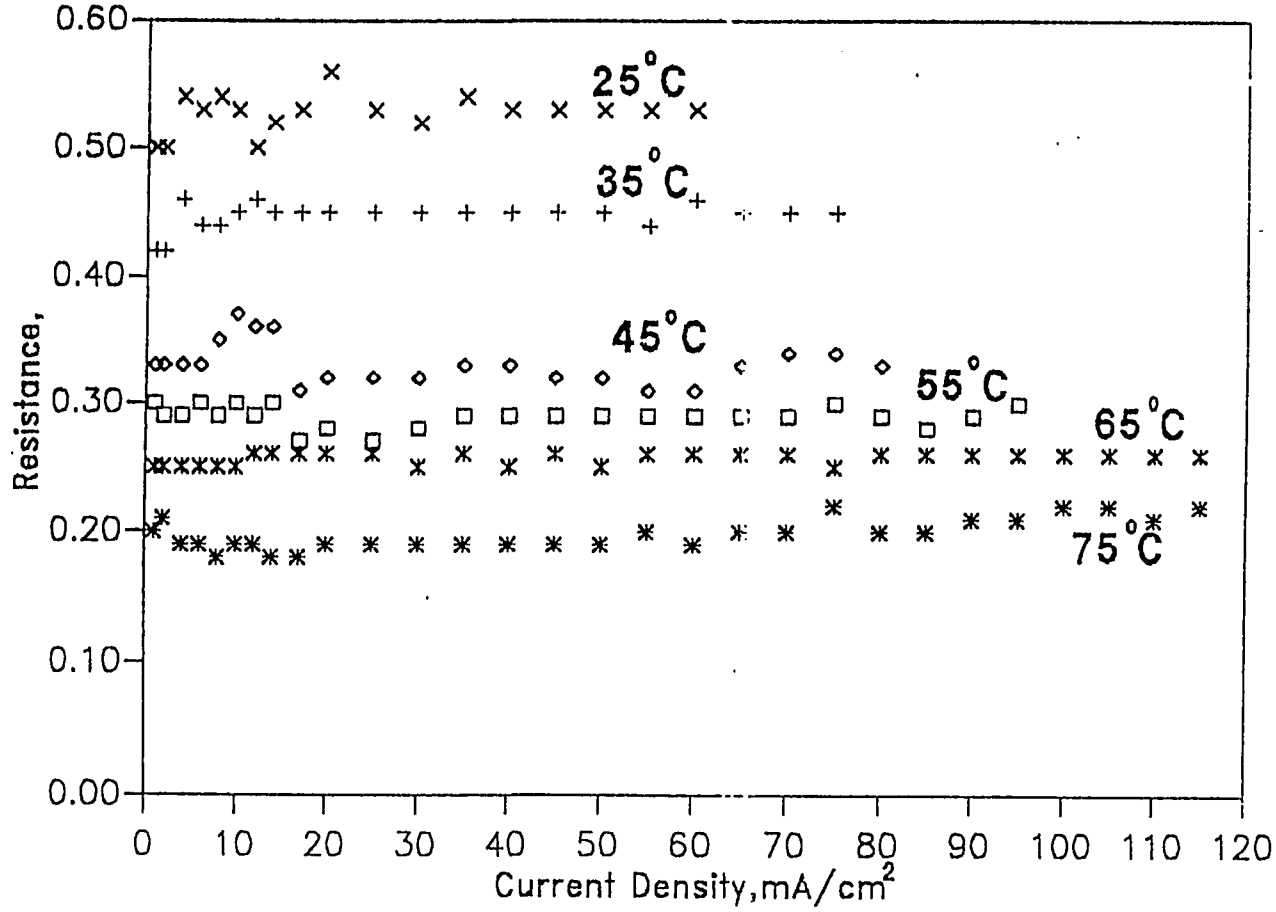

Fig. 7.3 Electrolyte Resistance as a Function of Temperature.

Table 7.1 Electrolyte Resistance as a Function of Temperarture

Temperature (°C)	Electrolyte Resistance (Ω)
25	0.527
35	0.447
45	0.331
55	0.2904
65	0.2565
75	0.1969

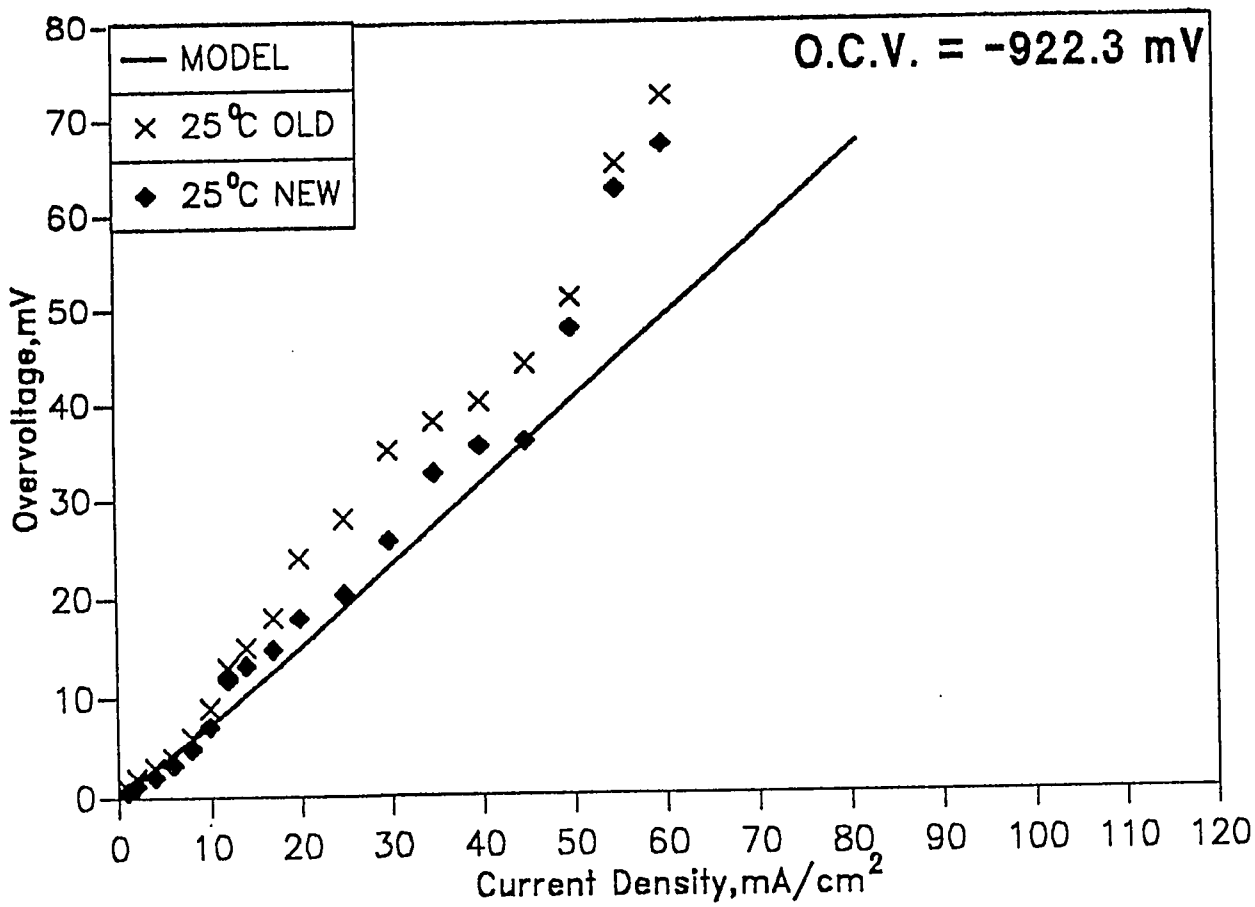

Fig. 7.4 Steady State Polarization Curve for Hydrogen Oxidation Reaction at 25°C.

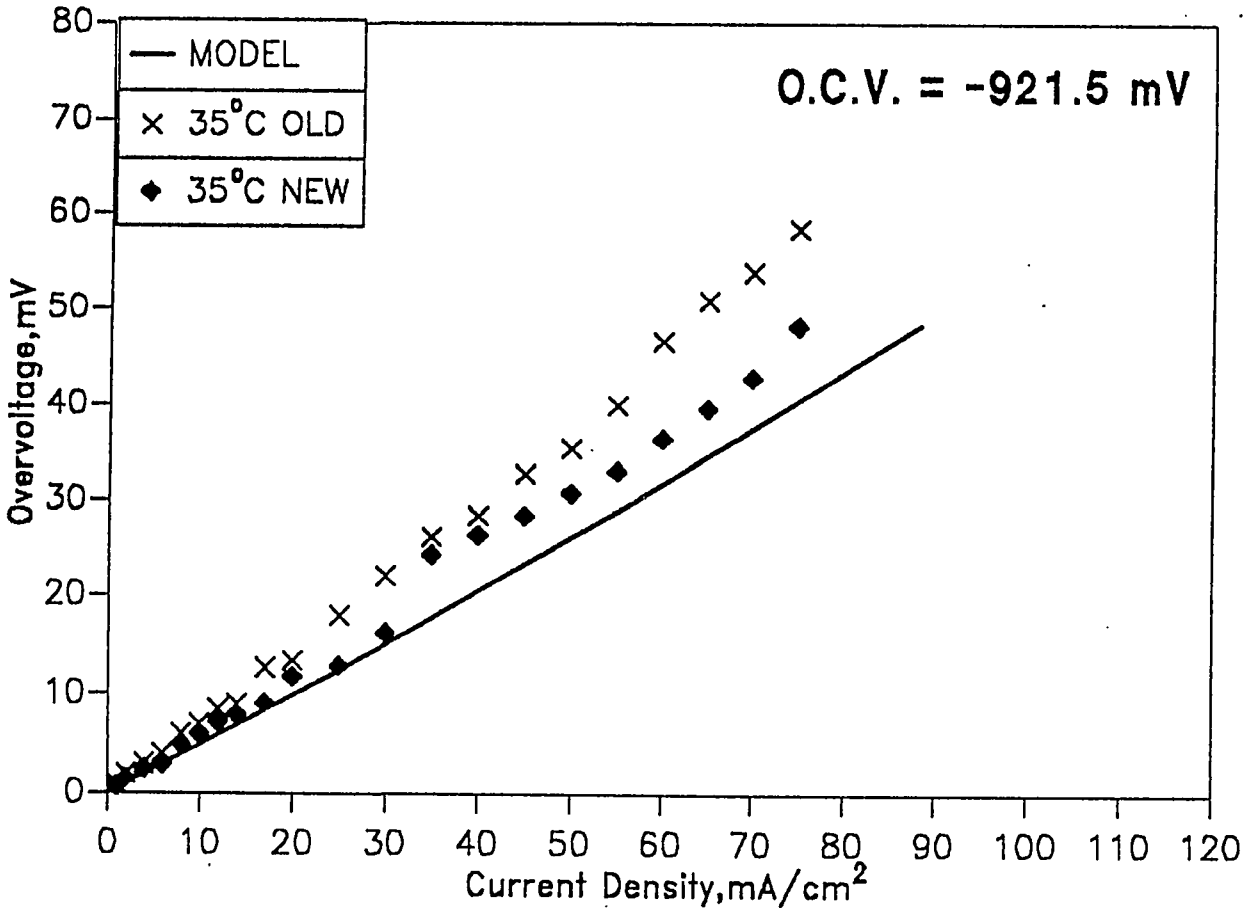

Fig. 7.5 Steady State Polarization Curve for Hydrogen Oxidation Reaction at 35°C.

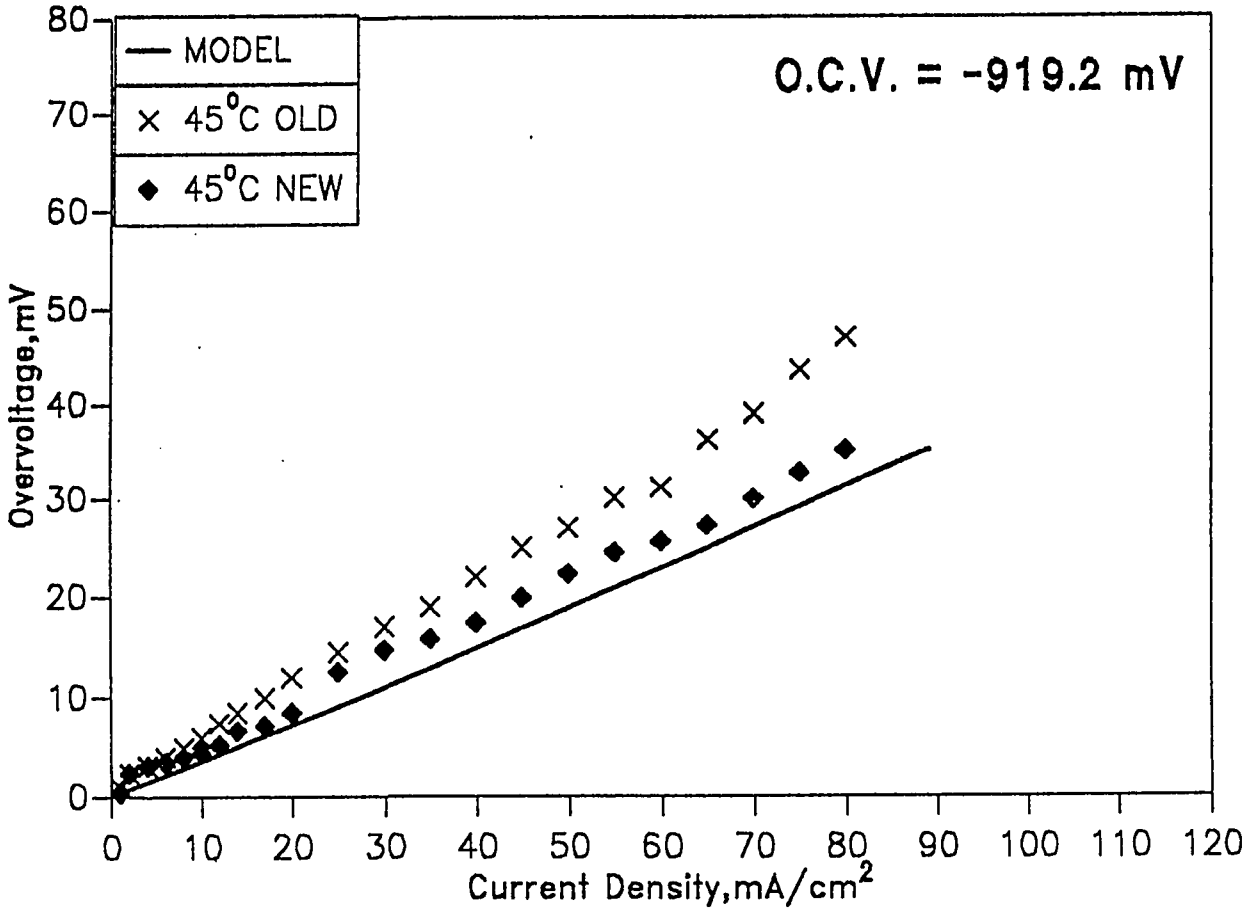

Fig. 7.6 Steady State Polarization Curve for Hydrogen Oxidation Reaction at 45°C.

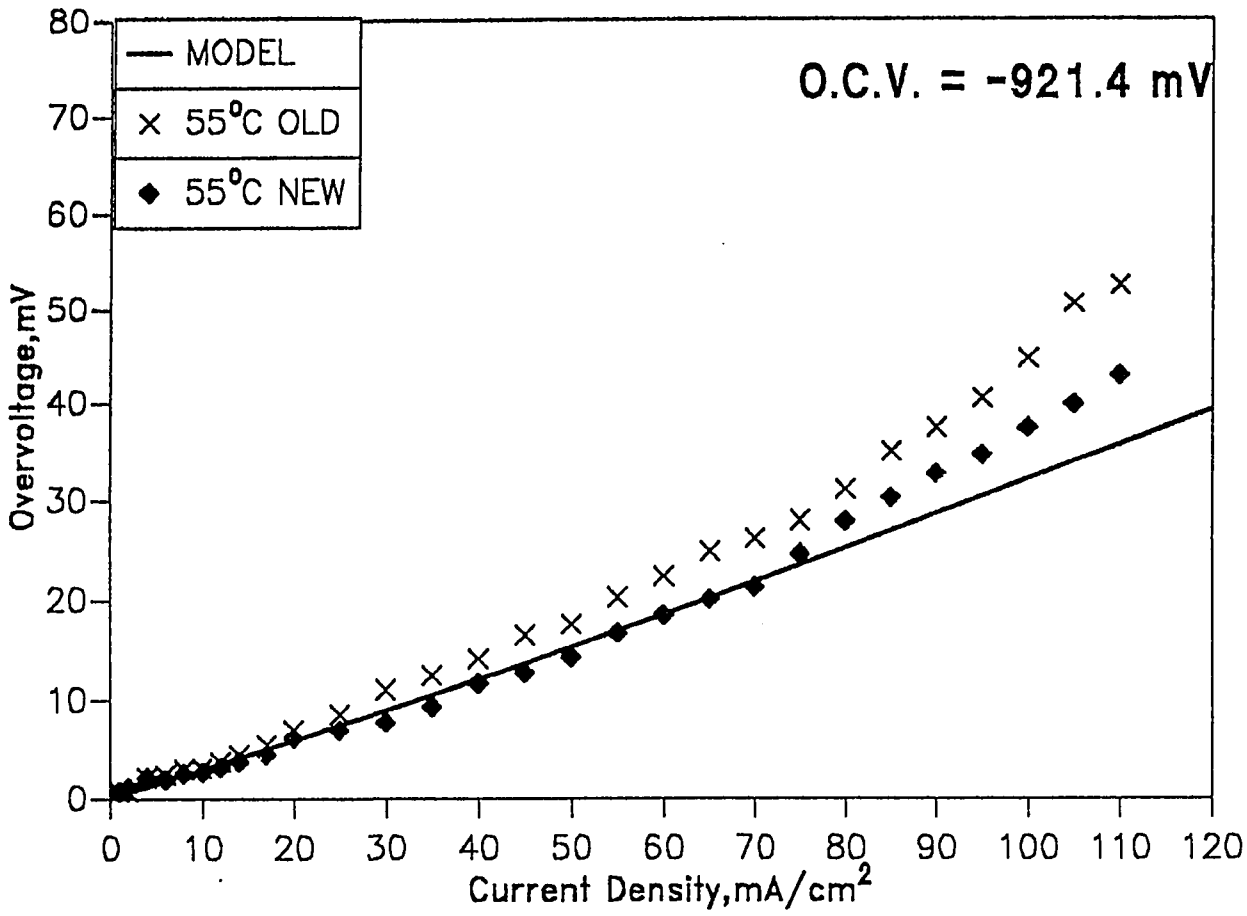

Fig. 7.7 Steady State Polarization Curve for Hydrogen Oxidation Reaction at 55°C.

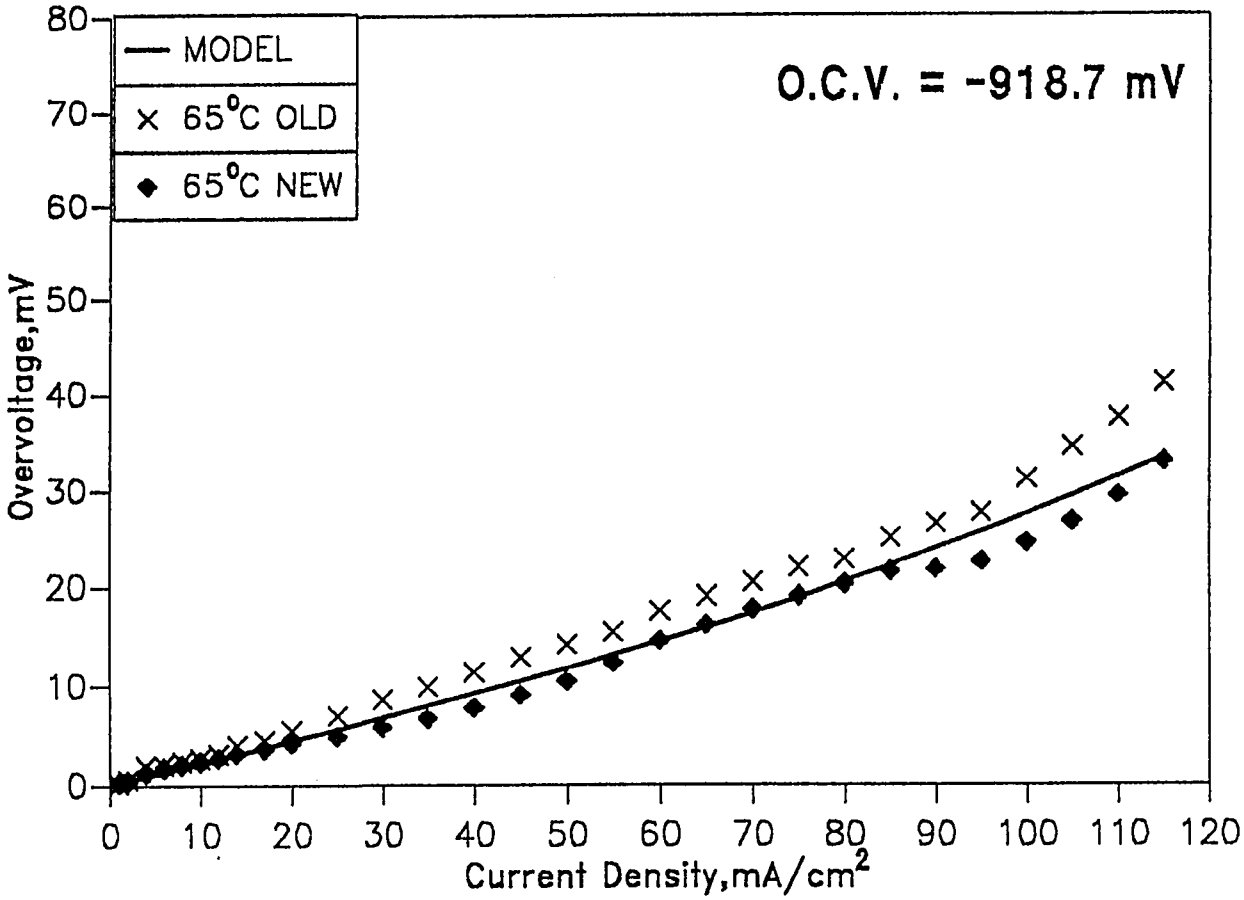

Fig. 7.8 Steady State Polarization Curve for Hydrogen Oxidation Reaction at 65°C.

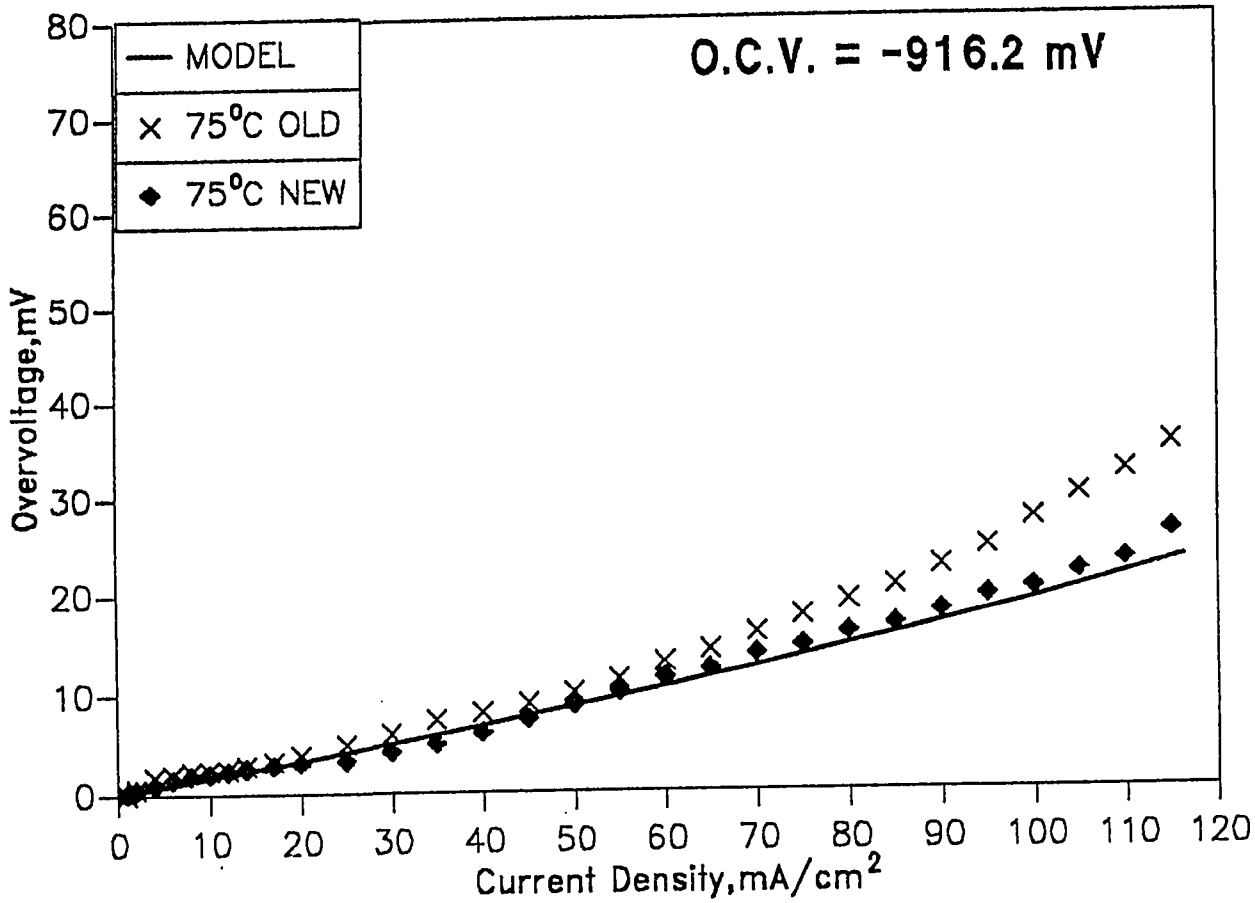

Fig. 7.9 Steady State Polarization Curve for Hydrogen Oxidation Reaction at 75°C.

7.2 Application of Spherical Raney Catalyst Grain Model

The spherical Raney catalyst grain model developed earlier (15) was applied to estimate the charge transfer coefficients and exchange current densities for the new electrode at different temperatures. The following model equation in dimensionless form ,

$$\frac{d^2\phi}{d\xi^2} = \frac{2nFD_iL^2}{\eta\kappa_i R} C_o(1-e^{-\frac{zF}{RT}\eta_o\phi})[\sqrt{\frac{i_o a}{nFD_iC_o}} Exp(\frac{\alpha zF\eta_o}{2RT}\phi) \coth\{R\sqrt{\frac{i_o a}{nFD_iC_o}}\exp(\frac{\alpha zF\eta_o}{2RT}\phi)\} - \frac{1}{R}] \tag{7.1}$$

with dimesionless boundary conditions is used for the parameter estimation.

B.C. 1 $\xi = 0$ $\phi = 1$

B.C. 2 $\xi = 1$ $\frac{d\phi}{dx} = 0$

Here,

φ = Dimensionless overvoltage $= \frac{\eta}{\eta_o}$

and ξ = Dimensionless electrode thickness $= \frac{x}{L}$

η_o is the measurable overvoltage at the electrolyte side of the electrode and L is thickness of the electrode.

difference method. The electrode current density at the electrolyte side of the electrode is given by

$$j(x) = -\kappa_e (1-\varepsilon_{mac}) \frac{d\eta}{dx}\Big|_{x=0} \tag{7.2}$$

Tables 7.2 and 7.3 gives respectively the temperature independent and temperature dependent input parameters used in the solution of equation 7.1.

Based on these parameters and experimental overvoltage values the model equation was solved to get theoretical current densities. The solid lines in figs. 7.4 to 7.9 also represents the current densities as predicted by the model.

7.3 Estimation of Kinetic Parameters

The spherical Raney-catalyst grain model was used to determine the kinetic parameters by comparing the predicted current density values with the observed experimental values and minimizing the sums of the squares of the difference between these two quantities. N data points from the experimental polarization curve were chosen and the objective function, S which was defined as the sum of the squares of the error

$$S = \sum_{1}^{N} (i_{cal} - i_{exp})^2$$

Table 7.2: Temperature -independent input parameters for Spherical Raney-Catalyst Grain Model

Stoichiometric Number	$z=1$
Electrons Transferred	$n=2$
Electrode Thickness	$L=380\mu m$
Avg. Grain Radius	$R=5\mu m$
Macroporosity	$\varepsilon_{mac}=0.3$
Microporosity	$\varepsilon_{mic}=0.4$
Tortuosity	$\tau_{mic}=2$
Active Surface Area	$f^{o}=8.3\times105\ cm^{-1}$
BET surface Area	$S=33.56\ m^2/g$
Catalyst Density	$\rho=4.117 g/cm^3$

Table 7.3: Temperature -dependent input parameters for Spherical Raney-Catalyst Grain Model

Temperature (°C)	25	35	45	55	65	75
Effective Diffusivity D_L (cm^2/s)*	1.6×10^{-5}	1.8×10^{-5}	2.0×10^{-5}	2.11×10^{-5}	2.32×10^{-5}	2.52×10^{-5}
Solubility Co (mol/cm^3)	2.0×10^{-7}	1.7×10^{-7}	1.4×10^{-7}	1.2×10^{-7}	0.92×10^{-7}	0.7×10^{-7}
Effective Electrical Conductivity κ_e ($\Omega^{-1}cm^{-1}$)*	0.254	0.300	0.344	0.390	0.434	0.480

*** Estimated from correlations in literature**

was evaluated by assuming a particular set of exchange current density (i_o) and charge transfer coefficient(α) values. The assumed values of i_o and α had upper and lower constraints based on physical considerations. At each temperature experimental data points were chosen on each polarization curve and the minimization procedure was carried out. Table 7.4 gives the best fitting values for i_o and α.

7.4 Apparent Activation Energy

The apparent activation energy, Ea for an electrochemical reaction is given at constant electrode potential by

$$E_a = \frac{R(\ln i_2 - \ln i_1)}{\frac{1}{T_2} - \frac{1}{T_1}} \qquad (7.3)$$

The potential of the reference electrode is dependent upon the temperature hence only apparent activation energies can be estimated.

The apparent activation energies for the new electrode for hydrogen oxidation reaction at overpotential, η = 10 mV, 25 mV and 50 mV were obtained from a plot(fig. 7.10) of logarithm of current density against the reciprocal of temperature. Table 7.5 gives the apparent activation energy for the electrode at different over voltages.

Table 7.4 Kinetic Parameters for Hydrogen Oxidation Reaction

Temperature °C	Charge Transfer Coefficient (α)	Exchange Current Density (i_o) mA/cm^2
25	0.57	6.6 E-6
35	0.59	15.1 E-6
45	0.60	31.0 E-6
55	0.61	52.7 E-6
65	0.63	118.5 E-6
75	0.65	310.0 E-6

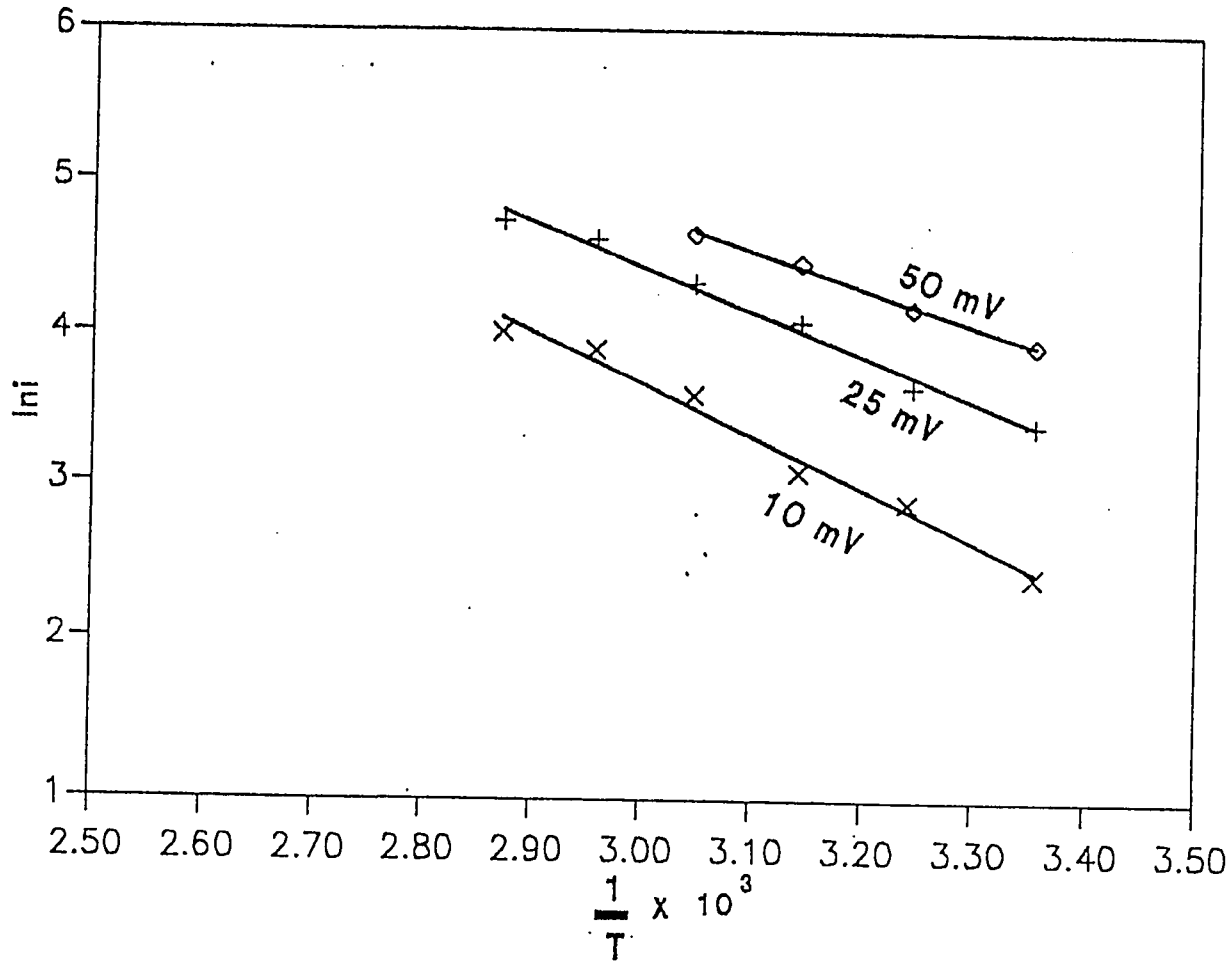

Fig. 7.10 Logarithm of Current Density(i) Vs 1/T for constant Overvoltage(η)

Table 7.5 Apparent Activation Energy at different Overvoltages

Overvoltage (mV)	Apparent Activation Energy (kJ/mol)
0	27.9
10	24.45
25	20.10
50	16.52

7.5 . Discussion of Polarization Results

It can be seen from figs. 7.4 to 7.9 that with increasing current density the IR free overvoltage i.e. losses also increase. For the range of current densities investigated it appears that the current density varies almost linearly with overpotential. This behavior is due to the fact that at lower polarization activation overpotential is very high while concentration and ohmic overpotentials are small.

From the figures it can be clearly discerned that the overvoltage at a given current density decreases with increase of electrolyte temperature. The reason behind this decrease in overvoltage at higher temperatures is still not clear. It is proposed that several different but partially co-operative and partially opposing processes are responsible for the experimentally observed phenomena of decrease in overvoltage with increase of temperature. Some of these processes are,

1. Change in electrolyte / gas hold up of the electrolyte.
2. Increase of electrolyte conductivity with increase of temperature.
3. Increase of exchange current density and charge transfer coefficient with temperature.

At 75°C the new electrode is able to support a current density of 115 mA/cm^2 at an overpotential of 24 mV(fig 7.9).While the old electrode could support the same current density at an overpotential of 35 mV. Under the experimental conditions kept for this study the overpotentials were always less than 70 mV. The polarization curve for the new electrode is always lower than that for the old electrode especially at higher current densities. This means the polarization resistance of the new electrode is smaller than the old electrode at

decrease in contact resistance(less Ohmic Polarization) brought about by copper present in the active layer and conducting grid. The new electrode also has a higher Electrocatalytic activity.

Fig. 7.3 shows the ohmic resistance of the electrolyte at various temperatures as a function of current density. From the figure it can be seen that the electrolyte resistance decreases with increase of temperature. This is because of the fact that at higher temperature the conductivity of KOH is more. In fact the conductivity of KOH increases more than twice from 25°C to 75°C as can be seen from the figure.

At 25°C (fig. 7.4) the electrode is not able to support current densities which are higher than 60 mA/cm^2. This implies that this is a limiting current density for the new electrode at 25°C. Thus the present value of limiting current density at 25°C makes the operation of the new electrode at room temperature very uneconomical. A through study of factors which affect the limiting current density is required to explain this decrease in limiting current density with decrease of temperature. The new electrode starts showing better performance at 55°C (fig. 7.6).

The apparent activation energy found for the new electrode at an overpotential of 10 mV is 28.63 kJ/mol. The activation energy for the new electrode at zero polarization is estimated to be 27.9 kJ/mol. For the previous electrode the activation energy was 31.35 kJ/mol. The lower value of activation energy indicates that lower activation energy results in lower polarization resistance. Which means better performance.

The kinetic parameters namely exchange current densities (i_o) and charge transfer coefficients(α) were estimated at different temperatures by using the spherical flooded Raney catalyst grain model and the experimental polarization curves. Table 7.4 gives the values of i_o and α for the new electrode. The exchange current density follows an exponential relation with temperature(fig.7.11). The exchange current densities and charge transfer coefficients estimated for the new electrode are greater than those for the previous electrode. For example at 75°C the i_o for the new electrode is found to be 3.10×10^{-4} A/cm^2 while for the old electrode it was 2.80×10^{-4}A/cm^2. The addition of Cu_2O to the catalyst is responsible for bringing about this increase in the exchange current density.

7.6 Experimental Results for Long Term performance Test

Steady state potentiostatic long term performance tests were carried out for the new electrode at various temperatures. The voltage between the test electrode and reference electrode was kept constant and current (i.e. Reaction rate) was monitored as a function of time.

For plotting the potentiostatic transient current decay experimental results the concept of Residual Electrode Activity (R.E.A.) was used. Residual electrode activity (R.E.A.) is defined as the ratio of electrode current density at any time = t to the initial electrode current density at time = 0. Thus,

$$\text{R.E.A.} = \frac{i_{t=t}}{i_{t=0}}$$

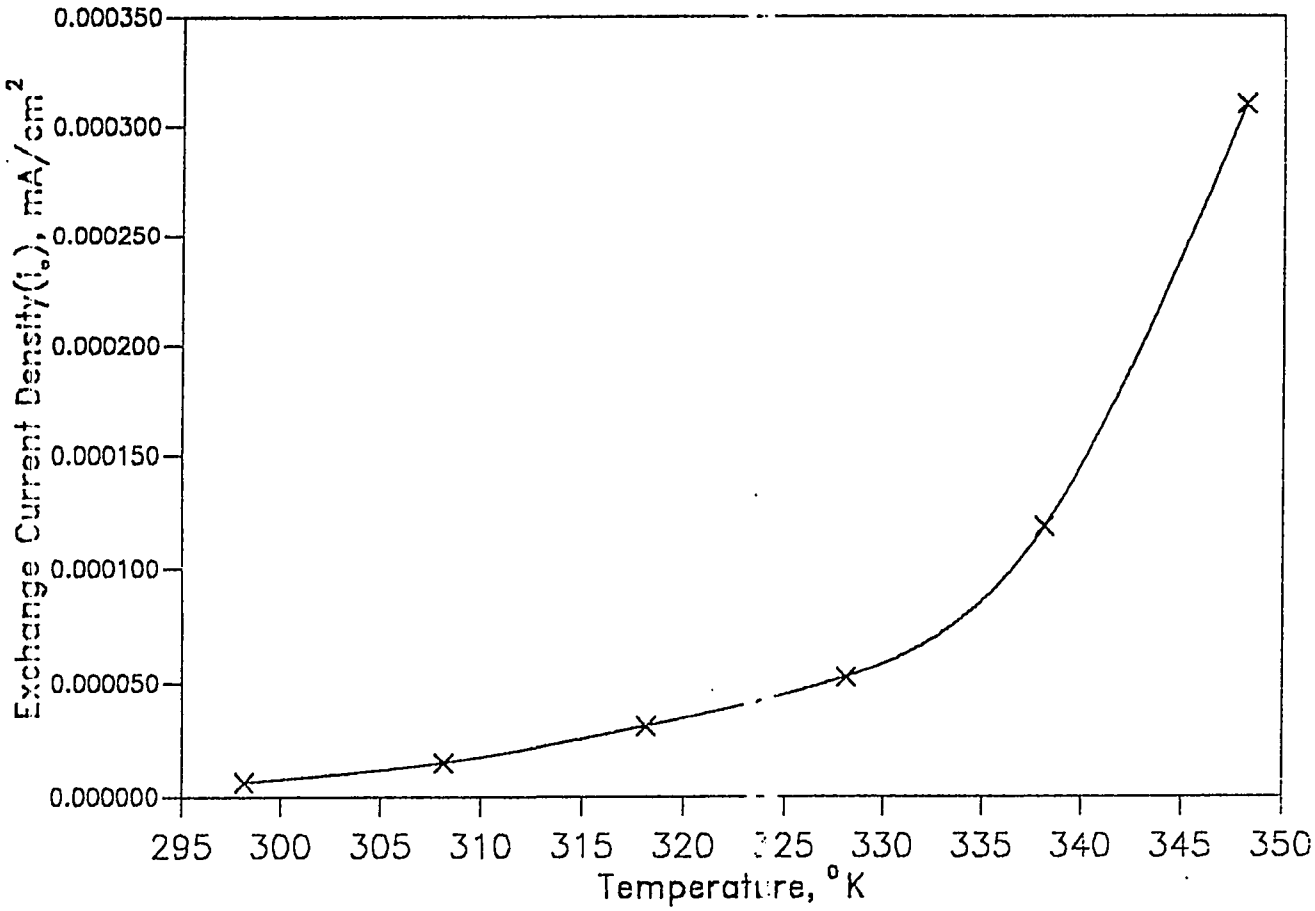

Fig. 7.11 Exchange Current Density as a Function of Temperature

Figs. 7.12 to 7.14 show the results of potentiostatic long term performance test on the new electrode at various temperatures.

Galvanostatic steady state long term performance test of the new electrode was also carried out for the new and previous electrode. For this particular test the current flowing through the half cell was kept constant and the potential of the test electrode was observed as a function of time. Fig. 7.15 shows the result of galvanostatic long term study.

7.7 Application of Deactivation Model

The spherical flooded Raney catalyst grain model has been modified to study the effect of deactivation phenomena in gas diffusion electrodes. The deactivation model assumes a first order reactant-gas-concentration-independent deactivation. The activity of the catalyst is then at any time t is given by

$$\bar{a} = \bar{a}_o \exp(-K_d t) \qquad (7.4)$$

Where a_o the activity of the catalyst at zero time as unity. The equation 7.4 can be written as

$$\text{R.E.A.} = \exp(-k_d t) \qquad (7.5)$$

The time dependent electrode current densities for an isothermal gas diffusion electrode with no gas diffusion limitation in the macropores is given by the following expression,

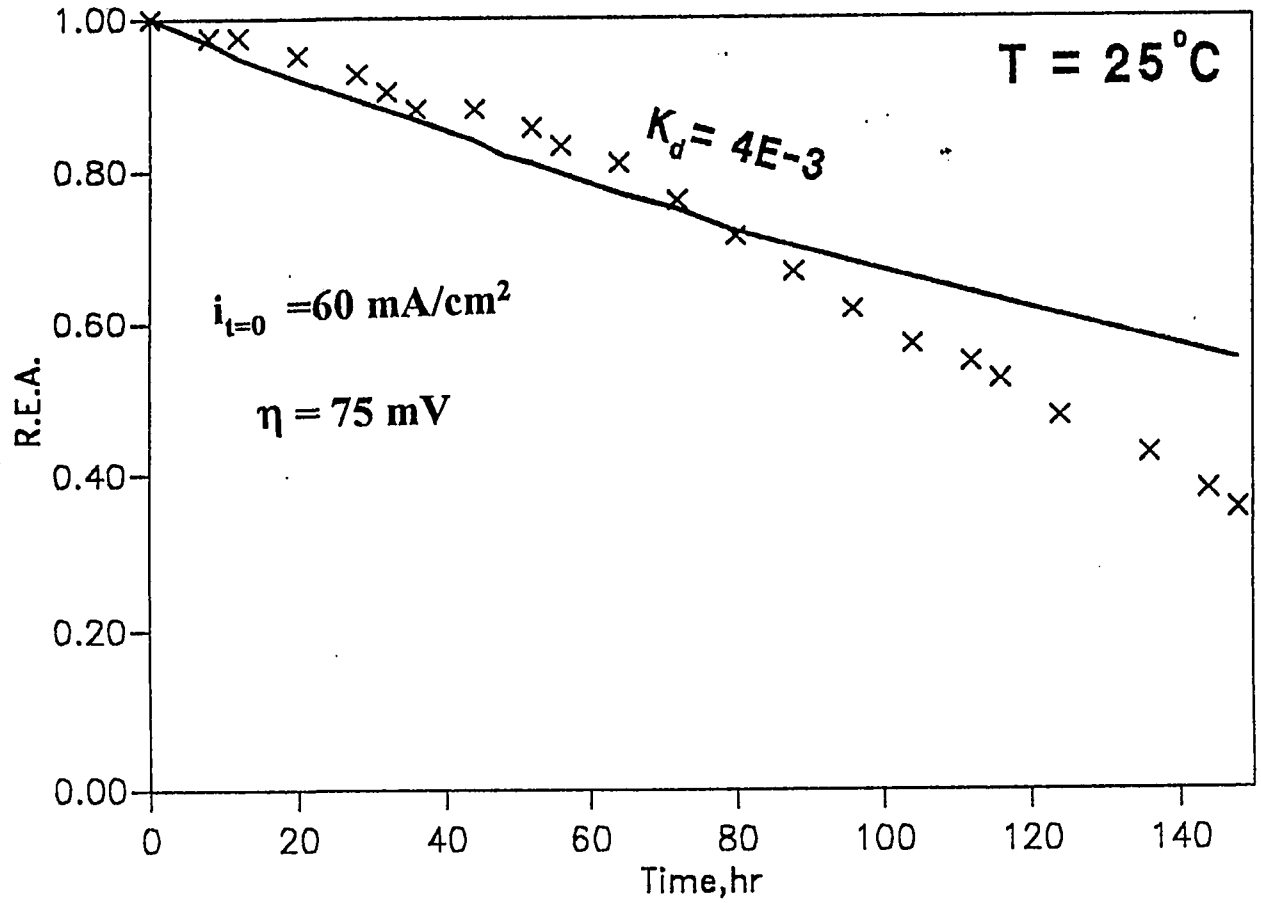

Fig. 7.12 Potentiostatic Long Term Performance Test at 25°C

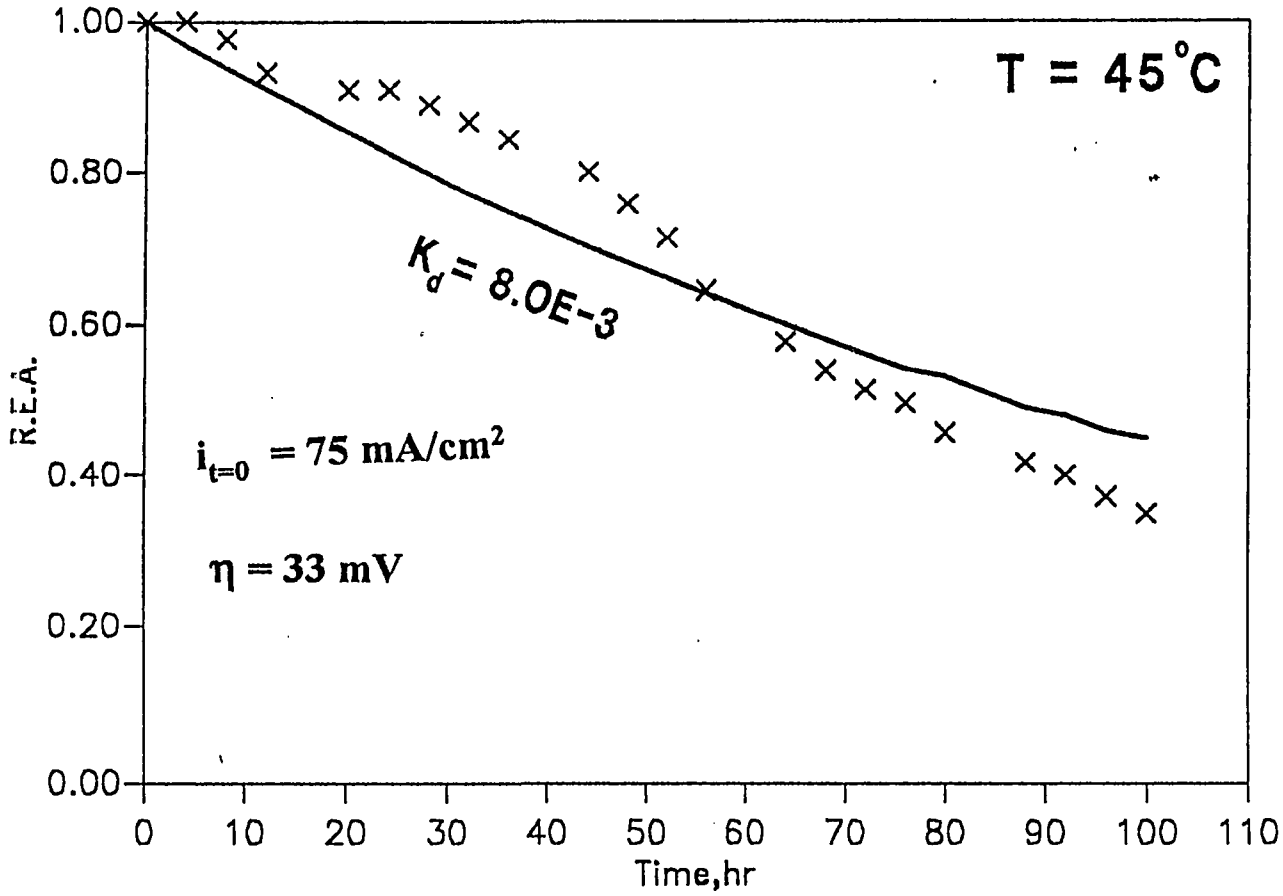

Fig. 7.13 Potentiostatic Long Term Performance Test at 45°C

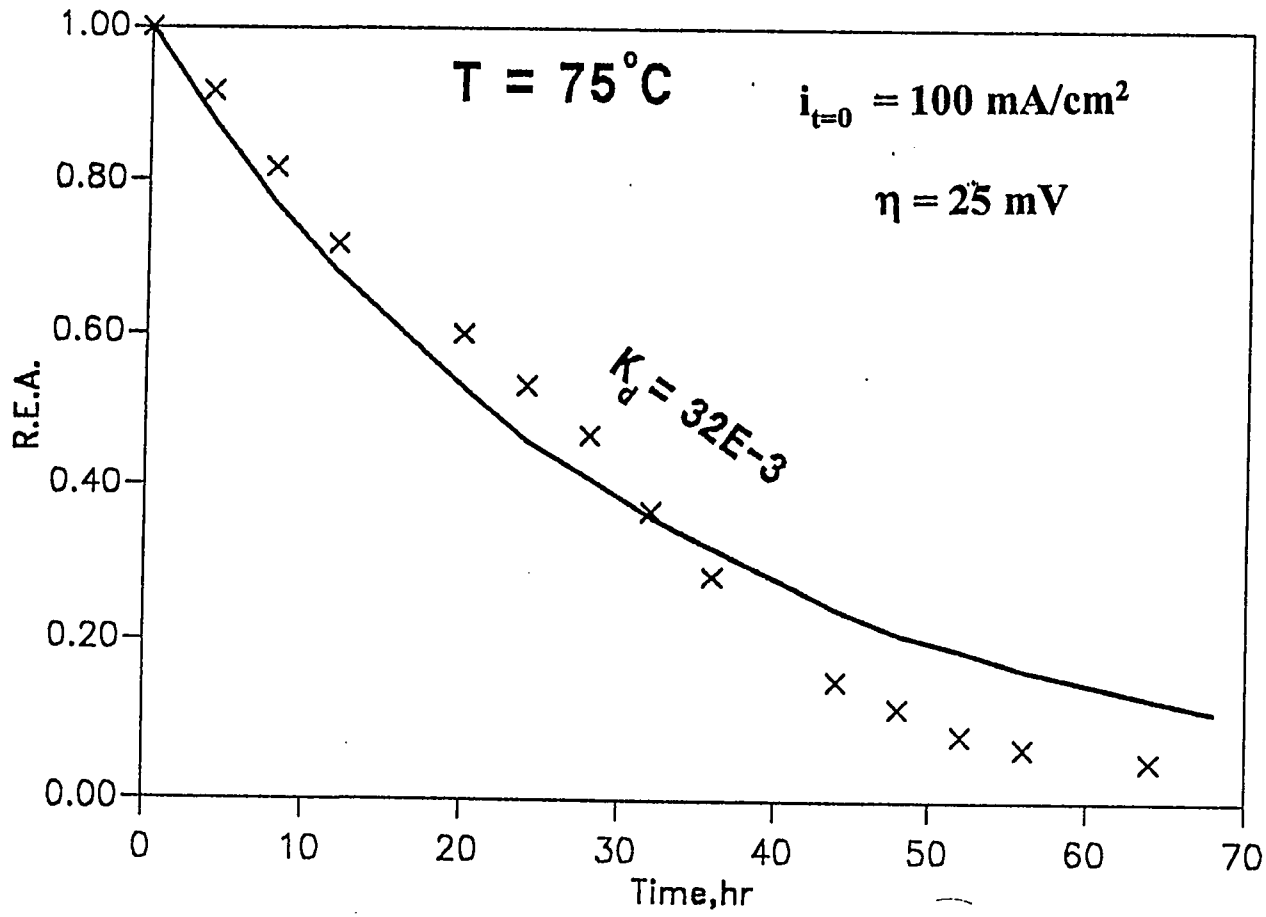

Fig. 7.14 Potentiostatic Long Term Performance Test at 75°C

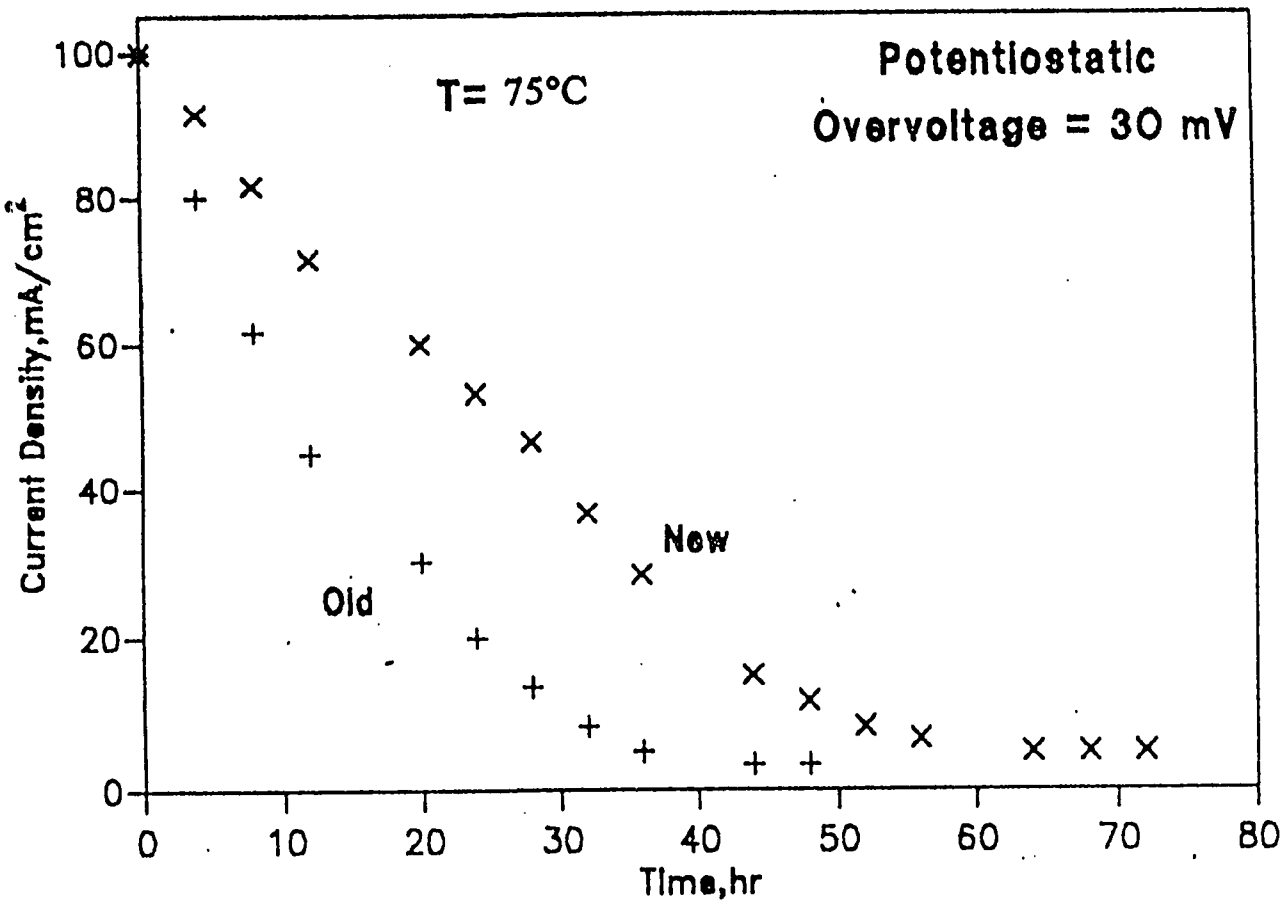

Fig. 7.15 Potentiostatic long term performance of the new and old electrode at 75°C

$$\frac{d^2\eta}{dx^2} = \frac{2nFD_L}{\kappa_e R} C_o (1 - \frac{A_3}{A_2})[\sqrt{\frac{i_o f^o}{nFD_L}} \exp(\frac{-K_d t}{2}) \sqrt{\frac{A_2}{C_o}} \coth\{\sqrt{\frac{i_o f^o}{nFD_L}} \exp(\frac{-K_d t}{2}) \sqrt{\frac{A_2}{C_o}} R\} - \frac{1}{R}] \tag{7.6}$$

with the boundary conditions as

B.C.1 x=0 $\eta = \eta_o$

B.C.2 x=1 $\frac{d\eta}{dx} = 0$

here,

$$A_2 = \exp(\frac{\alpha zF}{RT}\eta)$$

$$A_3 = \exp[\frac{-(1-\alpha)zF}{RT}\eta]$$

Equation 7.6 when solved with the above boundary conditions and a set of parameters including deactivation rate constant gives the time decay of electrode current densities.

7.8 Estimation of Deactivation Constant

The rate of reaction for an electrochemical reaction is given by current density. The decay of the electrode current density is assumed to be exponential with time. Therefore for estimating the apparent deactivation constant logarithm of the current density was plotted against time on stream. Fig. 7.16 gives the best fit

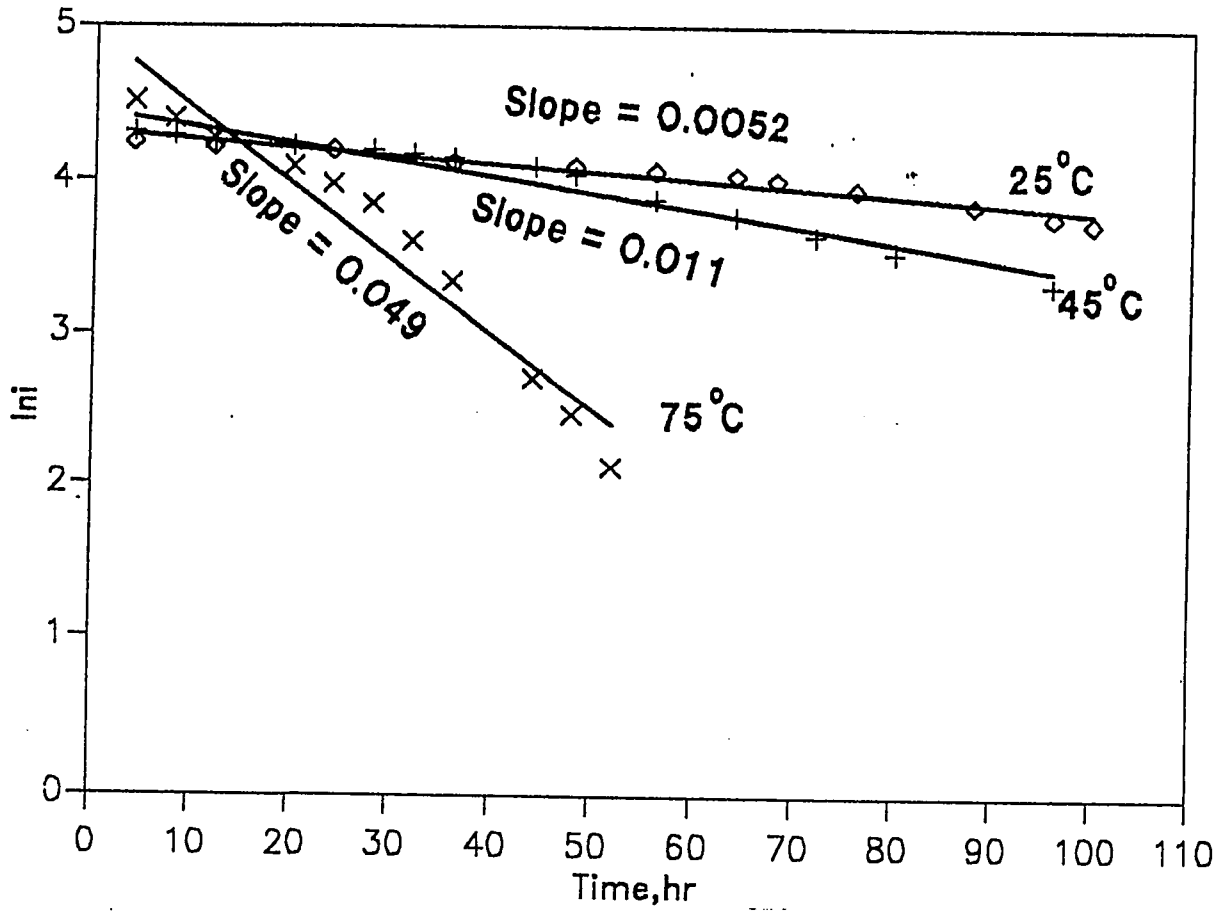

Fig. 7.16 Logarithm of Current Density as a Function of time on stream.

line to the lni versus t data. From the slopes of these lines the apparent deactivation constants are estimated at each temperature.

For estimating the deactivation constant by the modified spherical Raney catalyst grain model. The model was fit to the experimental R.E.A. versus time data by curve fitting with the deactivation rate constant(Figs. 7.12 to 7.14). The deactivation rate constant was determined by a similar approach as that was used for estimating i_o and α. However in this case the calculated and experimental current densities were functions of time only. The experimental R.E.A. versus time plots were used as a basis for the model equation to fit. N data points were chosen from the experimental curve and the function,$S = \sum(i_{cal}-i_{exp})^2$ was evaluated by assuming a particular value of K_d. In this case there was only one parameter for curve fitting therefore it was not possible to predict the new steady state reached by the electrode upon deactivation. Table 7.6 gives the apparent deactivation constants at three different temperatures.

7.9 Characterization of Deactivated Electrodes

The deactivated Raney-Ni/ PTFE electrode has been characterized by

1. BET Surface Area Measurement
2. X Ray Diffraction
3. Scanning Electron Microscopy

The main purpose behind carrying out this characterization was to find morphological and chemical changes due to deactivation. BET surface area measurement gave the surface area of the deactivated electrode sample to be $16.32 m^2/g$. The BET surface area for the fresh electrode was $24\ m^2/g$. The decrease in surface area of the electrode can be correlated with the deposition of

Table 7.6 Apparent Deactivation Constants at Different Temperatures

Temperature °C	App. Deactivation Constant (Model) hr^{-1}	App. Deactivation Constant(Plot) hr^{-1}
25	4.0 E-3	5.2 E-3
45	8.0 E-3	11.0 E-3
75	32.0E-3	49.0 E-3

KOH on the micropores. There was no K in the fresh electrode. The XRF analysis confirmed the presence of potassium in the deactivated sample. Fig. 7.17 gives a micro graph of the deactivated sample from the mesh side. Fig. 7.18 gives EDS spectra for the deactivated sample.

7.10 Discussion of Deactivation Results

The performance of a gas diffusion electrode depends on two main factors namely,

1. A suitable micro geometrical structure to have maximum gas-liquid interfacial area.
2. Improvement of the local intrinsic activity of the surface by using appropriate electrocatalyst.

The structure of the active layer or the reaction layer where electrochemical reaction occurs constitutes the most important part of a gas diffusion electrode. The steps which could control the current produced are

a) The supply of reactant gas to gas side of active layer.
b) Diffusion of reactant gas through the active layer to gas-liquid interface.
c) Diffusion of dissolved gas from gas-liquid interface to catalyst clusters.
d) Reaction at catalyst clusters.

The slowest step is the diffusion of dissolved gas to the catalyst clusters located throughout the reaction layer. More gas-liquid interfacial area throughout the reaction layer reduces the gas diffusion distance and thus improves the performance of gas diffusion electrode.

Fig. 7.17 SEM Micrograph of the Deactivated Electrode from mesh side.

```
SEEE\E\ETUP SSQ

SSQ: SSQ

SEMI-QUANTITATIVE ANALYSIS: M416: SAMP B,SQUARE
EL    NORM. K-RATIO

CU-K 0.43581 +- 0.00342
AL-K 0.00198 +- 0.00014
NI-K 0.51300 +- 0.00330
K -K 0.04636 +- 0.00054

ZAF CORRECTION        20.00 KV        40.00 Deg.

No. of Iterations  1
--      K      [Z]    [A]    [F]   [ZAF]  ATOM.%  WT.%
CU-K  0.435  1.032  1.000  1.000  1.032  40.47  44.13
AL-K  0.002  0.934  3.954  0.999  3.940   2.58   1.19  *
NI-K  0.513  0.986  1.000  1.000  0.986  49.43  49.69
K -K  0.041  0.9[illegible]  [illegible]  [illegible]  [illegible]  [illegible]  [illegible]
 * - High Absorbance

SSQ:

: TN-5500 UPM - Saudi Arabia JSM-840          SUN 21-FEB 9[illegible]  11:4[illegible]
:Cursor: 0.000KeV = 0          ROI      (1) 0.000: 9.640
```

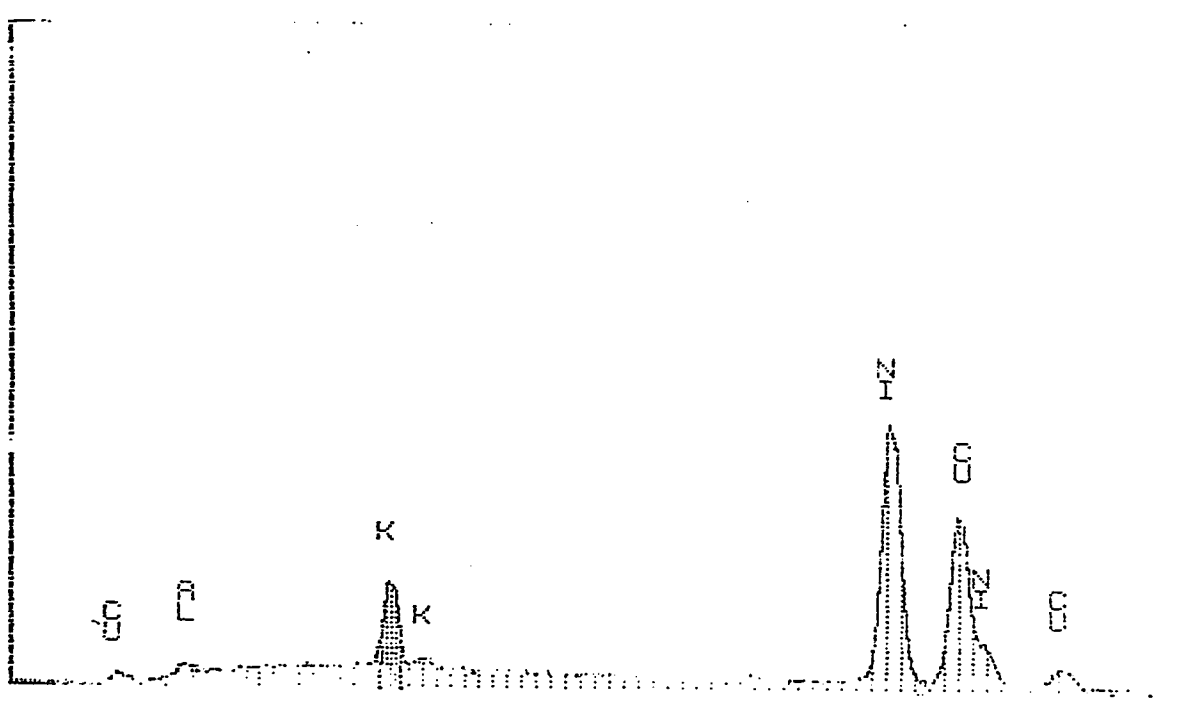

Fig. 7.18 EDS Spectra for the Deactivated Electrode.

The decay of electrode current density (figs. 7.12 - 7.14) with time on stream is a cumulative effect of combination of several independent processes.

Ewe, Justi and Selbach(26) have reported that the method of heat treatment employed during catalyst preparation affects stability of fuel cell electrodes. During catalyst preparation after leaching out Al- fraction of the basing Raney-Ni sponge obtained is dried in vacuum. This drying is accomplished by slow air oxidation of the sponge. This air oxidation of the catalyst produces α-$3Ni(OH)_2$ $2H_2O$ which is very active but unstable. Therefore further complicated heat treatment is done to convert α- hydroxide to more stable NiO. Not all α-hydroxide gets converted into NiO. During this heat treatment process a recrystallization of the strongly disordered Raney-Ni sponge occurs.

Maximovitch and Durand (61) have confirmed that α-$3Ni(OH)_2$ has a passivating effect on the hydrogen oxidation reaction. Moreover due to recrystallization of Raney-Ni sponge coarser catalyst grains are formed(26). Electrodes fabricated from coarser catalyst grains show lower performance due to slow hydrogen diffusion into the catalyst particles(20).

Uneven current and potential distribution in the active layer leads to electrode corrosion. Because of heterogenity of the electrode structure the current and potential distribution in the active layer are uneven. Therefore in some regions the local overvoltage may be quite high. This high overvoltage results in the anodic dissolution of copper thereby causing deactivation.(20)

Inability of hydrogen to reach the minor fractions of electrode. In the active layer macropores are filled with gas while micropores are flooded with

electrolyte. Not all hydrogen can reach the smaller pores of the active layer because of slow diffusion. The initial heat of adsorption for hydrogen on Raney-Ni is approximately 90 kJ/mol(62). This initial high heat of adsorption results in the evaporation of the electrolyte. This evaporated electrolyte then subsequently cools down and deposits on the gas diffusion pores. This deposition of electrolyte on the gas pores offers diffusion resistance to the diffusion of hydrogen. The gas diffusion process being slowest controls the generation of current in gas diffusion electrode.

Rotenberg and Srinivasan(63) have shown that KOH solution affects the hydrophobicity of PTFE. They carried out contact angle measurement experiments with KOH solution and teflon. They concluded that with increase in temperature and KOH concentration, PTFE undergoes chemical changes e.g. change of roughness. Thus the chemical change in hydrophobicity of PTFE brought about by KOH solution results in depletion of gas diffusion macropores. This affects the rate of current production.

Atmospheric carbondioxide dissolves in KOH solution and reacts with it. The reaction of CO_2 with the hydroxyl ions to form carbonate species which can precipitate and may block the micropores of Raney-Ni electrode. It can also stay as liquid and reduce the ionic conductivity of the electrolyte. Lower wettability and pH rise in the carbonate - containing electrodes results in lower performance when compared with pure KOH solution.(64)

The extent to which each of the above factors affect the decay of electrode current density requires further in-depth study of deactivation phenomena.

BET surface area measurement for the spoiled electrode indicate less surface area as compared to the fresh electrode. A significant part of the change in surface area is also brought about by the evaporation of water and deposition of KOH on the pores after removing the electrode from half cell. The presence of K in the active layer of the electrode has been confirmed by SEM and XRF analysis.

From figs. 7.12 to 7.14 it can be observed that initially the deactivation is slow. As the time on stream increases the deactivation becomes more rapid. This suggests the possibility of two deactivation mechanisms. This behavior can be explained by considering the diffusion resistance of the feed gas in the active layer of the electrode. Initially high heat of adsorption evaporates electrolyte. With increase of time on stream the KOH deposited in the pores increases diffusion resistance. Hence the rate of deactivation also increases.

From figs. 7.12 to 7.14 it can be easily seen that the decay of current density is more at higher temperature than at lower temperature. This behavior can be explained by the fact that at higher temperature more KOH gets evaporated. Also at higher temperatures nickel hydroxide is more unstable. It gets converted into NiO which passivates the electrode.

Table 7.6 gives the values of apparent deactivation constants at different temperatures estimated from lni vesus t plot and the deactivation model. From the table it can be deduced that the apparent deactivation constant estimated from the plot is lower than that of deactivation constant obtained by the deactivation model. This discrepancy is due to the negligence of mass transfer terms in the modified

spherical Raney catalyst grain model. From this it can be concluded that the diffusion limitation plays an important role in the deactivation behavior.

From potentiostatic long term performance test (ref. fig. 7.15) performed on the new and previous electrode it can be observed that the previous electrode decays faster than the new electrode. Copper impregnation adds to the stability of the new electrode. The activity of the new electrode for hydrogen oxidation at 75°C becomes very small in about 60 hrs while the previous electrode gets destroyed in 40 hrs at the same temperature. Thus it can be conferred that the long term performance of the new electrode is better than that of the previous electrode.

Chapter 8
CONCLUSIONS

1. The polarization of the new electrode is found to be less as compared to the electrode used in earlier studies in our laboratory. The performance of the new electrode is higher at higher current densities. Copper impregnation and improved micro geometry of the new electrode contribute to its better performance. The use of Cu mesh instead of Ni mesh reduces the contact resistance of the new electrode.

2. The values found for the exchange current densities for the new electrode were 6.6 E-6 A/cm^2(@ 25°C) and 3.1 E-4 A/cm^2(@ 75°C). While the charge transfer coefficient varied from 0.57 to 0.65 in the temperature range studied. The kinetic parameters namely exchange current density and charge transfer coefficient estimated for the hydrogen oxidation reaction on this new electrode are higher than that of the previous electrode. The higher value of the kinetic parameters for the new electrode gives less activation energy(28 kJ/mol). This shows better electrocatalytic activity.

3. The deactivation constant varied from 4 E-3 hr^{-1} at 25°C to 32 E-3 hr^{-1} at 75°C The deactivation constant estimated for the new electrode increases with temperature. Higher temperature and higher current densities are detrimental to the life of electrode. Copper improves the stability of the new electrode.

Chapter 9

RECOMMENDATIONS

1. The polarization behavior of the electrode should be investigated for higher current densities so as to obtain limiting current densities.

2. Impedance spectroscopy with an appropriate impedance model should be applied to the electrode so as to analyze the contribution of Ohmic, Faradaic and mass transport resistances to the effective impedance of the electrode.

3. The performance of electrode prepared by Dry Method and Wet Method should be investigated to arrive at the optimum fabrication technique. Attention should be paid to improve the gas-liquid interfacial area.

4. Raney - Ni should be alloyed with some other metals like Cr, Ti and impregnated with Copper to improve the electrocatalytic activity.

5. The effect of electrolyte concentration on the exchange current density and deactivation constant should be studied.

6. A deactivation model which takes into account the diffusion of reactant gas should be developed.

REFERENCES

1. Srinivasan, S."Fuel Cells for Extraterrestrial and Terrestrial Applications." J. of Electrochem. Soc.,136/2,1989:41C-48C.
2. Kleywegt,G.,J.and Willem L.,Driessen."Fuel Cells Revisited."Chemistry In Britain,May 1988:447-450.
3. Lindstorm,O."Fuel Cell Technology and Applications." Chemtech Aug. 1988 :490 - 495
4. Walsh, M.,P."The importance of fuel cells to address the global warming Problems" J.of Power Sources,29,1990:13-28.
5. Benjamin,T.,J.Camara and Marianowski."Handbook of Fuel Cell Performance " USDOE contract no.EC-77-C-03-1545:1980.
6. Prentice,G."Fuel Cells: Principles and Prospects."Chemtech, Nov.1984:684-694.
7. Broek,Vanden H."Alkaline Fuel Cells at ALENCO."J. Power Sources, 29,1990:201-206.
8. "Recent Developments in Fuel Cells", J. Electrochem. Soc. 139/10 October 1992:3008-3010.
9. Applby ,A.J. and Foulkes,F.R.`FUEL CELLS HANDBOOK.`Van Nostrand Reinhold,N.Y.,1989.
10. Bacon,Francis T."The Fuel Cell:Some Thoughts and Recollections."J. Elechem. Soc. Jan.,1979:7C-17C..
11. Fickette,A..,P."Fuel Cells."Encyclopedia of Physical Science and Technology, Vol.5,Academic Press Inc. 1987:629-639.
12. Strasser,K."The Design of AFC." J. Power Sources,29,1990:149-168.
13. Linden,D."Handbook of Batteries and Fuel Cells."Mc-Graw Hill,1983.

14. Kordesh ,K. and Jehangir, S. Electrochemica Acta 29,1989:1984-1988.

15. Celikar,H."Effect of carbon monoxide,carbon dioxide and nitrogen on the electrokinetics of Gas Diffusion Electrodes in Hydrogen/Oxygen Alkaine Fuel Cells." PhD Dissertation, KFUPM, OCT:1990.

16. Hammet, A. and Troughton,"Electrocatalysis and the Direct Methanol Fuel Cell." Chemistry and Industry,July 1992:482-483.

17. Kordesh,K.V.,J. Electrochem. Soc.,125(3),1978:77C.

18. Bacon,F.,T.,Adams,A..M. and Watson,R.G.H.,FUEL CELLS ,Chap.4, Ed.W. Mitchell,Academic Press,1963.

19. Niedrich,L. and Alford, H. R.,J. Elechem. Soc.,112,1977:117.

20. Jenseit,W.,Khalil, A.,Wendt,H.,J. of Applied Electrochemistry, 20:1990:893.

21. Mund,K.,Richter,G.,Von Sturm,F.,Journal Elechem. Soc.,124(1),1977

22. Ewe,H.,Justi,E.,Schmidt,A.,Energy Conversion,14,1975:35.

23. Tomido and Nakabayashi,J. Elechem. Soc.136(11),1989:3296

24. Ewe,H.,Justi,E., Schmidt,A.,Energy Conversion,20,1980:75.

25. Ewe,H.,Justi,E.,Selbach,H., Energy Conversion and Management, 23:1983:245.

26 Ewe,H.,Justi ,E.,Selbach,H.,Energy Conversion and Management, 4:1984:89.

27. Ewe,H.Justi,Selbach,H.,Energy Conversion and Management, 24:1984:94.

28. Brennecke,P.,W.,Ewe,Justi,and Selbach,Energy Conversion and Managemt, 24:1984:98.

29. Kenjo,T.,Bulletin Chemical Soc. Japan,54:1981:2553.

30. Kenjo,T.,Bulletin Chemical Soc. Japan,56,1983:1.

31. Candy,J.,P.,and Foilloux P.,J.Chemical Soc. Farady Trans.79,!983:823.

32. Markina,E.,L.,Tarasevich,M.,R.,Efremov,B.,Electrochimiya,24,1988:93.

33. Moren, C.,J.,Jouranl Elechem. Soc. 132(2)1985:383.

34. Padyukova,G.,L et. all Electrokhimiya,22,1986:247.

35. Kenjo,T.,J. Elechem. Soc.,132(2),1985:383.

36 Mund, K.,Richter, G.,Van Strum , "Electrocatalysts for the Reactions in AFC." Proceedings workshop on `Electrocatalysis of Fuel Cell Reactions. Vol.79- 2,Eds.Graday, Srinivasan, Dudley, 1978:67.

37. Pattabiraman,R. et. all `Transaction of the SAEST`,22(1),1987:25.

38. Grune,H.,Siemens, F.,Entwickl-Ber,12(5),1983:285.

39. Abramazon O. ,S., Chernyshov, Pshenickov, Electrochimiya, 12(11), 1976.

40 Al-Saleh ,Gultekin,Zakri and Celikar.,"Kinetics of Electrochemical Reactions:An Overview." Proceedings ofThird National Meeting of Chemist KFUPM, March, 1989:537-548.

41. Heitz,E. and Kreysa,G.,"Principles of Electrochemical Engineering." Extended version of a DECHEMA Experimental Course,FRG,1986.

42. Tilak,B.V.,Yeo and Srinivasan."Comprehensive Treatise of Electrochemistry."Plenum Press,1981:39.

43. Bockris,J.O.M and Reddy,A.K.N.,"Modern Electrochemistry." Vol. 2 Plenum Press ,1970.

44. Bockris,J.O.M. and Srinivasan,S."Fuel Cells:Their Electrochemistry." Chapter 9,McGraw Hill ,1969:469-510.

45. Austin,L.G., Ariet, M., Walker, Woods, Comyan, IEC Fundamentals 4:1965:321.

46. Chan, K. Y., Efthymiou, G. S., Cochetto, J.F. Electrochimica Acta 32,1987:1227.

47. Chirkov, Yu.G., Soviet Electrochemistry,8,1972:358.

48. Pshenichnikov,A.G., Kruyukov,Yu.K., Burshtein,R.Kh., Astakhov,I.I.,

Surikov,V.V. Soviet Electrochemistry, 12, 1976:1183.

49. Burshtein,R.Kh., Dribinskii,A.V., Tarasevich, M.R., Chimadzhev,Yu.A., Chirkov, Yu.G., Soviet Electrochemistry, 7, 1971:1762.

50. Chirkov, Yu. G., Soviet Electrochemistry, 11, 1975:36.

51. Lampinen,M.J. and Viitanen M. "A Mathematical Model and Optimization of the Structure for Porous Air Electrodes." J. Power Sources,32, 1990:207.

52. Giner, J., "From Electrocatalysis to Fuel Cells." Ed. G. Sandstede, University of Washington Press, Seattle, 1972.

53. Cutlip, M.B. "An Approximate Model for Mass Transfer with Reaction in Porous Gas Diffusion Electrodes." Electrochimica, 20, 1975:767-772.

54. Iczkowski, R.P. and Cutlip, M.B. " Voltage Losses in Fuel Cell Cathodes." J. Electrochemical Soc. 127, 1980:1433-1440.

55. Celikar,H., Al-Saleh,M.A., Gultekin, S. and Al-Zakri, A.S." Mathematical Model for the Performance of Raney Metal Gas Diffusion Electrodes." J. Electrochemical Society, 138/6, 1991:1671-1681.

56. Kimble, M.C.and White, R.E. " A Mathematical Model of a Hydrogen/oxygen Alkaline Fuel Cell." J. Electrochemical society, 138/11, 1991:3370-3382.

57. Kimble, M.C. and White, R.E. " Parameter Sensitivity and Optimization Prediction of a Hydrogen/Oxygen Alkaline Fuel Cell Model." J. Electrochem Society, 139/2, 1992:478-484.

58. Yang, Shian-Cherng and Bjornbom,P. "Modeling and Simulation of the Operation of AFC cathode by using concentrated electrolyte transport theory." Electrochimica Acta, 37/10, 1992:1831-1843.

59. Bolvin, K., Longhi, P. and Shnurnberger in Fuel Cell Seminar Abstract, Long Beach California, 1988:164.

60. Jung, M. and Dohren, H. V. DBP 1258 , 398 1968.

61. Maximovitch, S. and Durand, R. J. Electroanal. Chem. 149,1983:237-277.

62. Satterfield, C. N. " Heterogeneou Catalysis" MIT press, Cambridge, 1991.

63. Rotenberg, Y. and Srinivasan, S. J. Electroanal. Chem. 213, 1986:43-51.

64. Striebel, K. A., McLarnon, F. R. and Cairns, E. J., Journal Electrochem. Society, vol. 137, No. 11, Nov.1990:3360-3367.

Appendix A

STEADY STATE EXPERIMENTAL DATA

Temperature = 25°C

O.C.V= -922.3 mV

Current Density (mA/cm²)	Electrode Potential Hg/HgO (mV)	IR Drop (mV)	IR Free Overpotential (mV)	Ohmic Resistance (Ω)
1	-918.7	3	0.6	0.50
2	-915.1	6	1.2	0.50
4	-907.2	13	2.1	0.54
6	-900.0	19	3.3	0.53
8	-891.5	26	4.8	0.54
10	-883.2	32	7.1	0.53
12	-874.5	36	11.8	0.50
14	-865.1	44	13.2	0.52
17	-853.5	54	14.8	0.53
20	-836.4	68	17.9	0.56
25	-823.0	79	20.3	0.53
30	-802.6	94	25.7	0.52
35	-774.7	115	32.6	0.54
40	-759.9	127	35.4	0.53
45	-741.4	145	35.9	0.53
50	-716.6	158	47.7	0.53
55	-682.9	177	62.4	0.53
60	-662.3	193	67.0	0.53

Temperature = 45°C

O.C.V= -919.2 mV

Current Density (mA/cm²)	Electrode Potential Hg/HgO (mV)	IR Drop (mV)	IR Free Overpotential (mV)	Ohmic Resistance (Ω)
1	-916.7	2	0.5	0.33
2	-912.8	4	2.4	0.33
4	-908.1	8	3.1	0.33
6	-903.7	12	3.5	0.33
8	-898.2	17	4.0	0.35
10	-892.7	22	4.5	0.37
12	-887.9	26	5.3	0.36
14	-882.5	30	6.7	0.36
17	-880.0	32	7.2	0.31
20	-872.7	38	8.5	0.32
25	-858.6	48	12.6	0.32
30	-846.5	58	14.7	0.32
35	-833.4	70	15.8	0.33
40	-821.8	80	17.4	0.33
45	-812.3	87	19.9	0.32
50	-800.9	96	22.3	0.32
55	-792.7	102	24.5	0.31
60	-781.6	112	25.6	0.31
65	-762.0	130	27.2	0.33
70	-745.2	144	30.0	0.34
75	-734.5	152	32.7	0.34
80	-724.1	160	35.1	0.33

Temperature = 35°C

O.C.V= -921.5 mV

Current Density (mA/cm²)	Electrode Potential Hg/HgO (mV)	IR Drop (mV)	IR Free Overpotential (mV)	Ohmic Resistance (Ω)
1	-918.2	2.5	0.8	0.42
2	-915.0	5	1.5	0.42
4	-908.0	11	2.5	0.46
6	-902.5	16	3.0	0.44
8	-895.5	21	5.0	0.44
10	-888.5	27	6.0	0.45
12	-881.5	33	7.2	0.46
14	-875.5	38	8.0	0.45
17	-866.4	46	9.1	0.45
20	-855.7	54	11.8	0.45
25	-840.6	68	12.9	0.45
30	-824.2	81	16.3	0.45
35	-803.3	94	24.2	0.45
40	-787.2	108	26.3	0.45
45	-771.1	122	28.4	0.45
50	-755.7	135	30.8	0.45
55	-743.4	146	33.1	0.44
60	-723.0	165	36.5	0.46
65	-710.8	174	39.7	0.45
70	-694.6	188	42.9	0.45
75	-675.2	204	48.3	0.45

Temperature = 55°C

O.C.V= -921.4 mV

Current Density (mA/cm²)	Electrode Potential Hg/HgO (mV)	IR Drop (mV)	IR Free Overpotential (mV)	Ohmic Resistance (Ω)
1	-918.8	1.8	0.8	0.30
2	-916.7	3.5	1.2	0.29
4	-912.2	7	2.2	0.29
6	-908.4	11	2.0	0.30
8	-904.8	14	2.6	0.29
10	-900.7	18	2.7	0.30
12	-897.2	21	3.2	0.29
14	-892.6	25	3.8	0.30
17	-888.9	28	4.5	0.27
20	-882.2	33	6.2	0.28
25	-875.4	39	7.0	0.27
30	-863.6	50	7.8	0.28
35	-850.0	62	9.4	0.29
40	-839.7	70	11.7	0.29
45	-828.6	80	12.8	0.29
50	-819.1	88	14.3	0.29
55	-808.7	96	16.7	0.29
60	-796.9	106	18.5	0.29
65	-787.3	114	20.1	0.29
70	-776.1	124	21.3	0.29
75	-761.8	135	24.6	0.30
80	-754.5	139	27.9	0.29
85	-743.1	148	30.3	0.29
90	-726.7	162	32.7	0.30
95	-721.8	165	34.6	0.29
100	-712.0	172	37.4	0.29
105	-697.6	184	39.8	0.29
110	-686.6	192	42.8	0.30

Temperature = 65°C

O.C.V= -918.7 mV

Current Density (mA/cm²)	Electrode Potential Hg/HgO (mV)	IR Drop (mV)	IR Free Overpotential (mV)	Ohmic Resistance (Ω)
1	-916.9	1.5	0.3	0.25
2	-915.2	3	0.5	0.25
4	-911.4	6	1.3	0.25
6	-907.6	9	1.8	0.25
8	-904.3	12	2.1	0.25
10	-900.0	16	2.4	0.25
12	-896.7	19	2.7	0.26
14	-893.2	22	3.2	0.26
17	-887.7	27	3.7	0.26
20	-883.1	31	4.3	0.26
25	-874.5	39	4.9	0.26
30	-867.6	45	5.8	0.25
35	-857.7	54	6.7	0.26
40	-850.6	60	7.8	0.25
45	-839.3	70	9.1	0.26
50	-824.7	76	10.5	0.25
55	-822.0	84	12.4	0.26
60	-809.8	94	14.6	0.26
65	-800.2	102	16.2	0.26
70	-790.6	110	17.8	0.26
75	-785.3	114	19.1	0.25
80	-774.1	124	20.3	0.26
85	-763.8	133	21.6	0.26
90	-756.6	140	21.8	0.26
95	-747.8	148	22.6	0.26
100	-739.9	154	24.5	0.26
105	-727.7	164	26.7	0.26
110	-719.0	170	29.4	0.26
115	-706.4	179	33.0	0.26

Temperature = 75°C

O.C.V= -916.2 mV

Current Density (mA/cm²)	Electrode Potential Hg/HgO (mV)	IR Drop (mV)	IR Free Overpotential (mV)	Ohmic Resistance (Ω)
1	-914.8	1.2	0.2	0.20
2	-913.2	2.5	0.5	0.21
4	-910.7	4.5	1.0	0.19
6	-907.7	7	1.5	0.19
8	-905.3	9	1.9	0.18
10	-903.1	11	2.1	0.19
12	-899.9	14	2.3	0.19
14	-897.6	16	2.6	0.18
17	-895.3	18	2.9	0.18
20	-891.1	22	3.1	0.19
25	-883.9	29	3.3	0.19
30	-878.0	34	4.2	0.19
35	-870.2	41	5.0	0.19
40	-864.1	46	6.1	0.19
45	-856.8	52	7.4	0.19
50	-849.4	58	8.8	0.19
55	-840.1	66	10.1	0.20
60	-834.7	70	11.5	0.19
65	-825.9	78	12.3	0.19
70	-817.4	85	13.8	0.20
75	-808.6	93	14.6	0.20
80	-801.3	99	15.9	0.22
85	-793.5	106	16.7	0.20
90	-784.2	114	18.0	0.20
95	-778.7	118	19.5	0.21
100	-766.0	130	20.2	0.21
105	-760.4	134	21.8	0.22
110	-753.2	140	23.0	0.21
115	-740.2	150	26.0	0.22

Appendix B

Long Term Performance Experimental Data

Mode of Polarization: Potentiostatic O.C.V. = -920.1 mV

Overvoltage = 25 mV Temperature = 70°C

Time (hour)	Current Density (mA/cm^2)
0	100
4	91.7
8	81.7
12	71.7
20	60.0
24	53.3
28	46.7
32	36.7
36	28.3
44	15.0
48	11.7
52	8.3
56	6.7
64	5.0
68	5.0
72	5.0

Mode of Polarization: Potentiostatic

O.C.V = -919.5 mV

Overvoltage = 33 mV

Temperature = 45°C

Time (hour)	Current Density (mA/cm^2)
0	75.0
4	75.0
8	73.3
12	70.0
20	68.3
24	68.3
28	66.7
32	65.0
36	63.3
44	60.0
48	56.7
52	53.3
56	48.3
64	43.3
68	40.0
72	38.3
76	37.3
80	34.3
88	31.0
92	30.0
96	28
100	26.3
104	26.3

Mode of Polarization: Potentiostatic

O.C.V. = -922.3 mV

Overvoltage = 75 mV

Temperature = 25°C

Time (hour)	Current Density (mA/cm^2)
0	70.0
4	70.0
8	68.3
12	68.3
20	66.7
24	66.7
28	65.0
32	63.3
36	61.7
44	61.7
48	60.0
52	60.0
56	58.3
64	56.7
68	55.0
72	53.3
76	51.7
80	50.0
88	46.7
92	45.0
96	43.3
100	41.7
104	40.0
112	38.3
116	36.7
120	35.0
124	33.3
128	30.0
136	30.0
140	28.3
144	26.7
148	25.0

Mode of Polarization: Galvanostatic

O.C.V.=917.2 mV

Current Density(i)=100 (mA/cm^2)

Temperature = 70°C

Time (hour)	Overvoltage (mV)
0	22.7
4	22.8
8	22.7
12	23.2
20	26.5
24	28.9
28	30.6
32	35.7
36	43.6
44	55.3
48	63.6
52	77.8
56	92.6
64	107.5
68	500
72	1200

SAMPLE CALCULATIONS

Galvanostatic Polarization Run at 45°C

Open Circuit Voltage (O.C.V.)	=	-919.2 mV
Galvanostatic Current (I)	=	300 mA
Geometric Area of Electrode(A)	=	6 cm^2
Current Density (i)	=	50 mA/cm^2
Circuit Voltage (C.V.)	=	-800.9 mV
IR Drop in the Electrolyte	=	96 mV
Electrolyte Resistance	=	IR Drop/ I
	=	96/300
	=	0.32 Ω
IR free Overvoltage (η)	=	C.V. + IR -O.C.V.
	=	-800.9 - 9.6 + 919.2
	=	22.3 mV

```
C                                                                       H2500010
C       PARAMETERS @ 25 C                                               H2500020
C                                                                       H2500030
C   $JOB                                                                H2500040
C....SPECIFICATIONS FOR PARAMETERS                                      H2500050
C     IMPLICIT REAL*8(A-H,O-Z)                                          H2500060
      INTEGER LDYFIN,LDYINI,MXGRID,NEQNS,NINIT                          H2500070
      PARAMETER  ( MXGRID=100, NEQNS=2, NINIT=40, LDYFIN=NEQNS,         H2500080
     *           LDYINI=NEQNS)                                          H2500090
C.......                                                                H2500100
C.....                                                                  H2500110
      INTEGER I, J, NCUPBC, NFINAL, NLEFT, NOUT                         H2500120
      REAL  CONST, ERREST(NEQNS), FCNBC, FCNEQN, FCNJAC, FLOAT,         H2500130
     *      PISTEP, TOL, XFINAL(MXGRID), XINIT(NINIT), XLEFT,           H2500140
     *      XRIGHT, YFINAL(LDYFIN,MXGRID), YINIT(LDYINI,NINIT),         H2500150
     *      CURR(NINIT),RACURR(NINIT),XPRIM(NINIT)                      H2500160
C...                                                                    H2500170
      LOGICAL  LINEAR, PRINT                                            H2500180
      INTRINSIC FLOAT                                                   H2500190
      EXTERNAL  BVPFD, CONST, FCNBC, FCNEQN, FCNJAC, UMACH              H2500200
C...                                                                    H2500210
C.....       SET PARAMETERS                                             H2500220
C...                                                                    H2500230
      ETAO=0.075                                                        H2500240
      EPS=0.30                                                          H2500250
      EXCHI=6.60E-06                                                    H2500260
      ALPHA=0.57                                                        H2500270
      BARK=0.254                                                        H2500280
      R=0.5E-03                                                         H2500290
      T=298.15                                                          H2500300
      DEA=0.004                                                         H2500310
      TIM=20.0                                                          H2500320
      CONCO=2.0E-07                                                     H2500330
C     ALPHA=1.40                                                        H2500340
      DBAR=1.60E-05                                                     H2500350
      NLEFT = 1                                                         H2500360
      NCUPBC = 0                                                        H2500370
      TOL =0.01                                                         H2500380
      XLEFT = 0.0                                                       H2500390
C     XRIGHT = 0.020                                                    H2500400
      XRIGHT = 0.385E-01                                                H2500410
      PISTEP =0.0                                                       H2500420
      PRINT = .FALSE.                                                   H2500430
      LINEAR = .FALSE.                                                  H2500440
      EN=2.0                                                            H2500450
      Z=1.0                                                             H2500460
      CM2CM3=8.3E+05                                                    H2500470
C....                                                                   H2500480
C...   DEFINE XINIT AND YINIT                                           H2500490
C....                                                                   H2500500
      DO 10 I=1,NINIT                                                   H2500510
         XINIT(I)=XLEFT + FLOAT(I-1)*(XRIGHT-XLEFT)/FLOAT(NINIT-1)      H2500520
C        YINIT(1,I)=0.4*(XINIT(I)-XLEFT)*(XRIGHT-XINIT(I))              H2500530
C  CHANGE THE VALUE OF ETAO FOR DIFFERENT VALUES IN THE STAT. BELOW     H2500540
         YINIT(1,I)=0.0584-0.005*FLOAT(I)                               H2500550
```

```
      BARK=0.254                                                        H2501110
      R=0.5E-03                                                         H2501120
      F=96484.56                                                        H2501130
      CONCO=2.0E-07                                                     H2501140
      DBAR=1.6E-05                                                      H2501150
      Z=1.0                                                             H2501160
      GASC=8.314                                                        H2501170
      T=298.15                                                          H2501180
      EXCHI=6.60E-06                                                    H2501190
      ALPHA=0.57                                                        H2501200
      CM2CM3=8.30E+05                                                   H2501210
C     ALPHA=1.40                                                        H2501220
      DEA=0.004                                                         H2501230
      TIM=20.0                                                          H2501240
C                                                                       H2501250
C......CALCULATION OF C1,C2,C3,C4                                       H2501260
C                                                                       H2501270
      C1=(2.0*DBAR*EN*F*CONCO)/(BARK*R)                                 H2501280
      C2=(Z*F)/(GASC*T)                                                 H2501290
      C3=SQRT((EXCHI*CM2CM3*EXP(-DEA*TIM))/(EN*F*DBAR*CONCO))           H2501300
      C4=(ALPHA*C2)/2.0                                                 H2501310
      CC1=TANH(C3*R*EXP(C4*Y(1)))                                       H2501320
      CC2=EXP(-C2*Y(1))                                                 H2501330
      CC3=EXP(C4*Y(1))                                                  H2501340
C                                                                       H2501350
C.......DEFINE PDE                                                      H2501360
C                                                                       H2501370
      DYDX(1) = Y(2)                                                    H2501380
      DYDX(2) = C1*(1.0-EXP(-C2*Y(1)))*(C3*EXP(C4*Y(1))*1.0/            H2501390
     *          TANH(C3*R*EXP(C4*Y(1)))-1.0/R)                          H2501400
C     WRITE(7,*)'Y(2)= ',Y(2),'Y(1) = ',Y(1)                            H2501410
C     WRITE(7,*)'DYDX ',DYDX(2),Y(2),Y(1)                               H2501420
      RETURN                                                            H2501430
      END                                                               H2501440
C                                                                       H2501450
C                                                                       H2501460
      SUBROUTINE FCNJAC (NEQNS,X,Y,P,DYPDY)                             H2501470
C     IMPLICIT REAL*8(A-H,O-Z)                                          H2501480
      INTEGER NEQNS                                                     H2501490
      REAL X,Y(NEQNS),P,DYPDY(NEQNS,NEQNS),C1,C2,C3,C4,C5,EN,F,BARK,    H2501500
     *     R,DBAR,Z,GASC,T,EXCHI,CM2CM3,ALPHA                           H2501510
      REAL TANH,SINH,EXP,SQRT                                           H2501520
      INTRINSIC TANH,SINH,EXP,SQRT                                      H2501530
C                                                                       H2501540
C.....DEFINE PHYSICAL PARAMETERS                                        H2501550
C                                                                       H2501560
C     WRITE(7,*)'FCNJAC'                                                H2501570
      EN=2.0                                                            H2501580
      BARK=0.254                                                        H2501590
      R=0.5E-03                                                         H2501600
      F=96484.56                                                        H2501610
      CONCO=2.0E-07                                                     H2501620
      DBAR=1.6E-05                                                      H2501630
      Z=1.0                                                             H2501640
      GASC=8.314                                                        H2501650
```

```
      T=298.15                                                          H2501660
      EXCHI=6.60E-06                                                    H2501670
      ALPHA=0.57                                                        H2501680
      CM2CM3=8.30E+05                                                   H2501690
C     ALPHA=1.40                                                        H2501700
      DEA=0.004                                                         H2501710
      TIM=20.0                                                          H2501720
C                                                                       H2501730
C......CALCULATION OF C1,C2,C3,C4,C5                                    H2501740
C                                                                       H2501750
      C1=(2.0*DBAR*EN*F*CONCO)/(BARK*R)                                 H2501760
      C2=(Z*F)/(GASC*T)                                                 H2501770
      C3=SQRT((EXCHI*CM2CM3*EXP(-DEA*TIM))/(EN*F*DBAR*CONCO))           H2501780
      C4=(ALPHA*C2)/2.0                                                 H2501790
      C5=C4-C2                                                          H2501800
C                                                                       H2501810
C...        DEFINE   D(DYDX)/DY                                         H2501820
C                                                                       H2501830
      DYPDY(1,1)=0.0                                                    H2501840
      DYPDY(1,2)=1.0                                                    H2501850
C     DYPDY(2,1)=C1*C3*C4*EXP(C4*Y(1))*(1.0/TANH(C3*EXP(C4*Y(1)))+      H2501860
C    *           (-C3)*EXP(C4*Y(1))*1.0/SINH(C3*EXP(C4*Y(1)))**2.0)     H2501870
C    *          +C1*C3*C5*EXP(C5*Y(1))*(1.0/TANH(C3*EXP(C4*Y(1)))+      H2501880
C    *           (-C3)*EXP(C5*Y(1))*1.0/SINH(C3*EXP(C4*Y(1)))**2.0)     H2501890
C    *          -C1*(-C2)*EXP(-C2*Y(1))                                 H2501900
      DYPDY(2,1)=C1*C3*C4*EXP(C4*Y(1))*(1.0/TANH(C3*R*EXP(C4*Y(1)))+    H2501910
     *     (-C3)*R*EXP(C4*Y(1))*1.0/SINH(C3*R*EXP(C4*Y(1)))**2.0)       H2501920
     *          +C1*C3*EXP(C5*Y(1))*(1.0/TANH(C3*R*EXP(C4*Y(1)))+       H2501930
     *     (-C3)*R*C4*EXP(C4*Y(1))*1.0/SINH(C3*R*EXP(C4*Y(1)))**2.0)    H2501940
     *          +(C1*C2*EXP(-C2*Y(1)))/R                                H2501950
      DYPDY(2,2)=0.0                                                    H2501960
C     WRITE(7,*)'DYPDY ',DYPDY(2,1),Y(2),Y(1)                           H2501970
      RETURN                                                            H2501980
      END                                                               H2501990
C                                                                       H2502000
C                                                                       H2502010
      SUBROUTINE FCNBC (NEQNS,YLEFT,YRIGHT,P,F)                         H2502020
C     IMPLICIT REAL*8(A-H,O-Z)                                          H2502030
      INTEGER NEQNS                                                     H2502040
      REAL YLEFT(NEQNS), YRIGHT(NEQNS), P,F(NEQNS)                      H2502050
C                                                                       H2502060
C.......DEFINE BOUNDARY CONDITIONS                                      H2502070
C                                                                       H2502080
C     WRITE(7,*)'FCNBC'                                                 H2502090
C  CHANGE THE VALUE OF ETA0 FOR DIFFERENT VALUES IN THE STAT. BELOW     H2502100
      F(1)=YLEFT(1)-ETA0                                                H2502110
      F(2)=YRIGHT(2)                                                    H2502120
      RETURN                                                            H2502130
      END                                                               H2502140
```